ABSTRACT

Title of Thesis:	UNDERWATER OPTICAL WIRELESS COMMUNICATION LINK FOR SHORT-RANGE DATA TRANSMISSION: A PROOF OF CONCEPT STUDY
	Team OPTIC Gemstone Honors Program 2020
Thesis Directed By:	Dr. Ashok K. Agrawala Professor, Department of Computer Science

The purpose of this thesis is to lay the groundwork for the development of a cost-effective Underwater Optical Wireless Communications system. Currently, one of the largest barriers to the expansion of underwater enterprise and research is a lack of high-speed wireless communication systems. Wireless communication underwater is essential for safety, improving aquatic technology, and many other marine ventures, yet it is still technologically limited. Current methods, such as acoustic communication, are often power inefficient, cumbersome, and expensive. The proposed system would enable scuba divers and researchers to bridge the technological gaps in available underwater data transmission systems. This paper proposes using visible light to wirelessly transmit data underwater.

Visible light is an effective carrier wave underwater due to its large bandwidth and low absorption coefficient. Using light emitting diodes, silicon PIN photodetectors, waterproof enclosures, and consumer-grade microcontrollers, a model for the development of a wireless optical communications system is proposed. The system also adopts a modular design which allows each component to evolve as needed.

The proposed system can transmit and receive audio and vitals signals underwater, illustrating the potential of a technology that could make diving and other underwater endeavors safer and more efficient. Furthermore, the proposed data link shows the potential for this technology to be used in other underwater applications that were previously limited by data speeds or mobility. Above all, this technology seeks to build upon existing knowledge of optical wireless communication and advance the field of underwater science and technology.

UNDERWATER OPTICAL WIRELESS COMMUNICATION LINK FOR SHORT-RANGE DATA TRANSMISSION: A PROOF OF CONCEPT STUDY

by

Team OPTIC

Arjun Agarwal
Andrew Chen
Thomas Good
Miles Grissom
Daniel Klawson
Jacob Levit
William Nix
Michael Piqué
Edward Salvatierra
Nicholas Zhao

Thesis submitted in partial fulfillment of the requirements of the
Gemstone Honors Program
University of Maryland, College Park
2020

Advisory Committee:
Dr. Ashok Agrawala, Mentor
Dr. Christopher Davis
Dr. Yongzhang Leng
Dr. Thomas Murphy
Dr. Derek Paley
Dr. Steven Tretter

Acknowledgements

To Dr. Coale, Dr. Skendall, Dr. Hill, Dr. Tobin, and Jessica Lee, we appreciate your mentorship throughout the research process. To our librarian, Ms. Zdravkovska, thank you for preparing us for an undertaking of this magnitude. We would like to thank Dr. Akin, Dr. Davis, Dr. Murphy, Mr. Brigham, Mr. Mehrotra, and Mr. Quinn for furnishing the facilities and equipment to conduct our research. Thank you to our discussants, Drs. Davis, Leng, Murphy, Paley, and Tretter for taking time to review our findings and provide thoughtful feedback. Finally, we would be remiss without recognizing our mentor, Dr. Agrawala, without whom none of this would be possible. Thank you for your unwavering support of our endeavors and the academic process. Team OPTIC received support from Maryland Sea Grant under award NA14OAR4170090 (R/Ep/R-324) and NA18OAR4170070 (E/Ep/E-353) from the National Oceanic and Atmospheric Administration, U.S. Department of Commerce.

Table of Contents

List of Tables

List of Figures

Table of Abbreviations

Analog-to-Digital Converter	ADC
Application Programming Interface	API
Avalanche Photodiode	APD
Bill of Materials	BOM
Bipolar Junction Transistor	BJT
Bit Error Rate	BER
Direct Current	DC
Electromagnetic Interference	EMI
Entrance Pupil Diameter	EPD
Front Focal Length	FFL
Fuse Deposition Modeling	FDM
Ground Voltage	GND
Input Output	I/O
Institute of Electrical and Electronics Engineers	IEEE
International Convention on Standards of Training, Certification and Watchkeeping	STCW
International Safety Management	ISM
Light Emitting Diode	LED
Line of Sight	LoS
Lithium-Ion	Li-ion
Metal-Oxide-Semiconductor Field-Effect Transistor	MOSFET
Neutral Buoyancy Research Facility	NBRF
Nickel Metal-Hydride	Ni-Mh
On-Off Keying	OOK
Open Systems Interconnection	OSI
Operational Amplifier	Op-Amp
Photomultiplier Tube	PMT
p-i-n	PIN
Polyvinyl Chloride	PVC
Power Distribution Board	PDB
Printed Circuit Board	PCB
Radio Frequency	RF
Receiver	Rx
Signal to Noise Ratio	SNR
Safety of Life at Sea	SOLAS
Space-Division Multiple Access	SDMA
Transimpedance Amplifier	TIA
Transmitter	Tx
United Nations Convention of the Law of the Sea	UNCLOS
Underwater Optical Wireless Communications	UOWC
Universal Asynchronous Transmitter Receiver	UART
University of Maryland	UMD
User Interface	UI

Chapter 1. Introduction

Marine environments are the home for a number of multidisciplinary industries including biological research, resource extraction, and national defense [1], among others. These aquatic industries represent 2% of American employment and 1.7% of its annual gross domestic product, yet less than 5% of the Earth's oceans have been explored [2] [3]. In recent years, mounting environmental concerns, coupled with promising new technological developments, have placed more focus on marine affairs, conservation, research, or otherwise.

One of the most important considerations in dealing with marine environments is the ability to communicate underwater effectively, whether it is person-to-person, machine-to-machine, or a combination of the two. Certain systems have been developed for specific uses, such as acoustic communications for long-range low-throughput applications, or radio frequency (RF) communications for shallow land-to-ocean communication [4]. Still, underwater communication remains a field with much room for improvement, as most current underwater systems are overshadowed by their terrestrial counterparts.

The purpose of this study is to design, implement, and test an underwater optical wireless communications (UOWC) system built using consumer-grade components. One paradigm unaddressed by either acoustic or RF methods has been short-range, high-throughput, high-mobility communication for underwater ventures. The proposed system would allow underwater personnel to communicate speech, vital signs, and sensor readings while performing operations, increasing their capacity to work efficiently and safely.

UOWC represents the category of communication between devices underwater utilizing a wireless optical channel. In other words, light is used as a carrier to send and receive information. UOWC promises a much higher bandwidth than acoustic methods due to the higher frequency of light versus sound. It also permits smaller and lower cost components compared to both RF and acoustic systems, increasing the potential for mobility and reducing the cost.

This thesis proceeds with a literature review on existing investigations into UOWC as well as supplementary materials that hold relevance to this topic. Next, a methodology is included to demonstrate the approach to developing and integrating this model of UOWC. Afterwards, the results of the research are reviewed, followed by a discussion of the findings as well as suggestions for extrapolation and further investigations into this field. Finally, the thesis concludes by summarizing the general thrust and findings of this investigation.

Chapter 2. Literature Review

2.1. Overview of Established Underwater Networks

Electronic data transfer has become essential in nearly all facets of science, industry, and daily life. While terrestrial data transfer is an established field, there is a growing need for more underwater data transfer methods. To accommodate this increasing traffic, a diverse array of data transfer techniques can be utilized for differing scenarios. One example scenario is the monitoring of underwater oil and natural gas pipelines. Pipeline leakages and failures are supervised by longitudinal network cables. However, these monitoring systems are inherently unreliable because a single severed connection would cause large-scale network failure. This makes underwater wired connections limited in their application due to the inaccessible environment and the need for a physical connection between two points, which is much less certain underwater than above water. For this reason, among others that will be discussed, wireless communications are increasingly being explored to supplant or supplement wired connections underwater [5].

Current methods of wirelessly transmitting data underwater utilize the acoustic, RF, and visible light spectrums. Underwater acoustic waves have become a common option for transmitting data because they propagate faster in water than in air and have low rates of attenuation [6] [7]. However, their lower relative speed and frequency in comparison to electromagnetic waves results in less bandwidth, slower data rates, and higher latency [8]. In addition, acoustic transceivers are large, energy-intensive devices, which have the potential to harm surrounding marine life [9]. Finally, factors such as

pressure and deflection of acoustic waves off the ocean's surface have limited their use to long-range deep-sea communication [7].

Transmitting data in the RF spectrum is effective for terrestrial networks in the form of Wi-Fi, offering high data speeds and large bandwidth [10]. However, the effectiveness of RF decreases drastically underwater; as the frequency of an underwater RF wave increases, its absorption increases dramatically. This effect is further worsened in saltwater due to its higher conductivity compared to freshwater. This means that the frequency of the RF waves underwater must be orders of magnitude less than the frequency of RF waves on land [9]. This decreased frequency minimizes the absorption, but compromises the speed and bandwidth of the signal [7] [11]. Furthermore, RF communication underwater necessitates large antennae due to the long wavelengths required as a byproduct of low frequency [11].

The third method is using the visible light spectrum to transmit data. Visible light communications, one subset being UOWC, has a number of qualities that match or surpass other existing underwater communications technologies. UOWC, with a signal in a focused direction, creates a relatively secure connection, meaning that another party cannot intercept the signal unless it is able to see and demodulate the light transmission. Such a quality lends itself well to commercial and defense applications in underwater surveillance [1]. UOWC also allows for high data rates that can be used to stream video and transfer large amounts of data, since the frequency of the carrier signal is higher in UOWC than in RF or acoustic. Moreover, UOWC's fundamental components, light emitting diodes (LEDs)/lasers and photodiodes, are relatively small compared to their RF and acoustic counterparts and can be scaled to meet application

parameters. Finally, in terms of power consumption, UOWC systems generally require much less power than their acoustic and RF counterparts due to the low power consumption of LEDs and photodiodes [11]. Therefore, for short-range, high-bandwidth applications, UOWC presents itself as a promising alternative to existing methods.

2.2. Non-Technical Considerations

2.2.1. Overview

UOWC, acoustic, and RF systems each have their own unique safety, regulatory, and environmental considerations. When designing a communications system, these factors must all be acknowledged. This section compares and contrasts the non-technical considerations regarding the aforementioned underwater communications systems.

2.2.2. Safety

The primary procedure for underwater communication between scuba divers is hand signaling. There is a need to provide commercial divers with a more effective means of communication while submerged because, often times, hand signals lack the range and throughput necessary for their work environment [12] [13] [14]. One study found that 86% of scuba diving-related fatalities occur when divers become separated from one another or are diving alone [15]. These casualties could be lessened by the use of a UOWC system, which would provide a more comprehensive means of communication to divers. Moreover, underwater working conditions could be improved in terms of safety and efficiency with the introduction of a UOWC system. For example, there is still no viable means of communication to help divers mitigate the uncertainty and risk associated with underwater debris management [14]. Another study supervised the temporary implementation of a UOWC system that used lasers to assist diver communications on a public works project in underwater rock-blasting [14]. The study found that workers were able to work efficiently and minimize

potentially hazardous situations with a clearer line of communication, however the laser-based system was too costly to broadly implement [14]. In this regard, a UOWC system using LEDs may show promise as a feasible improvement to underwater labor conditions.

2.2.3. Regulation

UOWC is relatively unregulated compared to existing methods such as RF or acoustic communications – RF bands are heavily sanctioned, and measures are being taken to reduce the noise pollution of acoustic sources [16] [17] [18]. The recency of UOWC, when compared to its counterparts, is underscored by a lack of institutions dictating its use [16] [19]. This can be an advantage for researchers as their use of UOWC may be less restricted, especially in international waters where the expectations and restrictions on RF and acoustic communications are thoroughly entrenched [12] [18]. As such, UOWC presents a novel opportunity to work around existing marine constraints. In this regard, the current regulation of UOWC may present previously inaccessible opportunities in underwater communications.

As should be apparent, while presently less restricted, UOWC is subject to some of the same standards and expectations as all other underwater technology [20]. The Regulations set forth by institutions such as the United Nations Convention of the Law of the Sea (UNCLOS), Safety of Life at Sea (SOLAS), International Convention on Standards of Training, Certification and Watchkeeping (STCW), and the International Safety Management (ISM) code limit and specify the conditions and context under which use of marine technology and apparatuses is permissible [21]. The general of

these establishments is to protect the marine environments, including conservation of ecosystems, noninterference with wildlife, and ensuring ethical procedures [21] [22]. For a list of these regulations, see Appendix A.

2.2.4. Environmental Impact

One of the most promising qualities of UOWC has been its potential to limit the impact of human interference in underwater environments [1]. The use of acoustics underwater has been shown to interfere with individual animals and the environment as a whole – for instance, acoustic emitters can interfere with the life cycle of cetaceans [3] [12] [22]. Acoustic communications can impact not only their immediate environment but have the potential to harm the surrounding ecosystem for thousands of kilometers as well [22]. To the contrary, early studies have shown that LEDs may interfere less with an ecosystem, especially when used during the day [1]. Marine flora and fauna may be less affected by UOWC under the right conditions, permitting more empirical results from research and a lessened impact on the ecosystem [9] [20].

2.3. Underwater Optical Wireless Systems

2.3.1. Overview

As UOWC is the focus of this research, the following subsections will discuss different system setups, the drawbacks to using light to transmit data through water, the commercial products available for UOWC systems, and the current and potential uses for UOWC systems.

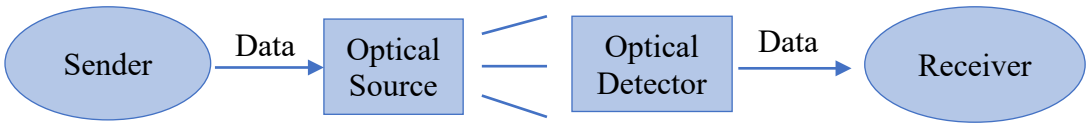

Figure 1: Example of underwater optical communication

UOWC represents a promising new subdiscipline in the field of underwater technology. UOWC transmission works by modulating data via a light source, typically an LED or laser, which is received by a photodetector. This process can be seen in Figure 1. The received signal is then processed and demodulated, resulting in the original data. Currently, research on UOWC is accelerating, yet there are few commercial products that use this technology. Many research papers on UOWC do not actually test underwater; instead, studies have employed rigs which are used on either side of encased water [23] [24]. These studies seek to optimize individual components of UOWC, such as the optical link, rather than entire UOWC systems. These aforementioned points demonstrate that there is currently a lack of research into creating a usable consumer-grade UOWC system.

2.3.2. Optical Links

There are three types of links, or data connections established between two points, possible for an UOWC system: a line of sight (LoS) link, a modulating retroreflector link, or a reflective link. Each of these links provide high data rates at short ranges and are adversely affected by the attenuation of water.

LoS links are the most common system used for UOWC. In this setup, the transmitter emits the light beam in the direction of the receiver. An ideal link would have the transmitter and the receiver pointed directly at each other at the closest range possible because data losses would increase as either the angle of effect or the transmission distance increases [25]. The majority of research uses LoS because the optical power is the strongest [25] [26] [27].

The next system is an alternate approach to having a two-way channel: a modulating retroreflector is used as the link. The modulating retroreflector link is used in scenarios where there is a central communication hub with much greater computing capabilities compared to the peripheral devices with which it communicates. For example, a submarine has an abundant supply of energy and processing power in comparison to a battery powered transceiver on a scuba diver. Therefore, the submarine would act as a hub and transmit data to the diver, whose modulating retroreflector would return the diver's data transmission [25]. As seen in Figure 2 , the retroreflector is another potential way of establishing a two-way link between underwater systems. However, this method is less effective than having a transceiver on both systems, as the necessary transmission distance is essentially doubled for a given separation

distance. Thus, the link's strength is optimized by having a light source on either side [26].

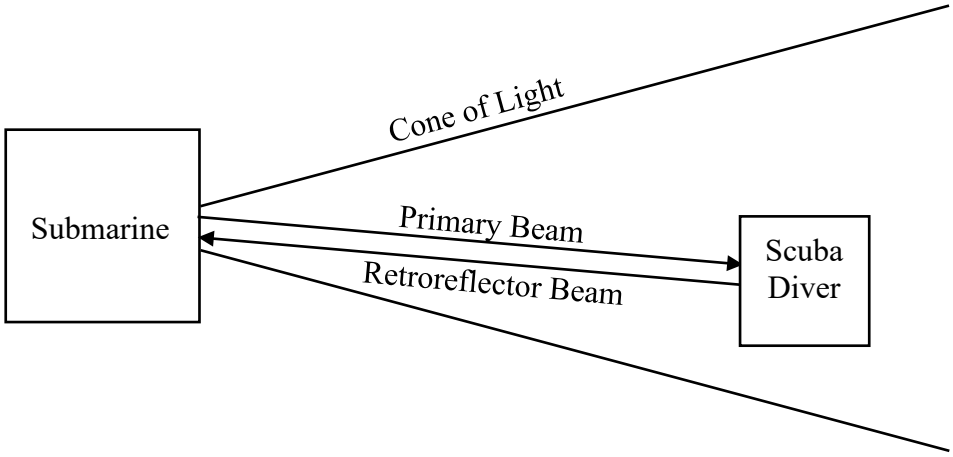

Figure 2: Modulating retroreflector communication link example

The last technique is the reflective communication link. This link may be used when there is an obstruction in the way, blocking a LoS link. In this system, a transmitter emits a cone of light, defined by inner and outer angles θ_{min} and θ_{max}, in the upward direction, using the water's surface to reflect light back down and around obstacles, as seen in Figure 3 [25]. While this technique may be more robust because it does not require a LoS link, the light transmitted has more attenuation compared to a LoS link. This is because the light is travelling a greater distance, so more light is scattered from reflecting off of the ocean's surface, which is not a flat plane. Finally, although this technique forgoes a LoS link, the effective area that the signal can transmit to is limited by θ_{min} and θ_{max}, which means this technique requires the same amount of precision as the LoS and modulating retroreflector link. However, it has still been shown that it can perform better than an LoS link; a Monte Carlo simulation

demonstrated a reflective link capable of 20MHz bandwidth at a distance of 20m in clear conditions, which is a significant reduction in channel bandwidth compared to the LoS simulation [27].

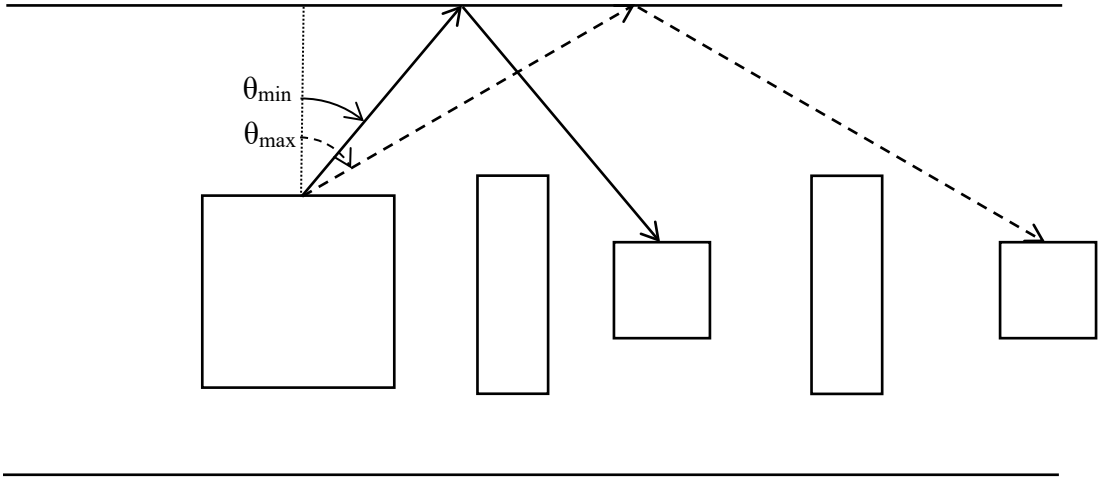

Figure 3: Reflective communication link example

2.3.3. Signal Modulation

Modulation in a communication system is the process of altering the carrier wave in order to represent the desired data. In the case of UOWC, the modulation scheme determines how the light signal is changed based on the transmitted data. Several different modulation schemes exist to support UOWC, with each varying in complexity, implementation cost, bit error rate (BER), robustness to noise, power consumption, and bandwidth. The simplest scheme is on-off keying (OOK), wherein a light switched on represents a bit, either 0 or 1, and a light switched off represents the other bit [28]. For example, a 2.3Gbps UOWC system was designed using a green wavelength laser and OOK, showing that there is more than enough bandwidth

available to consider OOK a viable modulation scheme [10]. Other more complex modulation schemes include pulse position modulation, frequency shift keying, phase shift keying, and quadrature amplitude modulation [28] [29].

2.3.4. Factors that Affect Underwater Optical Wireless Systems

The different optical links used in UOWC networks pose several unique problems for this type of data transmission. Similar to other wireless communication methods such as acoustic and RF, UOWC is severely affected by the transmission medium [11]. Additionally, LoS is critical to nearly all UOWC implementations, regardless of the medium through which it passes. This makes the optical data transmission link between sender and receiver more precarious compared to other data transmission schemes which are omni-directional and can transmit through objects. The details of these effects will be further explained in the review of the transmitter.

2.3.5. Existing Underwater Wireless Systems

Currently, there are a number of companies that sell underwater wireless communications systems. However, few companies exist that actually manufacture UOWC systems, while the rest use acoustics to transmit data wirelessly.

One of the communications companies that manufactures acoustic systems is Evo Logics. All of their products, designed for short, medium, or long-distance communications, can only achieve limited data rates due to the inherent properties of sound waves. For example, one of their products, the S2C Underwater Acoustic Modem, can achieve a maximum of 31.2kbps at an operating range of 1000m [30].

With this slow of a data rate, only certain applications such as low-quality voice transmission, basic data collection, and signaling are viable. However, with the use of optics, much faster data rates are achieved by a company called Sonardyne.

Sonardyne manufactures three different underwater optical communications systems, each for a unique application. All three of the products use a simple digital modulation scheme, and the systems can be utilized in both saltwater and freshwater. Compared to acoustic systems, these UOWC systems perform well enough to stream video back to a receiver onboard a ship or on land [31]. These systems allow for short-range, high-bandwidth applications unafforded by acoustics.

Sonardyne offers two ambient light systems and one directed light product. The ambient light systems use an array of LEDs to transmit data. In shallow water, where there is interference from sunlight and organic matter, data rates of 1 to 5Mbps can be achieved from up to 15m [31]. In deeper, darker water, data rates of 2.5 to 12.5Mbps can be reached from up to 100m [32]. Their last product transmits data using lasers, which are much narrower beams of light. The range of this system is only 7m; however, because laser diodes can be modulated much more quickly than LEDs, they can transmit data at a higher rate, achieving speeds of 500Mbps [33].

The UOWC systems that are present today clearly illustrate that underwater optical communications provide superior data rates to acoustic systems [30] [31] [32] [33]. However, acoustic systems have the benefit of much larger ranges. There is a significant trade-off between bandwidth and range with acoustic and optical systems, so the user must choose according to their system requirements. These existing systems, however, all fall short of achieving the goal of supporting diver communications due

to expensive costs, lack of physical mobility, flexibility in network structure, or diver specific user interface implementation.

2.4. System Design

2.4.1. Overview

The following subsections of System Design outline the different components of a UOWC system, starting with the transmitter and receiver, followed by the circuit design implementation, and then ending with the software used to control the transmission of data.

2.4.2. Transmitter

2.4.2.1. Overview

In a UOWC system, the role of the transmitter is to convert a binary signal into a modulated optical signal that can be transmitted through water. The design of the transmitter can be divided into two components: the optical source used to project the data through the medium, and the switching circuit used to modulate the data on the optical source. This section discusses the different technologies available for these two components as well as their strengths and weaknesses.

2.4.2.2. Optical Source

In UOWC, megabit and gigabit data rates are only feasible using semiconductor devices such as lasers or LEDs because of these devices' ability to be modulated at high frequencies [34]. Lasers and LEDs each have distinct advantages and disadvantages which make them suitable for different communication applications. Lasers offer a more powerful, focused beam of light that can be modulated on the order of gigahertz, allowing for high data rates [11]. Additionally, lasers transmit light with a narrow wavelength range, meaning that filters can be designed on the receiving end

to filter out all but the relevant wavelengths, thus reducing noise injected by other sources of light [11]. The major weakness associated with lasers for UOWC is that this transmission scheme requires greater spatial precision and is more adversely affected by obstacles in the medium [28]. While LEDs have lower possible modulation frequencies on the order of megahertz, less power, and lower transmission wavelength precision, these devices are cheaper and do not rely on a precise transmitter-to-receiver link due to their wider emission angle [28]. As a result, LEDs are the preferred optical source for short-range, wide-angle applications [11].

One major challenge for UOWC systems, regardless of the transmission source used, is the effects of the underwater environment on the propagation of light. The two main mechanisms that affect the propagation of light underwater are absorption and scattering. The overall attenuation associated with a light wave traveling underwater is given by the sum of these two mechanisms, *i.e.*

$$c(\lambda) = a(\lambda) + b(\lambda) \qquad (1)$$

where $a(\lambda)$ is the wavelength-dependent absorption coefficient and $b(\lambda)$ is the wavelength-dependent scattering coefficient [35]. Absorption is the process of the light wave's optical intensity being reduced as it travels through a medium and ionizes the atoms that it encounters [35]. On the other hand, scattering occurs when light waves change directions due to interference with wavelength-sized particles or larger particulate matter with a different index of refraction [35]. Quantitative studies have consistently shown that the scattering coefficient decreases linearly with increasing wavelengths in clear oceanic environments [36]. Additionally, the scattering coefficient is directly linked to the turbidity of the ocean environment. Suspended

particulate matter and macroscopic organisms can cause light to deflect in different directions, meaning the scattering coefficient is lowest in freshwater, followed by open ocean water, and highest in coastal ocean and harbor water due to their increased concentration of particulates [11].

Absorption, however, is more complicated. There are several factors that impact the absorption spectrum and can drastically vary which wavelength of light is attenuated the least [11]. The absorption coefficient of pure seawater is minimized for blue-green wavelengths due to dissolved salts in the water, but the wavelength of light that is least absorbed changes in the presence of particulate matter and microorganisms [11]. For example, photosynthetic organisms contain chlorophyll which absorbs light in the blue-green spectrum, thus increasing the minimal absorption wavelength [11]. Additionally, organic matter also increases absorption in the blue-green spectrum due to the chemicals released when this matter decays, and this also causes the minimum absorption frequency to increase [11]. In summation, absorption is the dominant factor in the attenuation, and the wavelength of light used to transmit should be dependent on the environment [35].

2.4.2.3. Switching Circuit

In addition to the optical transmission source, another important aspect of the transmitter in a UOWC system is how the light is modulated. This modulation is performed using a switching circuit, which is a type of circuit that uses a control signal to turn on and off power delivered to a load [37]. One of the simplest ways to implement

the switching circuit is using a transistor in the common source configuration, shown in Figure 4 [38]:

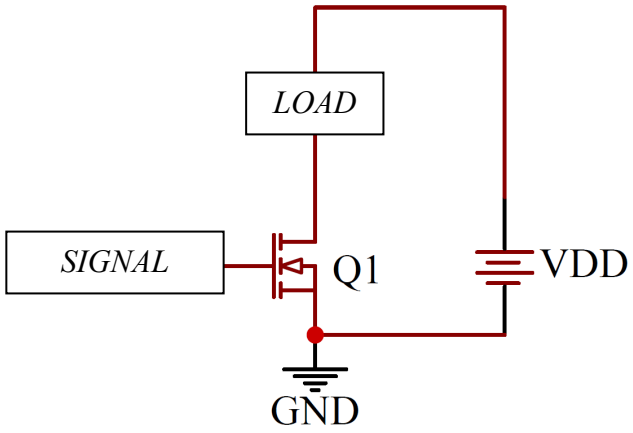

Figure 4: Simple transistor switching circuit

In this circuit, a digital signal is used to control whether the transistor acts as an open or closed circuit, thus modulating the current passing through the load. The two predominant transistor architectures used in switching circuits are the bipolar junction transistor (BJT) and the metal-oxide semiconductor field-effect transistor (MOSFET), the latter of which is used in Figure 4. Although these two devices serve the same purpose, there are significant differences in how these devices modulate current and how effective these devices are for switching applications – more details can be found in Appendix B.

Regardless of the transistor architecture used, this switching circuit allows a high current device, such as an LED or a laser, to be driven by a low current signal, such as a digital output signal from a microcontroller or other signal processing unit. In the case of the load, there have been numerous experimental optical transmitters that have used LED arrays to increase the luminous intensity and transmission angle of their

UOWC transmitters [11] [28]. However, implementing arrays of LEDs introduces problems such as thermal runaway, a destructive positive-feedback mechanism that can occur when LEDs are wired in parallel in a circuit [39]. Each parallel LED branch will have the same voltage drop; however, each individual LED has a slightly different current-voltage relationship due to variations in the illuminated semiconductor junction caused by the manufacturing process. As a result, there will be a small current imbalance between the parallel branches. The temperature of the LED branch receiving the higher current increases at the semiconductor junction, which further increases its current compared to the adjacent branches [40]. This current imbalance will continue to worsen until the temperature and current exceed the safe operating limits of the LEDs, at which point they burn out.

One way to mitigate the effects of thermal runaway is by implementing a current mirror, shown in Figure 5. Using this configuration, it can be shown that the current through Q_1 is roughly equal to the current through Q_2 due to the identical biasing of the gate and source terminals [38]. By maintaining equal currents, this circuit configuration effectively counteracts fluctuations in current that are caused by changing LED temperatures, and thus lessens the effect of the thermal runaway feedback loop.

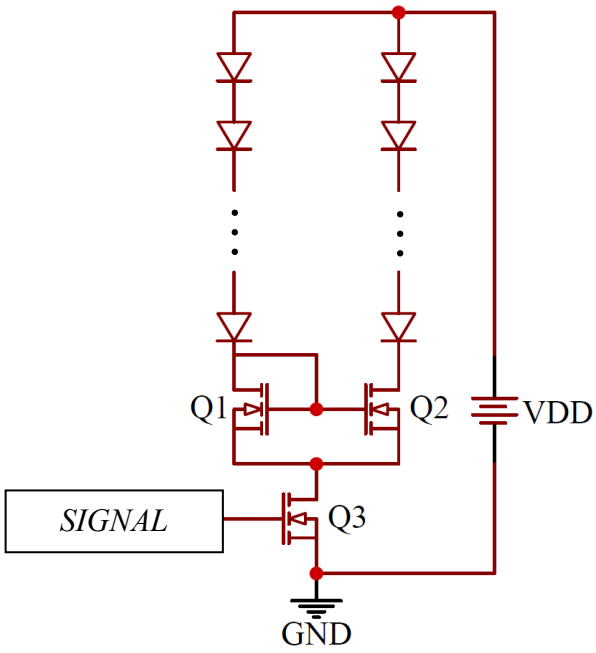

Figure 5: Switching circuit implemented using a simple current mirror

A current mirror, or feedback mechanism, is not the only method used to reduce the effects of thermal runaway in semiconductor devices. Another method involves making modifications to the semiconductor device that allow for greater heat dissipation. For example, heat sinks can be used to divert thermal energy produced by semiconductor devices, thus keeping these devices at a more constant temperature [39]. Heat sinks are made of materials with high thermal conductivities, which are designed to maximize the diffusion of thermal energy from a concentrated source into the surrounding environment [41]. This is done by maximizing the surface-area-to-volume ratio of the heat generating device, thus increasing the rate at which thermal energy escapes. There are many novel ways that this can be accomplished. For example, there have been honeycomb heat sink designs which have been used to maximize heat dissipation with minimal added weight in high power LEDs [41]. However, there are

trade-offs – rudimentary heat sinks may weigh much more than some of the more novel heat sink designs, but they are much simpler to design and implement [41]. Overall, thermal management is an extremely important aspect of any high-power LED circuit because the performance and reliability of LEDs is contingent on these devices operating within their thermal limits.

2.4.3. Receiver

2.4.3.1. Overview

In a UOWC system, the role of the receiver is to convert the received optical signal into a usable voltage for processing. A typical receiver consists of an optical collection system and a detector. The optical collection system, a lens, gathers and focuses the incident light onto the detector. The detector then converts the optical signal to an electrical one. First, this section will detail the different detectors commonly used in UOWC systems. Then, some of the common noise sources in detectors will be discussed. Finally, this section will review important design considerations when using lenses.

2.4.3.2. Detectors

Photomultiplier tubes (PMTs), also called vacuum photodiodes, are extremely sensitive detectors of ultraviolet, visible, and near-infrared electromagnetic radiation. Incident photons are multiplied exponentially by one to two dozen electron-multiplying dynodes to produce a large current. In such devices, a single photon can produce a current hundreds of thousands of times stronger when amplified through a PMT [42].

Thus, PMTs are often used in detecting very low power signals in low noise settings, as any noise incident on the system would also be amplified exponentially.

For UOWC, PMTs allow for an increased signal-to-noise ratio (SNR) without increasing the transmitted power, which is advantageous for increasing range in low noise environments such as the deep sea. For example, a laser diode transmitter and a PMT detector for an UOWC link were used for two autonomous underwater vehicles – data rate of 20Mbps at a range of 120m and a depth of 700m was achieved [43]. Since the experiment was conducted at such depth, there was minimal ambient light, thus decreasing the noise in the system and enabling the use of a PMT. A similar system was produced by Sonardyne called the Bluecomm 200, as mentioned in the review of existing underwater wireless systems. This device uses a PMT detector to enable communication at up to 100m. These operating conditions are only possible at depth or during night, when ambient light is minimized [44]. To summarize, PMTs allow for extremely high signal gain, but are limited to low-light operating conditions due to their low noise tolerance.

The next detector to review is the avalanche photodiode (APD). Much like PMTs, APDs have a high internal current gain. Rather than using electron-amplifying dynodes, APDs are solid-state semiconductor devices that employ avalanche breakdown to increase the device's output current [42]. Avalanche breakdown is a mechanism in which an electron is amplified in a solid-state device through cascaded electron-freeing lattice collisions, producing a high internal photocurrent gain [42]. As compared to PMTs, APDs generally have a higher quantum efficiency in the infrared range whereas PMTs have higher efficiency in the visible light spectrum. Accordingly,

APDs are widely used for infrared wavelength fiber optic systems but can still be adapted for UOWC systems [45]. For example, a laser diode transmitter and an APD detector were used to achieve 2.5Gbps over a distance of 60m, demonstrating that APDs are still suitable for underwater applications [46].

The final detector to discuss is the silicon p-i-n (PIN) diode. The PIN diode is a solid-state semiconductor device consisting of a P-type, intrinsic, and N-type semiconductor junction. It uses this junction to produce a weak photocurrent when subjected to photons. A schematic can be seen in Figure 6.

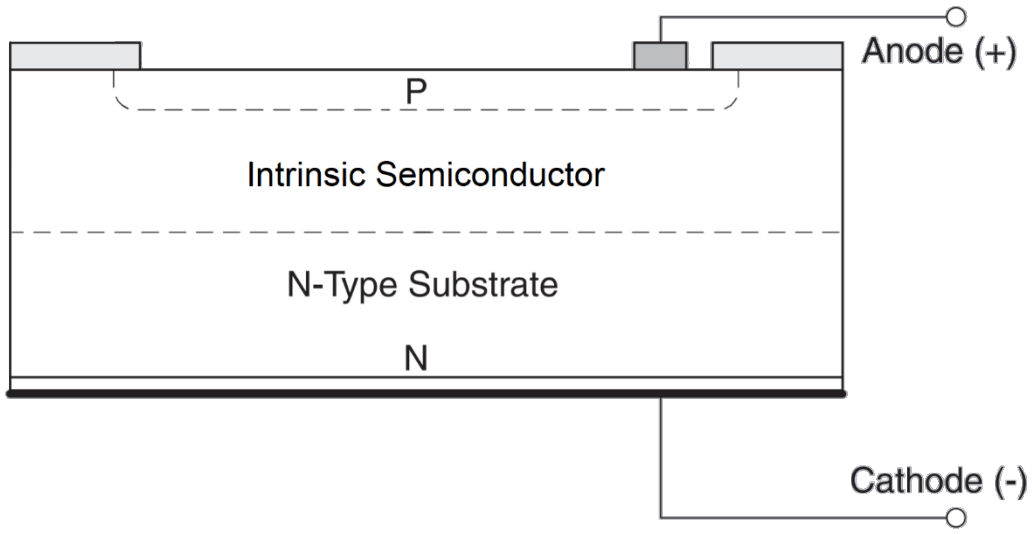

Figure 6: Schematic of a PIN diode

The PIN diode is unlike the PMT and the APD in that it has no internal gain. Therefore, an external gain circuit is necessary. This circuit is called a Transimpedance Amplifier (TIA). The TIA converts a weak photocurrent to a measurable voltage. This conversion is critical because most measuring devices require a voltage signal rather

than a current signal for operation. A circuit schematic for a typical TIA can be seen in Figure 7.

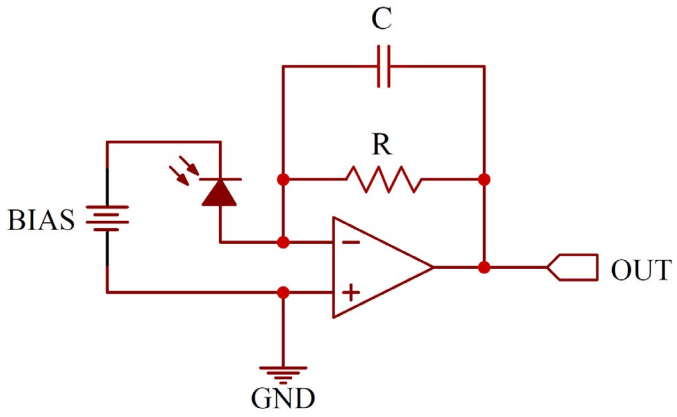

Figure 7: Circuit diagram for a TIA

In this circuit, the photodiode is reverse biased to increase the output photocurrent and decrease the junction capacitance [47]. Furthermore, a resistor and capacitor in parallel provide negative feedback to an operational amplifier. The feedback resistor supplies a low frequency gain to the photodiode current, with the gain being proportional to the resistance value. Additionally, the feedback resistor value limits the bandwidth, to which it is inversely proportional. The feedback capacitor also dictates the bandwidth of the amplifier, where the capacitance holds an inversely proportional relationship [38].

The use of a TIA circuit injects more noise into a PIN diode receiver as compared to a PMT or APD receiver, as they have internal gain. Thus, PIN diodes are not often used for OWC applications, let alone UOWC systems, as the increase in noise decreases the SNR. However, performance notwithstanding, PIN diodes often cost tens to hundreds of times less than APDs and PMTs.

2.4.3.3. Noise Sources

Two types of noise dominate in detectors: shot noise and Johnson noise. Since these are inherent to detectors, they exist in PMTs, APDs, and PINs. This section will briefly explain the origins of shot and Johnson noise, and introduce the power spectral density equations for both.

Shot noise is caused by random fluctuations in the arrival of photons to the detector. On average, the incoming signal provides a constant optical power to the detector. However, since the photon arrival varies stochastically, there is also random fluctuation in the photocurrent, which adds to the noise in an optical communications system. The shot noise power is shown below, where e is the charge of an electron, $\underline{i}$ is the average photocurrent, and f is the signal bandwidth [42].

$$\langle i_N^2 \rangle = 2ei\Delta f \qquad (2)$$

Johnson noise, also called thermal noise, is noise caused by fluctuation in temperature in resistive circuit elements. These temperature fluctuations cause localized electric potentials, which agitate electrons and thus create an unwanted current. Any circuit with resistors operating above absolute zero temperature will encounter Johnson noise. In the noise power equation below, k is Boltzmann's constant, T is the temperature, f is the signal bandwidth, and R is the resistance [42].

$$\langle i_N^2 \rangle = \frac{4kT}{R}\Delta f \qquad (3)$$

2.4.3.4. Lenses

The objective of a lens in an optical communications system is to collect and focus incoming light onto the detector. There are three main considerations when using lenses – entrance pupil diameter (EPD), spot size, and focal length. This subsection will explain the roles of each of these variables in an optical collection system.

The EPD of a lens corresponds to the active area in which incident light will be properly focused. The larger the EPD of a lens, the more light it can collect. However, the EPD increases monotonically with the spot size. The spot size refers to the diameter of the focused beam after the incident light propagates through the lens. In an optical communications system, an ideal spot size should be smaller than the active area of the detector. This ensures that all incident light on the lens is focused onto the detector, which occurs at the focal length of the lens. The focal length is the location of the smallest spot size, the location at which the incident light is focused. A simple way of utilizing the focal length in optical system design is with the front focal length (FFL), or the distance from the front of the lens to the spot. Another trade off occurs here – the focal length decreases monotonically as the spot size increases. All three of these parameters must be considered when designing an optical collection system. They can be seen with an example biconvex singlet lens in Figure 8.

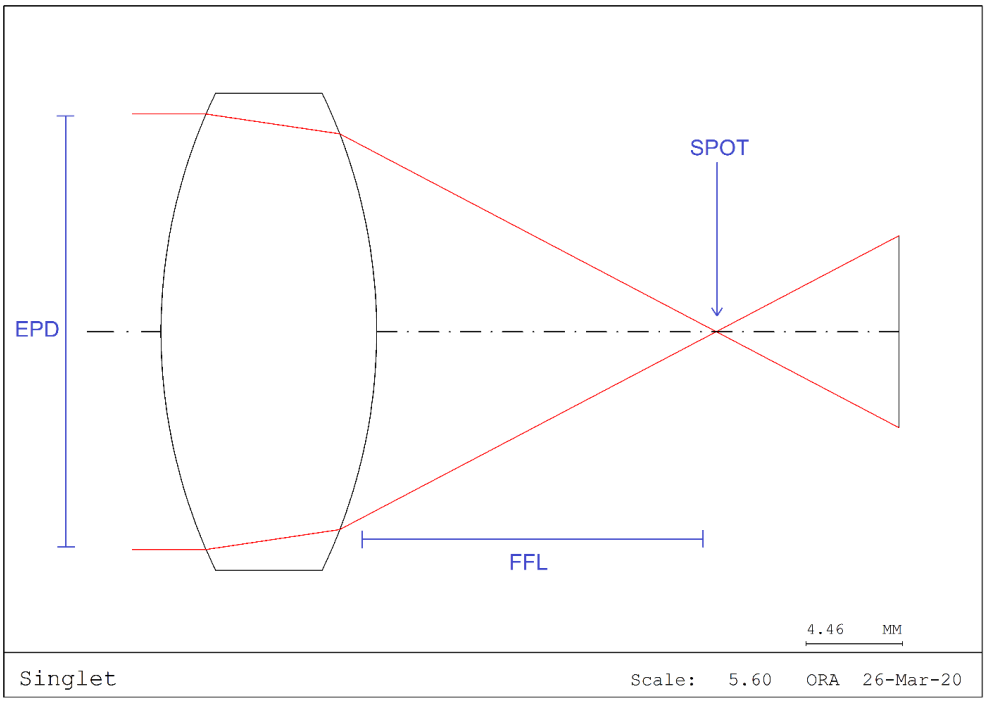

Figure 8: EPD, FFL, and spot of a sample lens

2.4.4. Power

2.4.4.1. Overview

A self-contained UOWC system, like other portable electronic devices such as cameras, phones, and laptops, must be battery powered because it is designed to operate in remote environments. As a result, this section focuses on how portable electronic devices are powered – this can be broadly divided into two categories: power generation and power distribution. The focus of power generation will be on the different battery technologies that are available for portable electronic devices, and the focus of power distribution will be how a single source can be used to power multiple components in a portable electronic device.

2.4.4.2. Power Generation

Powering a portable electronic device requires the use of batteries, and there is a wide selection of battery chemistries to choose from. Battery types for portable electronic devices can broadly be broken up into rechargeable and disposable. Alkaline batteries are the dominant disposable battery, while the rechargeable battery market is currently divided between Nickel-Metal Hydride (Ni-MH) and Lithium-ion (Li-ion) [48] [49]. Although lead acid and Nickel-Cadmium batteries are two other forms of rechargeable batteries, these older battery designs are currently being phased out by newer rechargeable battery technologies because of their lower energy densities [49]. Between Li-ion and Ni-MH, the newer Li-ion batteries are superior in nearly every metric excluding cost, making them the popular choice for more expensive portable electronic devices, as seen in Table 1 [49]. It is important to note, however, that there are distinct advantages to disposable batteries over the established rechargeable batteries. Alkaline batteries have higher energy densities compared to Ni-MH batteries, and the operating voltages of alkaline batteries is greater than comparable Li-ion cells. Additionally, alkaline batteries are less expensive than Li-ion [48].

Characteristic	Ni-MH	Li-ion
Volumetric energy density $\left(\frac{Wh}{L}\right)$	60-120	170-250
Cycle life (number of charges)[1]	1000	500-2000
Self-discharge per month (%)	30	<10
Fast charging time (hr)	1-4	<1

Table 1: Comparison between key performance metrics of Ni-MH and Li-ion batteries

2.4.4.3. Power Distribution

In addition to a power source, a portable electronic device needs additional hardware to perform voltage conversions and provide circuit protections. Most portable electronic devices are powered using a battery with a single direct current (DC) voltage. However, electrical devices often contain various circuits that require different DC input voltages, and those are obtained using DC-DC converters. The simplest form of a DC-DC converter is a linear regulator, which is a device that steps down an input voltage by dissipating excess energy from the input. These regulators are low-cost, and more importantly, they produce minimal voltage ripple [50]. Voltage ripple is a metric which describes how much the DC voltage output from a converter deviates from its desired value. It is an extremely important factor when selecting a power converter because circuits rely on constant input voltages to ensure operations within the device execute correctly [51]. For example, analog-to-digital converter (ADC) circuits can

[1] Cycle life represents the number of times the battery can be recharged before its maximum charge drops below 80% of the initial capacity.

use the source voltage as a reference when quantizing input signals. If there are fluctuations in the source voltage, then there is no longer a stable reference voltage, which means inputs into the ADC will no longer be quantized correctly [52]. However, linear regulators are extremely power-inefficient because the excess energy inputted to the regulator is purely transformed into heat [50]. If a linear regulator is stepping down a voltage from V_{in} to V_{out} to power a load with current I_L, the power dissipated in the regulator is approximately equal to the following expression [50]:

$$P_{dissipated} = (V_{in} - V_{out})(I_L) \qquad (4)$$

This expression, coupled with the fact that most linear regulators require the input to be a certain number of volts higher than the output, means that there are always intrinsic power losses within the device [50]. For example, the typical maximum efficiency of a 5V regulator is 71%, and this efficiency can be even lower if the power source used has a higher nominal voltage than ideal operating conditions [50].

Another form that DC-DC converters can take are switching regulators, which use pulse-width modulation (PWM) and energy storage elements such as capacitors and inductors to convert an input DC voltage into a different output DC voltage [53]. Three common switching regulator topologies are buck, boost, and buck-boost. All three make use of switching elements (typically transistors and diodes), inductors, and capacitors, as seen in Appendix C.

The buck converter takes an input DC voltage and produces an output DC voltage of lesser magnitude. The boost converter takes an input DC voltage and produces an output DC voltage of greater magnitude. The buck-boost converter can produce an output DC voltage of either greater or lesser magnitude than the input DC

voltage depending on the switching duty cycle. Some of the main advantages of switching regulators include increased flexibility and higher efficiencies than with linear regulators. For example, switching regulators in normal operation can boast efficiencies of 80 to 89% [53]. On the other hand, switching regulators are more complicated and have a higher cost. Additionally, these devices exhibit higher output noise, including electromagnetic interference (EMI) and output voltage ripple when compared to linear regulators [54].

2.4.5. Printed Circuit Board Design

2.4.5.1. Overview

Circuit design for the different hardware components in a UOWC system, and more generally any system design containing electric circuits, necessitates rapid prototyping. The following section reviews the prototyping process and how circuits transition from designs to a finished printed circuit board (PCB) that is implemented in a system. This section will also discuss sources of noise in PCBs and design guidelines that can be followed to improve the performance of the hardware.

2.4.5.2. Circuit Prototyping

A breadboard, shown in Figure 9, allows designers to modify a circuit quickly, but these circuits are often noisier and more difficult to use in system integration. The noise of the breadboard comes from a stray capacitance of about 2 to 20pF at the point of contact limiting the frequency of the circuit to approximately 10MHz [55]. Breadboards are also difficult to use in system integrations because the circuit is not permanent – the whole system can be disrupted by a component coming loose from the

breadboard. Given these issues, developers transition their breadboard circuits into PCBs after circuit design is thoroughly tested and finalized. Once a circuit is fabricated onto a PCB, the layout is unchangeable.

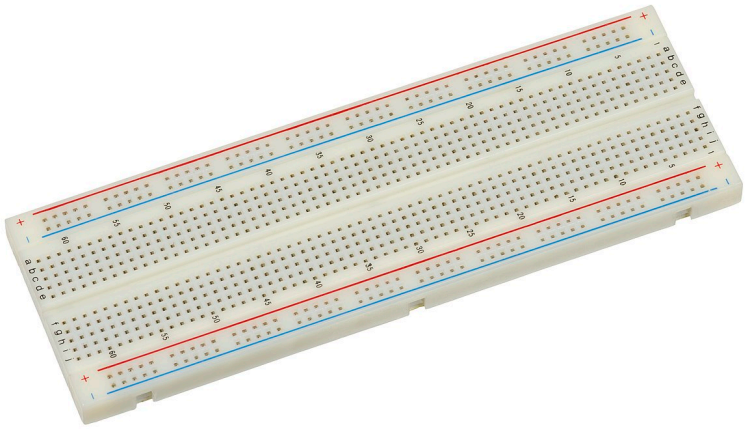

Figure 9: Solderless breadboard used for rapid circuit prototyping

2.4.5.3. Sources of Noise in PCB Designs

The sources of the noise in a PCB are often related to EMI and are caused by loops in the circuit that act as antennae, projecting electromagnetic energy onto neighboring components [56]. This noise could be negligible in some applications, but when a voltage or current needs to be stable, then the entire circuit could fail. One specific example of EMI that is prominent in PCB designs is crosstalk. Crosstalk is when the signal properties of one trace affect the signal of another, either through capacitive or inductive coupling. This phenomenon occurs when two signal traces, or wires printed to the top and bottom layers of the PCB, are routed parallel to one another. In capacitive crosstalk, a sharp rise in the voltage on one signal trace induces a current on a coupled trace [56]. Inductive crosstalk, meanwhile, occurs when large conductor loops on a PCB create a magnetic field that affects other parts of the circuit [56].

2.4.5.4. Design Guidelines to Improve Performance

Design guidelines exist to help designers develop layouts that limit the noise associated with crosstalk, and more generally, EMI. One significant tool used to reduce EMI is return loops. A loop in any circuit could be a signal and its return path, a voltage regulator and its bypassing capacitor, or the power and ground lines between an active device [56]. Noise in a loop will take the path of least impedance to return to the same location where the noise was generated, which is useful because designers can control the properties of the return path [56]. For example, designating a plane, or layer in the PCB, as ground can be utilized to greatly reduce trace lengths. Rather than extending a trace across a PCB to connect a ground terminal, a hole can be drilled into the PCB next to the terminal and lined with copper to electrically connect the two planes. This hole, known as a via, is used to connect the terminal to the ground plane, thus greatly reducing trace lengths [56]. Additionally, components such as bypass capacitors can be used to separate noise from a trace on a PCB. These capacitors provide connections between the signal or power and ground, offering a low-impedance loop for noise. As a result, noise is diverted away from the signal or power line [50].

In the case of high frequency devices, the major performance concern is inductive and capacitive crosstalk. This concern is addressed by the physical design of the PCB – as previously addressed, the positioning of traces directly impacts the effects of crosstalk [56]. One way of reducing inductive crosstalk is to decrease the loop size and increase the distance between loops as much as possible [50]. The general guidelines for capacitive crosstalk are to separate digital and analog signals and to isolate high frequency lines that would be affected by the capacitance between lines

[50]. A capacitor's impedance decreases with frequency, so high frequency digital signals can be capacitively coupled to adjacent traces, which severely degrades the quality of precise analog signals [56]. Additionally, a basic rule is to place all the fastest data logic close to the power supply and place slower logic further away [50]. As a result of these guidelines, PCBs are typically partitioned into blocks that house different types of signals; Figure 10 shows an example of how a PCB may be laid out to reduce EMI [50].

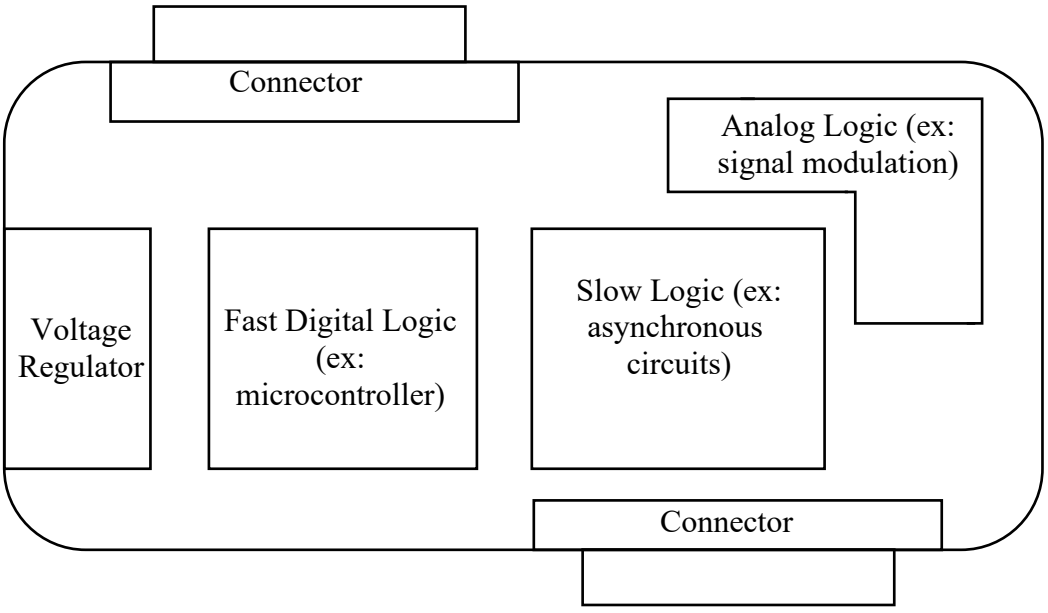

Figure 10: Simple PCB layout example

Another set of guidelines to improve performance in a PCB design is the size and placement of traces. Any trace in a PCB is essentially a resistor whose resistance directly relates to the length, width, and height of a trace [50]. Due to this relationship, traces that carry large amounts of current, such as those for power and ground signals, are typically wider. Power dissipation and heat generation are greater with increased

current, so trace width is increased to lower the resistivity of the trace and reduce the dissipative energy losses [50].

2.4.6. Software

2.4.6.1. Overview

Digressing from hardware design, one of the most promising avenues for innovation in the realm of underwater communication networks is in higher-level networking software. The lowest layer of the networking stack, the physical level, has been studied quite thoroughly [1]. In order to realize a fully operational underwater communication network, higher-level networking algorithms and software must be studied further [1]. A diagram of the most common model of networking, the Open Systems Interconnection (OSI) model, is presented in Table 2. The physical layer, mostly a hardware consideration, was discussed previously so it will not be discussed in this section.

Layer	Name	Description
7	Application	High-level application programming interfaces (APIs), including resource sharing, remote file access
6	Presentation	Translation of data between a networking service and an application
5	Session	Managing communication sessions
4	Transport	Reliable transmission of data segments between points on a network
3	Network	Structuring and managing a multi-node network
2	Data Link	Reliable transmission of data frames between two nodes connected by a physical layer
1	Physical	Transmission and reception of raw bit streams over a physical medium

Table 2: OSI model

2.4.6.2. Data Link

The first networking level to explore is the data link layer. At this stage, underwater networks must balance the robustness and speed of communication between individual points, which optionally includes error correcting codes. Error correction techniques are not unique to underwater networks, and only need to be considered when comparing results to the theoretical maximum correctable BER of approximately one error per every 2,600 bits [57]. The most room for optimization lies in multiple-access, which controls how each network node relays traffic from several connected neighbors. This is typically accomplished by separating each connected channel's signal over some dimension, like frequency band or symbol timing. While

there are abundant techniques for this, space-division multiple access (SDMA) appears to be one of the most promising [1]. SDMA works by separating the different signals spatially, which requires that the signals not to interfere in free space, so it can take advantage of the line-of-sight nature of optical communications to achieve data throughput ten times higher than the more commonly used time-division multiple access, which separates the channels temporally [58].

2.4.6.3. Network and Transport

Moving higher in the networking stack, even less specialization for underwater communications can be found. The network layer determines the routing of data to its desired endpoint. While there are many possible intricacies, underwater communication systems are limited to using a relaying algorithm due to the relatively short maximum distance between nodes [59]. One step higher lies the transport layer, which is easily the least explored for underwater communications [1]. The transport information must maintain connectivity, reliability, and congestion control, each of which presents unique challenges in the underwater domain. The session and presentation layers have received very little attention in UOWC research [1]. Existing methods at this level should work independent of the environment, and underwater networks offer no unique challenges at this level.

2.4.6.4. Application

Finally, the application layer can be developed for underwater purposes. The application layer should inherently be independent of the underlying network

architecture, so it may be developed without consideration for underwater restraints. However, many applications are instead developed to take advantage of optical properties in water. Underwater positioning is a popular use case, and different techniques like “time of arrival” or “received signal strength” have different solutions and problems in the underwater channel, and show great potential for replacing existing acoustic systems [60]. Additional use cases can also take advantage of developments encompassed in underwater networking. The most significant new concept, underwater internet of things, requires development in routing, scheduling, and data analysis, which requires significant coordination between every layer of the networking stack [61].

Chapter 3. Methodology

3.1. System Overview

The proposed UOWC system is comprised of a transmitter and receiver module which enable unidirectional communication. Figure 11 displays the process in which the transmitter sends information to the receiver, which is explained in this section.

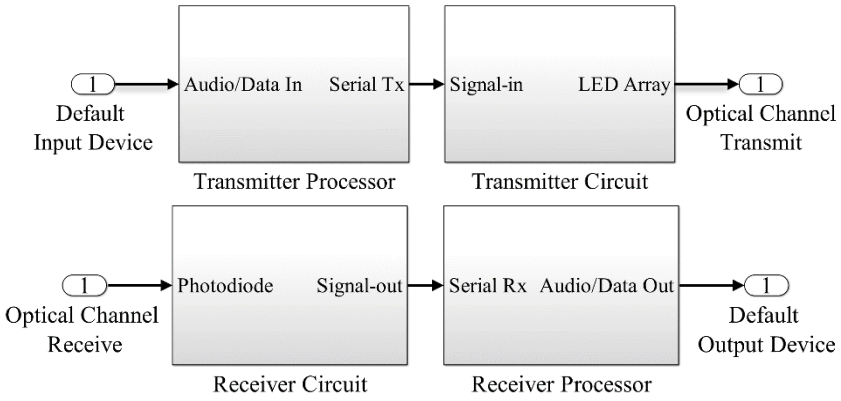

Figure 11: System flowchart.

Firstly, the transmitter's Raspberry Pi single board computer reads in a dataset. This dataset could manifest as a binary file representing various sensor data, or it could be a live audio stream from an external microphone. Then, over the serial port, the microprocessor outputs this encoded digital signal to the transmitter circuit, modulating the LED array. The modulation scheme chosen for the UOWC prototype was OOK because of its simplicity and performance as described in the review of modulation schemes. At this stage, the electrical signal is converted to an optical signal, which is sent through water to the receiver module.

The receiver uses a lens to collect and focus the optical signal onto the photodiode. This diode converts the optical signal back to an electrical signal in the

form of a photocurrent. Then, the photocurrent is fed through an amplifier circuit, where it is converted to a readable voltage bitstream for software processing. This bitstream is then read into another Raspberry Pi 3B+ via the serial port, where it converts the electrical signal back into its original audio or sensor data form. LoS was chosen as the intended optical link between the transmitter and receiver because it was the most established, and it was the simplest to implement as described in the review of optical links.

Both the transmitter and receiver modules are encased in dive cases. These cases are waterproof and pressure proof deeper than 18.3m and have an optical grade glass interface through which the signals propagate – each entire system is contained within these cases. Accordingly, they are both powered by on-board batteries which deliver the proper current and voltage to each component.

3.2. Transmitter

3.2.1. Overview

The design of the transmitter is divided into two sections: the optical source and the switching circuit. The following sections discuss the design decisions made for the optical transmitter as well as the rationale behind each decision. Starting with the optical source, the two architectures considered were LEDs and lasers. As discussed in the review of the transmitter, lasers offer a more powerful, directed beam of light. However, transmission of data is severely dependent on precisely directing the transmitter at the receiver [28]. The focus of this research is to design a robust and cost-effective proof-of-concept system that can transmit and receive data with little calibration, so lasers were ultimately not investigated in the design of the transmitter. These project constraints made it clear that LEDs should be used in the transmitter: they are cost-effective, can be modulated at frequencies high enough for audio transmission, and have a much wider transmission angle.

3.2.2. LED Selection

The main design choices that needed to be made regarding LEDs were transmission wavelength, rise and fall times, luminous intensity, and power requirements. Transmission wavelength was most important; as discussed in the review of the transmitter, attenuation of light underwater is largely dependent on the transmission wavelength [35]. Since the system proposed is a proof-of-concept, it was originally designed to function in clear water conditions. As a result, the LEDs chosen

for the transmitter had transmission wavelengths in the blue 450nm to 490nm range due to their minimal absorption in clear water [11].

The next important design feature that needed to be considered was the LEDs' rise and fall times, or how quickly the LED can be turned on and off. One of the limiting factors in a UOWC system is how fast the light source can be modulated to produce the desired digital signal that is transmitted, so the physical limitations of the optical sources used must be investigated. The proposed system was designed to transmit text and audio data, so the Institute of Electrical and Electronics Engineers (IEEE) Advanced Audio Coding Standard was used as a benchmark for data transmission rates. The coding standard defines output bitstreams for lossy audio signals to be in the range of 16kbps to 96kbps [62]. Although this range does not include the additional bits needed when sending data using a packet structure, it presents the minimum speed required for audio communications.

The luminous intensity of the LED must also be considered; the inverse square law gives the basic relationship between intensity and distance [63]:

$$Intensity \propto \frac{1}{Distance^2} \qquad (5)$$

So, choosing LEDs with greater luminous intensities will consequently yield further transmission distances. Finally, the voltage and current requirements for the LED must be considered; these will dictate the size and layout of the LED array that can be used in the transmitter circuit given the power constraints of the system.

Using the design criterion described above, two LEDs were initially selected for testing: the Young Sun LED Technology Co. YSL-R1042B5C-D13 and the Kingbright WP7113QBC/G. The key product specifications are listed in Table 3.

Specification	Units	YSL-R1042B5C-D13 [64]	WP7113QBC/G [65]
Operating Wavelength	nm	465 – 470 (Blue)	461 – 465 (Blue)
LED Size	mm	10	5
Rise Time[2]	ns	51.2	45.5
Fall Time[3]	ns	6.1	6.1
Luminous Intensity	mcd	8000-10000	4200-6000
Forward Voltage Range	V	3.0 – 3.4	3.3 – 4
Peak Forward Current	mA	120	150
DC Forward Current	mA	80	30

Table 3: LED comparison

Based upon the two LEDs tested, the YSL-R1042B5C-D13 was initially selected because of its higher luminous intensity and lower forward voltage. The rise and fall times for both LEDs were both beyond adequate for the desired switching frequency; a 50% duty cycle square wave oscillating at 96kHz is low/high for approximately $10.4\mu s$, meaning that ideally the YSL-R1042B5C-D13's transitions take up less than one 1% of the time for which the signal is set high or low. For all of these reasons, the YSL-R1042B5C-D13 was used for all the different transmitter revisions. There were other LEDs considered later in the design process, such as the Cree C503B-BAS, which had a greater luminous intensity at 11000mcd. However, these new LEDs ultimately were not used in the prototype due to the time that would

[2] Rise times were calculated by measuring the voltage across the LEDs using an oscilloscope when the input voltage was modulated at various frequencies.

[3] Fall times were calculated in the same manner as rise times.

be required to incorporate the new LEDs into the PCBs and transmitter housing design [66].

3.2.3. Transmitter Circuit Revision 0

The switching circuit design built upon the basic transistor switching circuit discussed in the Literature Review. The initial circuit featured eight LEDs and used a P2N2222A BJT for switching purposes. The circuit schematic, as well as a photo of the transmitter soldered to a perforated prototyping board (perfboard), are shown in Figure 12.

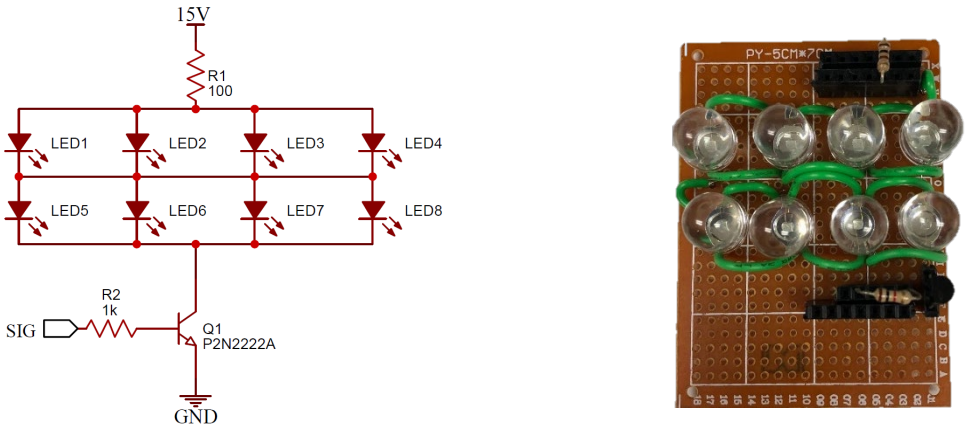

(a) (b)

Figure 12: Circuit schematic (a) and physical design (b) of transmitter Revision 0

The P2N2222A BJT was initially selected because it was cost-effective, readily accessible in the lab, and supported collector currents that were high enough to drive multiple branches of LEDs. As seen in Figure 12a, R_1 was adjustable and was used to

limit the current through the LEDs, and R_2 was used to limit the current sourced from the microcontroller to prevent excessive current draw from the microcontroller digital pins.

While this revision was used for initial testing, there were several problems with the circuit that needed to be addressed in future iterations. Firstly, using multiple branches of LEDs in parallel can induce LED thermal runaway, as discussed in the Literature Review. A brief experiment showed the effect of thermal runaway; the circuit shown in Figure 12 was left in the "ON" state for one hour, with the currents through each LED being measured every five minutes. The results are shown in Figure 13a:

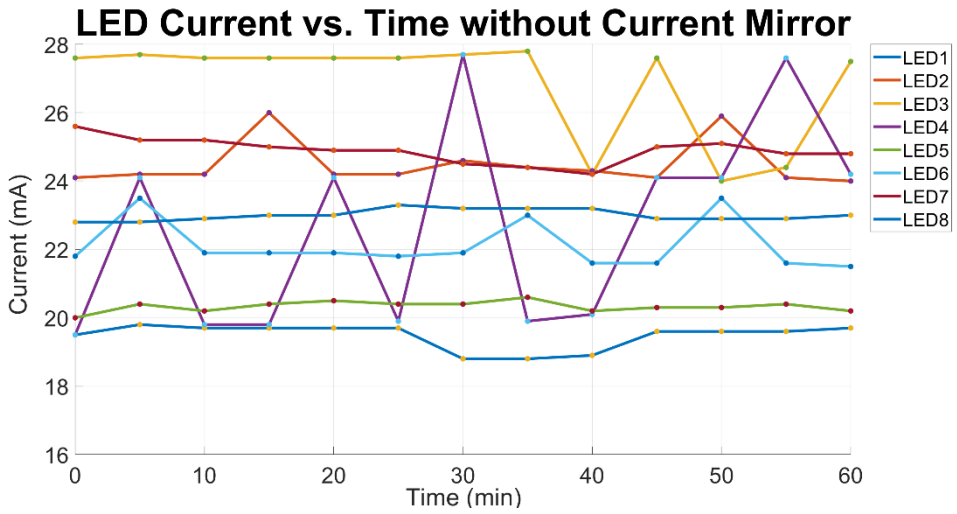

(a)

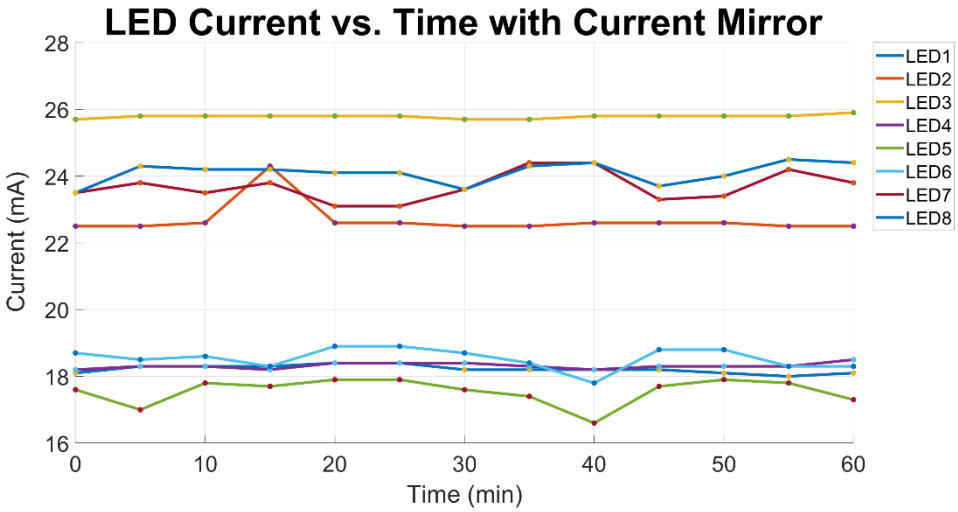

(b)

Figure 13: Current vs. time for transmitter Rev. 0 without (a) and with (b) a current mirror

As seen in the figure, there were numerous current fluctuations in several of the LEDs in the array. In order to reduce the variance in the LED currents, a simple current mirror was introduced, as seen in Figure 14.

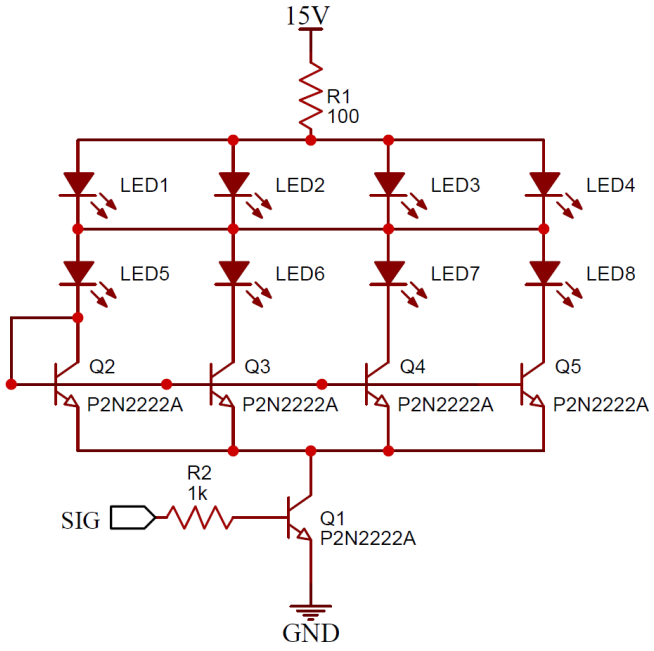

Figure 14: Revision 0 of the transmitter circuit, now using a current mirror.

A current mirror was ultimately chosen over other thermal protection devices such as a heat sink due to the design of the LEDs and the ease of implementation of the current mirror. The YSL-R1042B5C-D13 LEDs used in the transmitter were encased in a thick insulating package, which meant that little thermal energy was released to the outer edges of the insulating package, making it difficult to further redirect thermal energy away from the semiconductor junction. Although the current mirror did not equally distribute the currents through each LED in the parallel branches, it greatly reduced the current fluctuations as seen in Figure 13b. As mentioned in the review of the switching circuit, changes in LED currents results in temperature fluctuations at the semiconductor junctions, which degrades the lifetime of the LEDs [39]. Therefore, more stable currents produced by the current mirror circuit not only kept the brightness

of the LEDs more consistent, but also increased the lifetime of the LEDs by reducing the temperature fluctuations.

Additionally, the value of R_1 (100Ω) was determined such that the maximum continuous current would be kept well below the maximum current rating of the LEDs. Figure 13 shows that the current passing through the LEDs was between approximately 20 to 30% of the DC current limit. In subsequent iterations, the resistance was lowered to 10Ω per LED branch, increasing the maximum current through the LED array which increased the brightness and range of the transmitter circuit.

Finally, the transistor used in the circuit, the P2N2222A BJT, was replaced due to several reasons. As discussed in Appendix B, BJTs inherently suffer in comparison to MOSFETs when used for switching applications: it takes a longer period of time for BJTs to change the polarity of the internal p-n junctions compared to MOSFETs, and therefore, their switching speeds are reduced. Additionally, it was discovered through extended use of Revision 0 of the transmitter that the P2N2222A BJT would burn out at collector currents less than the maximum DC current rating of 600mA, effectively turning the BJT into a resistor when the device was in the "OFF" state. As a result, the subsequent transistors selected had a maximum current rating well beyond the theoretical maximum current load.

3.2.4. Transmitter Circuit Revision 1

As discussed previously, a new transistor was selected to be used in the switching circuit. Ultimately, two MOSFETs were used in Revision 1 because of their

very similar operating characteristics. Table 4 summarizes the significant differences between the two new MOSFETs as well as the old BJT:

Parameter	**Units**	**P2N2222A BJT** [67]	**TN0702 MOSFET** [68]	**VN0300 MOSFET** [69]
Max DC Channel Current	A	0.6	1	0.640
Max Power Dissipation at $T = 25$ ℃	W	0.625	1	1
Rise Time	ns	25	20	30
Fall Time	ns	60	20	30

Table 4: Relevant characteristics of transistors used for switching

As seen in Table 4, the rise and fall time differences between the three devices are negligible given that the target switching speeds are for reliable audio transmission. However, the more critical difference is the maximum power dissipation: the new transistors selected could dissipate more power, meaning they were suitable for higher currents. In addition to reducing the current-limiting resistor, there were other changes made in the second revision. As the transceiver prototype developed, a portable power supply was adopted and the nominal voltage was increased to 24V, as explained in the discussion of the Power Distribution Board (PDB) design. This increased nominal voltage allowed for the LED array to be revised; Revision 1 used only two branches of LEDs, with six LEDs per branch, thus increasing the total luminous output while also reducing the transistors needed in the circuit.

There were additional elements added as well to improve the robustness of the transmitter circuit. For example, a pull-down resistor was added to the gate that

controlled the current through the LEDs to prevent inadvertent charge accumulation at the gate (see Appendix B). Additionally, a Schottky diode was added to provide reverse polarity protection. Revision 1 is shown in Figure 15:

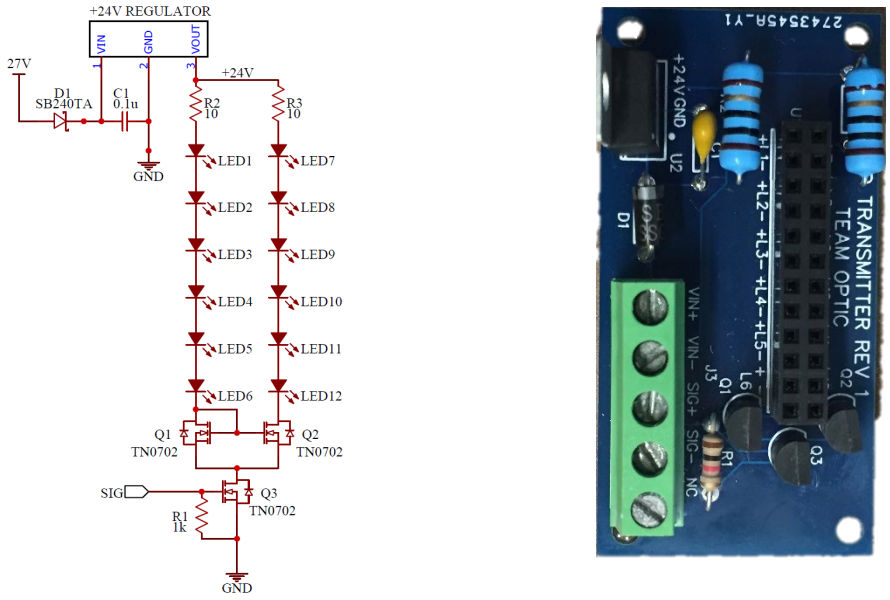

(a) (b)

Figure 15: Circuit schematic (a) and physical design (b) transmitter Revision 1

3.2.5. Performance Analysis

DC measurements for Revision 1 of the transmitter circuit are shown in Figure 16. As seen in the figure, the DC current through the LEDs was now roughly 165mA, which exceeds the maximum rated forward current for the LEDs used. However, the current passed through the LEDs is modulated, meaning the LEDs were only on for a short period of time before being turned off again. Therefore, the higher current did not have a significantly detrimental impact on the lifetime of the LED; there were no LED burnouts while using Revision 1 of the transmitter. As seen in Figure 16, the DC voltages show that the circuit operates as expected. The LED voltages are

approximately within the operating range, the MOSFETs in the current mirror are in the saturation regime, and the MOSFET being used as a switch is in the triode regime due to the high gate voltage being applied.

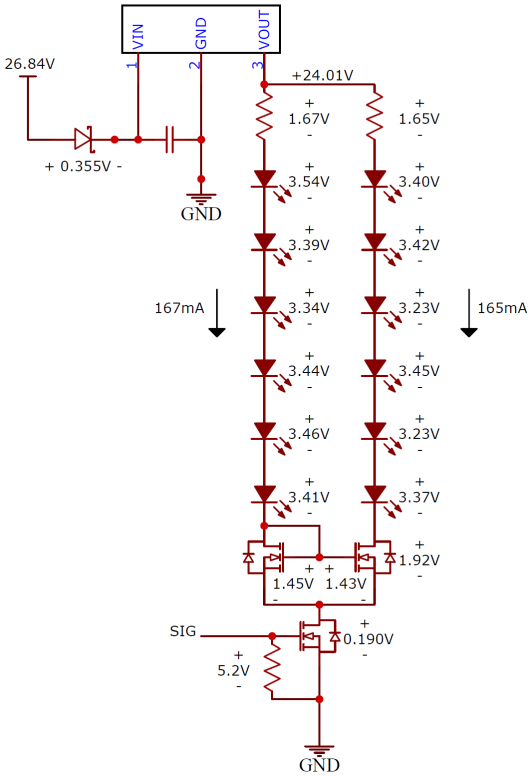

Figure 16: DC voltages for Revision 1 of the transmitter circuit.

The rise and fall times for the transmitter circuit were also measured, this time taking the measurements from receiver circuit discussed in the following section. Due to intrinsic delays in the receiver circuit, it was difficult to measure the rise and fall times of the LED transmitter circuit on its own. However, the times measured reflect the realistic operating characteristics of the transmitter circuit; the tests performed to measure the rise and fall times used the hardware that is found in the prototype, therefore accurately depicting the rise and fall times of the entire transmitter-receiver

system. Figure 17 shows a screenshot of a sample 50kHz waveform received by receiver circuit. The resulting rise time was 470ns and the resulting fall time was 410ns.

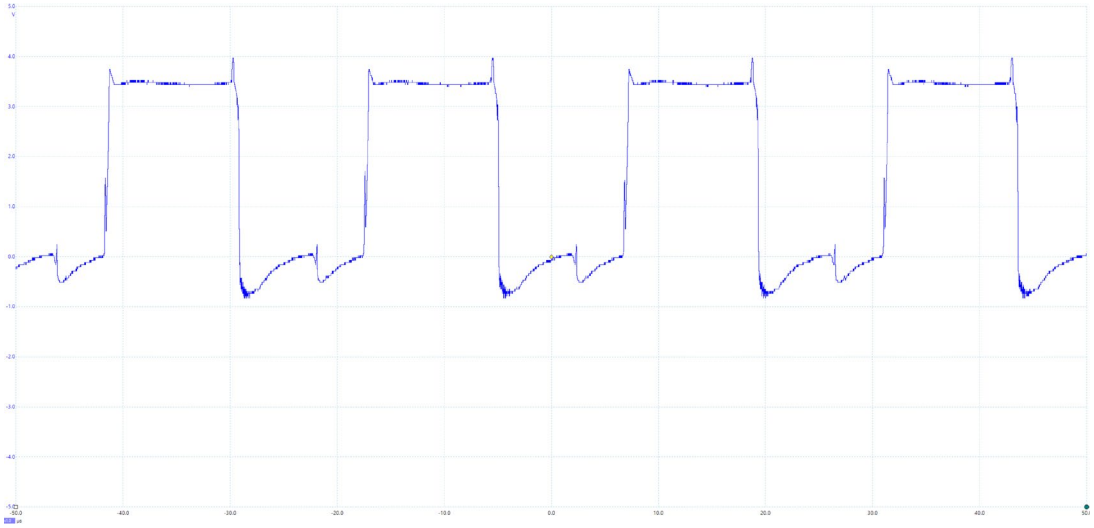

Figure 17: 50kHz LED transmitter signal received by the receiver circuit.

Although the rise and fall times of the system are greater than the initial rise and fall times measured when first choosing LEDs to use in the transmitter circuit, they are still suitable for audio transmission. As mentioned previously, a 96kHz waveform with a duty cycle of 50% is low/high for approximately $10.4\mu s$, meaning a 470ns rise time only occupies 4.52% of the high period.

3.3. Receiver

3.3.1. Overview

The receiver is a multi-faceted hardware system, consisting of the optical collection system, detector, and TIA circuit. The optical collection system concentrates the incoming light onto a detector, which produces an electrical signal in response. The TIA circuit amplifies this weak signal to a usable voltage signal that can be processed by the microprocessor. In this section, the design choices and development of these subsystems are discussed. Additionally, a performance analysis of the optical collection system is presented at the end of the section.

The design process for the receiver largely differed from the design process for the transmitter. The primary changes and revisions made to the receiver were to component selection and placement, while revisions to the transmitter were mostly on a system design level. This is particularly evident in the development of the TIA circuit since the basic circuit design is well-known. As a result, the iterative revisions of the TIA circuit instead focused on board type and layout.

3.3.2. Detector Selection

The first decision for designing the receiver was to choose a class of detector. Of the three detectors mentioned in the literature review, the PMT, APD, and PIN, the main consideration was cost. PMTs and APDs cost thousands of dollars, whereas PIN diodes cost less than one hundred. With this consideration alone, the PIN diode was chosen as its low price was necessary in designing a cost-effective prototype.

Three possible photodiodes were chosen: Thorlabs FDS1010, Thorlabs FDS100, and FirstSensor PS13-6b. Three criteria were used for selection – rise time, responsivity, and price. The active area was not considered for the final decision because a lens was used to focus the signal to a single, confined spot. The decision factors for each of the three photodiodes can be seen in Table 5:

Photodiode	Rise Time (ns)	Responsivity at 470nm (A/W)	Price (USD)
FDS1010 [70]	65	0.14	52.53
FDS100 [71]	10	0.14	14.08
PS13-6b [72]	140	0.33	33.31

Table 5: PIN diode characteristics

The first criteria to assess was the rise time. As discussed in the design of the transmitter, a rise time within the order of microseconds was required. Thus, all the nanosecond rise times for the three photodiodes were sufficient. Then, the responsivity was considered. At 0.33A/W, the FirstSensor photodiode had over double the responsivity of the two ThorLabs detectors. This advantage would allow for greater SNR at a constant received power. Finally, the price was analyzed. All three of the photodiodes were priced at around $50 or less. These criteria led to the choice of the PS13-6b diode due to its greater responsivity. Since a PIN diode was chosen, a TIA circuit was designed to provide external gain.

3.3.3. Transimpedance Amplifier Circuit Design

As mentioned in the review of the receiver, the purpose of a TIA is to convert a weak current into a usable voltage that can be measured. In the case of this research,

the TIA converts a photocurrent into a voltage, which is then amplified in both the transimpedance and secondary gain stages.

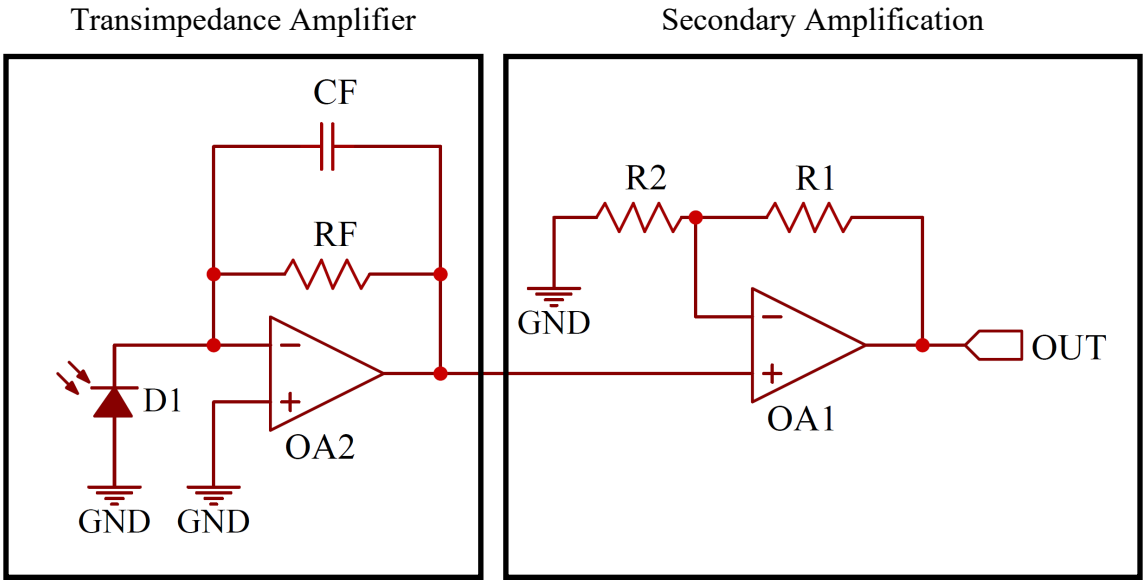

Figure 18: Basic receiver

As shown in Figure 18, designing the receiver, which consists of both the TIA and secondary amplification stage, required selection of several components. These include the operational amplifiers (op-amps), the feedback resistor and capacitor, and both of the secondary amplification resistors.

The criteria for selecting an op-amp model included a high gain-bandwidth product, reasonable cost, low noise, and availability in a dual in-line package. The packaging criteria was important so that rapid prototyping and testing could be performed on breadboards. The OP37E op-amp from Analog Devices provided all of the necessary features with a GBW of 63MHz and demonstrated effectiveness in the receiver design during testing. The high GBW allowed the secondary amplification

stage to have a large voltage gain while maintaining sufficient bandwidth to avoid bottlenecking the system's data rates.

A value of 1pF was selected for the feedback capacitor based on typical industry designs [47]. The next design decision to be made was selecting the feedback resistor [73]. Given that the system expects to receive a transmitted signal with a frequency on the order of 10 to 100kHz, the feedback resistor could not have too large a value. Otherwise, the bandwidth of the receiver would be limited since the OP37E op-amps have a finite GBW. A value of 47kΩ was selected after preliminary testing was performed – the chosen capacitance and resistance allowed the circuit to have a maximum bandwidth of 400kHz. Next, the ratio of the values of the resistors in the secondary amplification stage needed to be determined. Since the individual resistance values can fall within a wide range so long as their ratio provides the appropriate gain, the resistor R_2 was given a value of 1kΩ for simplicity. In order to determine an appropriate value for the resistor R_1, the schematic presented in Figure 18 must be analyzed. Using Kirchoff's Voltage Law and Kirchoff's Current Law the gain equation below was derived:

$$Gain\ \left(\frac{V}{A}\right) = \left(\frac{R_F}{1+sR_FC_F}\right)\left(1+\frac{R_1}{R_2}\right) \qquad (6)$$

Considering that the value of the feedback capacitor is only a single picofarad and the receiver will be operating on the order of kilohertz, the gain equation was approximated and rewritten as shown below:

$$Gain\ \left(\frac{V}{A}\right) = \frac{V_{out}}{I_{in}} = R_F\left(1+\frac{R_1}{R_2}\right) \qquad (7)$$

$$R_1 = R_2\left(\frac{V_{out}}{I_{in}R_F} - 1\right) \qquad (8)$$

The receiver is designed to output 3.3V, the required microcontroller digital input pin voltage, when the photodiode detects a power signal above the noise threshold. Given that the target threshold output voltage of the OP37E is 3.3V and the photodiode outputs ~150nA for low power signals as determined experimentally, R_1 was selected to be 470kΩ.

3.3.3.1. Receiver Circuit Revision 0

After designing the receiver circuit, the first physical implementation was on a breadboard as shown in Figure 19a. Although the breadboard allowed for quick prototyping and swapping of components, the parasitic capacitances inherent in the breadboard's construction greatly decreased the receiver's functional bandwidth, as discussed in the review of circuit design guidelines. As a result, the next implementation of the receiver was on a perfboard (Figure 19b). Perfboard holes are electrically isolated from each other, thus improving performance at higher signal frequencies. However, one drawback to using perfboards is that they require soldering, which increases development time. The perfboard functioned as expected and increased the maximum transmittable signal frequency. With reassurance that the design worked as expected, the next step was to develop a receiver PCB. The Revision 0 PCB is shown in Figure 19c and it provided a low-cost receiver with a smaller footprint than either the breadboard or the perfboard. The PCB outperformed the breadboard but did not demonstrate significant performance improvements over the perfboard due to various inefficiencies. Revision 0 wasted silicon area and contained long signal traces. As

discussed in the Literature Review, long traces can pick up electrical noise, decreasing SNR and increasing BER once the signal is processed.

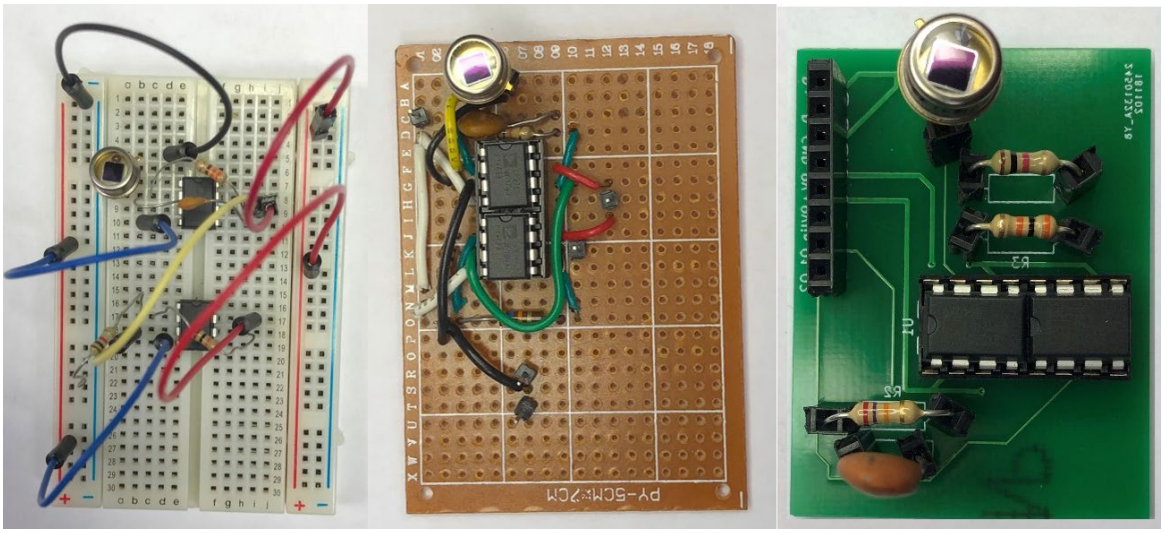

Figure 19: Breadboard (a), perfboard (b), and PCB (c)

3.3.3.2. Receiver Circuit Revision 1

In an effort to improve the frequency performance of the receiver, a receiver Revision 1 PCB (Figure 20) was designed. This revision further reduced the receiver's footprint, removed redundant or unnecessary inputs and outputs, and improved the receiver's high frequency performance. However, this design still used the standard 2.54mm header pins for the input and output and required the linear voltage regulators to be located on a separate perfboard. Standard header pins were not ideal for the input and output terminals since they did not offer a secure or durable connection. They also

only interface with standard jumper wires, which are unshielded and have a low current rating.

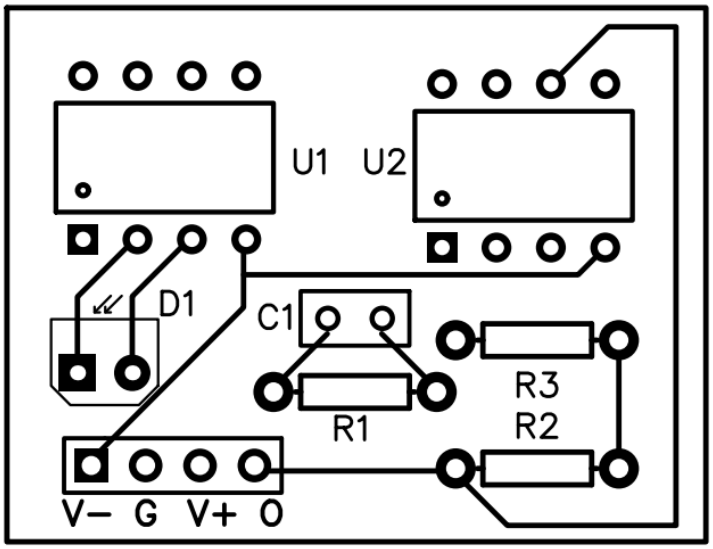

Figure 20: Receiver Revision 1 PCB

3.3.3.3. Receiver Circuit Revision 2

The design flaws mentioned in receiver Revision 1 PCB design drove the need for a second revision. The new design, designated receiver Revision 2 PCB, is shown in Figure 21. The first significant improvement was moving the linear voltage regulators onto the receiver PCB. Not including batteries, this condensed the receiver hardware onto a single PCB. Additionally, the input and output terminal types were changed from header pins to screw terminals. The screw terminals held the wires more securely than standard header pins, which improved the ease of future testing. Similar to the changes made from Revision 0 to Revision 1, signal trace lengths were further shortened with an improved layout of components. Finally, mounting holes were placed

in the corners of the PCB. Unfortunately, the on-board power regulation led to significant EMI, decreasing the receiver output signal quality.

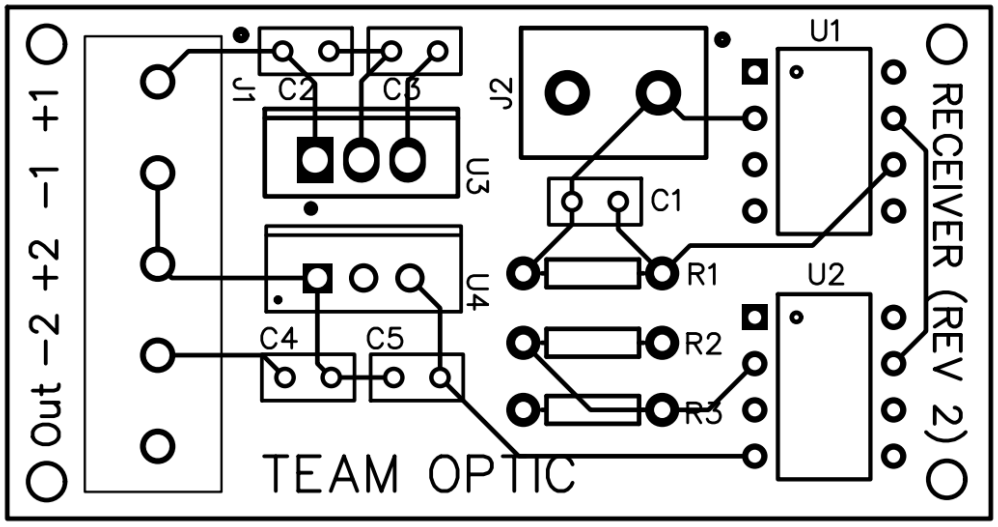

Figure 21: Receiver Revision 2 PCB

3.3.3.4. Performance Analysis

As mentioned previously, the receiver Revision 2 PCB exhibited significant EMI as a result of the linear voltage regulators being positioned close to the signal traces. To address this, a PDB was designed to contain all power regulation and conversion components; this system is presented in the following section. Due to time constraints, the PDB PCB was not produced and the receiver reverted to the Revision 1 PCB for testing. To address issues with input noise to the amplifier infrequently causing negative voltages to appear on the output, a Schottky diode and pull-down resistor were added to the receiver output.

3.3.4. Optical Collection System

3.3.4.1. Lens Revision 0

The first iteration of the optical collection system used the Thorlabs LA1951, a 25.4mm diameter plano-convex singlet, to focus the oncoming optical signal onto the photodiode. The plano-convex lens was chosen because it was a cost-effective, simple to use converging lens. For this design iteration, the lens was only required to focus on-axis light, so angled transmission was not considered. This was to test the feasibility of a point-to-point UOWC system rather than optimize it, which came in later revisions. Therefore, the plano-convex lens had a small angle of operation. As the transmitting angle increased, the spot size also increased, thus decreasing the incident power on the photodiode. To reiterate, the photodiode has a diameter of 3.61mm – as mentioned in the lenses literature review, ideally the lens should have had a spot size such that the entire signal was confined onto the active area of the photodiode. A plot of spot size versus incidence angle can be seen in Figure 22.

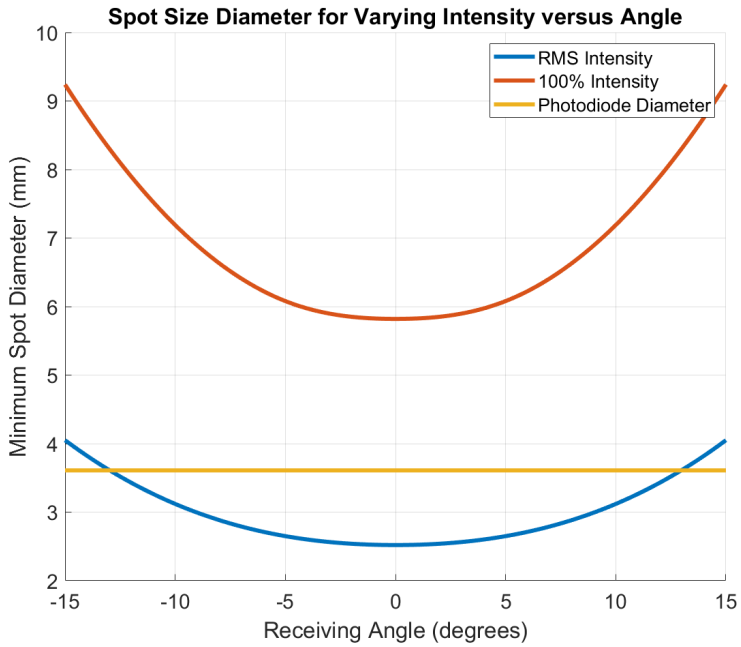

Figure 22: Spot size diameter versus angle for the singlet lens

This figure was generated with the quick spot function in Code V for angles from -15 to 15°, with a 5° step size. This spot diagrams can be seen in Appendix D. Then, the intermediate points were interpolated in MATLAB using one-dimensional splines. The blue line shows the root mean square (RMS) intensity, or 71% intensity, and the red line shows 100% intensity. The orange line represents the diameter of the photodiode. For example, at 5° incidence, 71% of the signal intensity was confined to a diameter of 2.65mm, and 100% of the signal intensity was confined to a diameter of 6.08mm. Even at 0° incidence, this lens did not focus all the incoming light onto the photodiode, as the 100% intensity diameter is 5.82mm. Thus, a better lens was required.

3.3.4.2. Lens Revision 1

The final iteration of the optical collection system used the Thorlabs AC508-075-A, a 50.8mm diameter achromatic doublet. An achromatic doublet was chosen over a singlet because this class of lens has less spherical aberration and a smaller spot size, resulting in a more uniform focus. Furthermore, this lens has twice the diameter of the singlet, so it has four times the active area. A plot of spot size versus incidence angle can be seen in Figure 23, and the Code V spot diagrams can also be found in Appendix D.

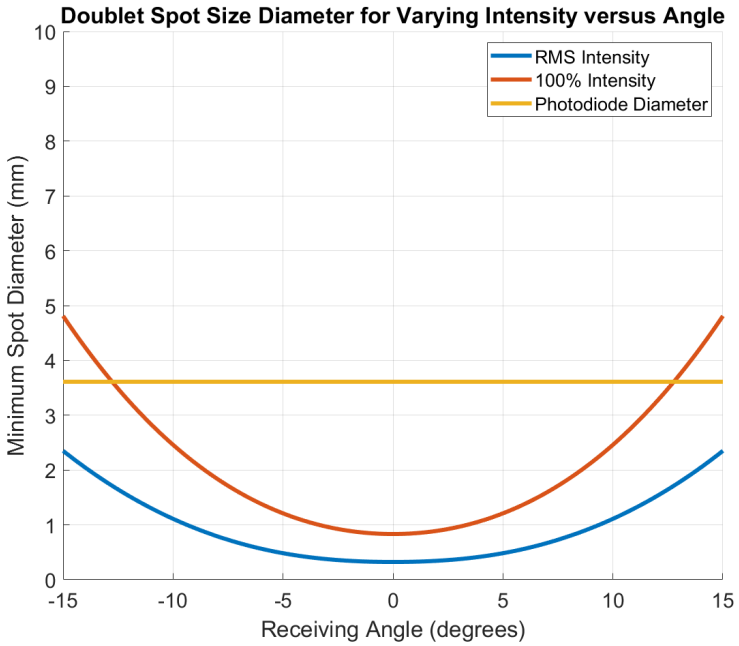

Figure 23: Spot size diameter versus angle for the doublet lens

As can be seen in Figure 23, the doublet has much better performance than the singlet. The entire spot diameter was less than the diameter of the photodiode up until 11.5° from 0, which allowed for a much larger effective area. While the location of the focused spot was offset as the incidence angle changes, this offset was a negligible tens to hundreds of microns. Thus, it is clear from these simulations that the achromatic

doublet offers superior performance as compared to the plano-convex singlet. The following step was to test the receiving angles of the two lenses verses transmission distance, which will be detailed next.

3.3.5. Performance Analysis

3.3.5.1. Receiving Angle versus Distance

Two different receiving angles versus distance were tested through air as shown in the diagrams in Figure 24 and Figure 25. In these figures, RX denotes the receiver and TX denotes the transmitter. Two angles were recorded – theta (θ) and phi (ϕ), which are functions of D, the horizontal component of the distance between the transmitter and receiver. Theta is the maximum angle between the hypotenuse (the line segment from RX to TX) and the horizontal, measured while TX is always facing directly towards RX. Phi is the maximum angle that TX can be tilted from the horizontal, measured with TX on the horizontal.

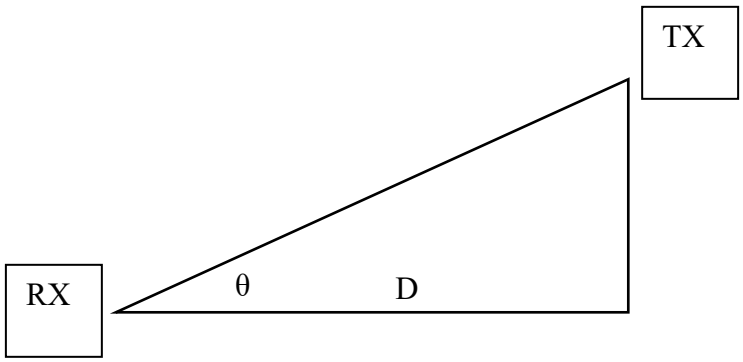

Figure 24: Theta experimental setup.

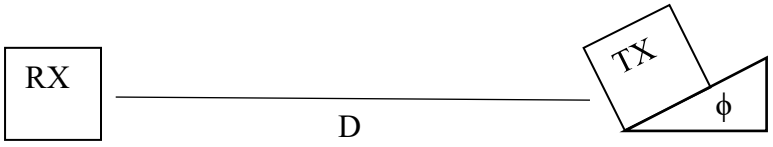

Figure 25: Phi experimental setup

Theta was measured by first aligning the transmitter and receiver at normal incidence at a short distance. Then, the angle of the receiver was slowly increased until data transmission failed. After this, the range was increased, and the test was repeated. The test concluded when the system could no longer transmit at normal incidence. This test was completed for both the plano-convex singlet and the achromatic doublet.

Phi was measured similarly to theta, except the receiver was static and the transmitter was dynamic. First, the system was aligned at a short distance at normal incidence. Then, the transmitter was angled until data transmission failed. The range was then increased, and the test repeated until reaching the maximum range at normal incidence. Plots of theta versus distance and phi versus distance can be seen in Figure 26.

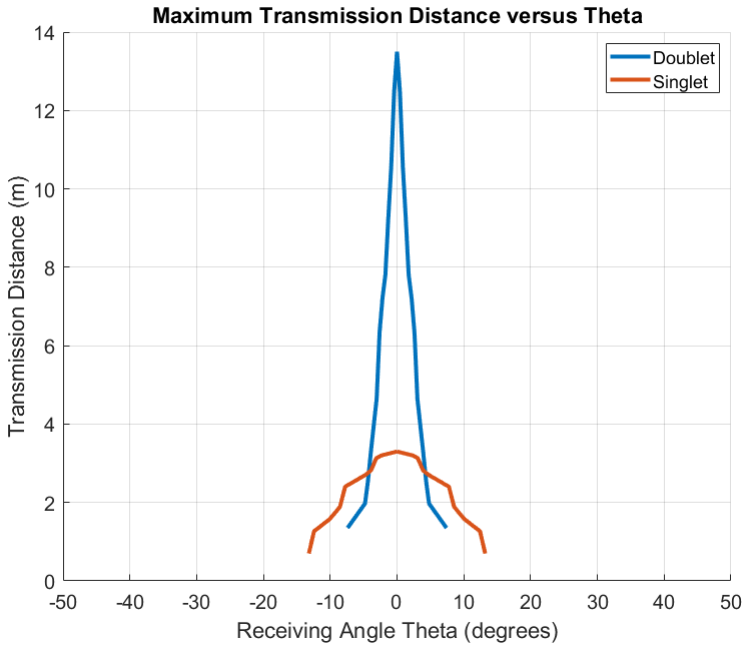

(a)

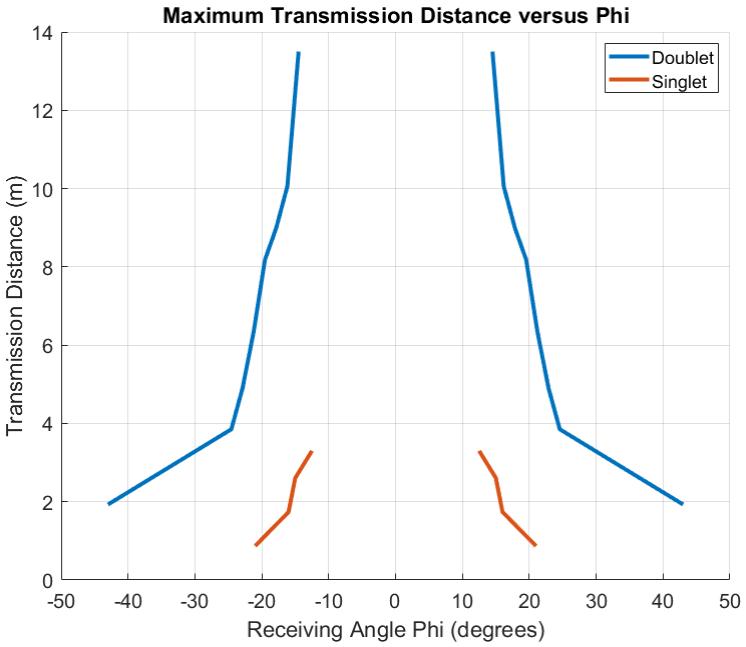

(b)

Figure 26: Theta vs. distance (a) and phi vs. distance for the singlet and doublet lenses (b)

Firstly, discrete data points were taken and linearly interpolated over a uniform set of angles in MATLAB. Then, these data points were normalized to the maximum distance over air for each lens – 13.5m for the doublet and 3.3m for the singlet. Normalization mitigated differences between tests that can be attributed to battery charge instead of the lens. It is assumed that individual tests, such as the theta measurement for the singlet, were performed quickly enough such that battery drain did not have a significant impact on each individual distance measurement. Therefore, normalizing the data to the maximum range allowed for a valid comparison of theta and phi for the singlet and doublet.

The plot of theta versus distance in Figure 26 showed that the singlet has a wider on-axis tolerance at the cost of distance, whereas the doublet has a longer distance with less receiver axis tolerance. This is because angling the receiver drastically changes the location of the focused spot. Since the singlet has a wider, less focused spot, changing the receiver angle still focuses some of the large spot onto the photodiode. Conversely, the tight spot of the doublet allows maximal optical power to be focused on the photodiode, but minimal tolerance for angle shifts.

Furthermore, the Figure 26 plot of phi versus distance confirmed the theoretical simulations from earlier in the section. The simulations showed that the doublet had a superior transmission angle tolerance than the singlet – in the plot of phi versus distance, the doublet has a 10 to 20° advantage at a given transmission distance over the singlet. This is because the low spherical aberration of the doublet lens leads to a tight focused spot, loosely dependent on incident angle. Therefore, the Code V simulations and angle experiments demonstrate the doublet's superior performance over the singlet.

3.3.5.2. Signal-to-Noise Ratio

SNR and BER simulations were conducted in MATLAB for the plano-convex singlet and the achromatic doublet. The detector was assumed to be shot and Johnson noise limited, so the following noise equation was used:

$$N = 2q_e(I_s + I_d)\Delta f + \frac{4kT\Delta f}{R} \qquad (9)$$

The first term is the shot noise; q_e is the elementary charge, I_s is the signal current, I_d is the detector dark current, and Δf is the signal bandwidth. The second term in the noise equation is the Johnson noise: k is the Boltzmann constant, T is the operating temperature, and R is the resistance.

The signal power was calculated by propagating the LED signal through each optical element. Firstly, the power loss due to LED beam divergence was calculated, which is given by:

$$P_{div} = \frac{P_{LED}a^2}{4d^2\tan(\theta_{LED})^2} \qquad (10)$$

In this equation, a is the diameter of the lens, d is the propagation distance, and θ_{LED} is the divergence angle of the LEDs. Next, the power propagation through the optical system was calculated using the solid acceptance angle. This is given by the solid angle

$$\delta\omega = \frac{\pi a^2}{d^2} \qquad (11)$$

and resulting power equation

$$P_{in} = \frac{P_{div}\delta\omega}{4\pi} \qquad (12)$$

Then, the responsivity ℜ of the photodiode was considered, giving the optical power converted to electrical power by the diode. This is given by

$$P_{PIN} = \Re P_{in} \qquad (13)$$

Additionally, the intensity loss due to the spot size area was factored in. The SNR and BER curves were calculated at normal incidence – accordingly, the 0° spot size diameters from the Code V simulations were used. For the plano-convex singlet, 71% of the signal was confined to a diameter of 2.52mm, and 100% of the signal was confined to a diameter of 5.82mm. A linear approximation was used to estimate the intensity at the photodiode diameter of 3.61mm, which yielded a power scaling factor *A* of 0.805. For the achromatic doublet, the entire spot was focused on the photodiode active area, so a scaling factor of 1 was used. The following linear relationship between scaling factor and power was used.

$$P_{spot} = AP_{PIN} \qquad (14)$$

Finally, the Beer-Lambert law was used to calculate the attenuation of the optical signal through the aquatic medium. This relationship is shown below, where α is the attenuation coefficient of light through calm, clear water.

$$P_{total} = P_{spot}e^{-\alpha d} \qquad (15)$$

To calculate SNR, the total power was divided by the noise power and converted to decibels, as seen in the following equation.

$$SNR_{dB} = 10log_{10}\left(\frac{P_{total}}{N}\right) \qquad (16)$$

The SNR versus distance for the singlet and doublet were plotted in MATLAB and can be seen in Figure 27.

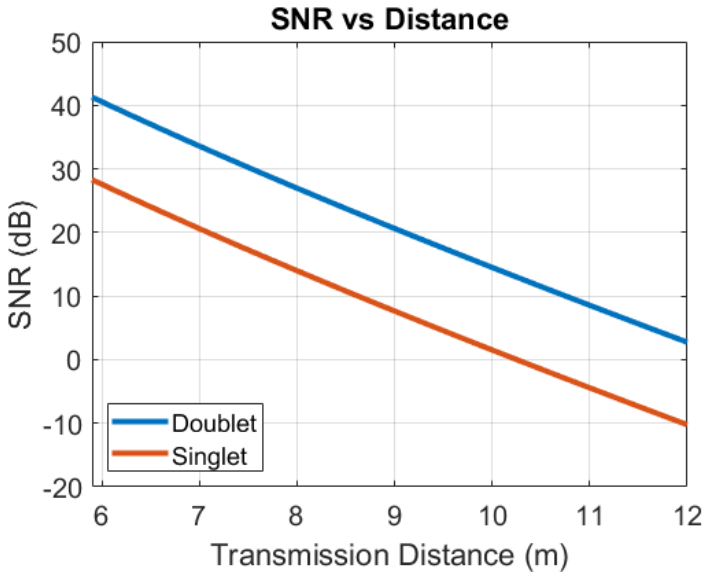

Figure 27: SNR versus distance for the singlet and doublet lenses

The SNR was then used to calculate the BER using the following relationship, as described in the *International Journal of Computer Applications* [29].

$$BER = \text{erf}\left(\frac{1}{2}\sqrt{\frac{P_{total}}{2N}}\right) \qquad (17)$$

In this equation, *erf* is the Gaussian error function. The BER versus distance on a logarithmic scale was plotted in MATLAB and can be seen in Figure 28.

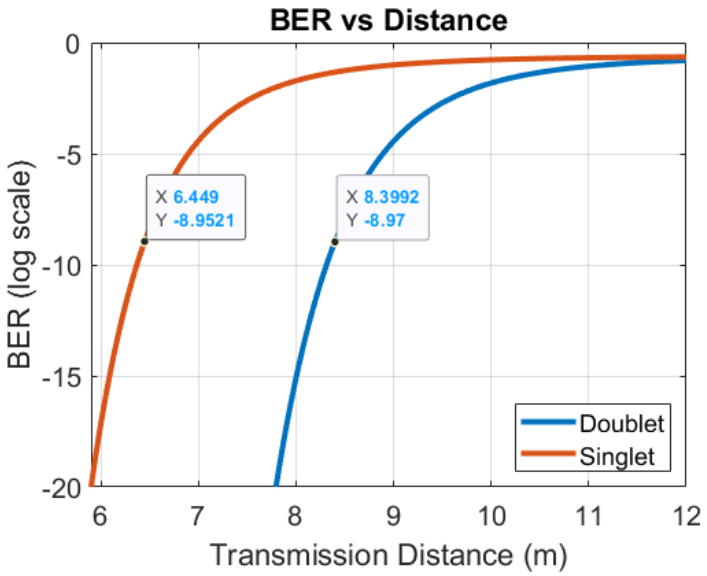

Figure 28: BER versus distance for the singlet and doublet lenses

As seen in Figure 28, the doublet gave superior performance at normal incidence as compared to the singlet. For 10^{-9} bit errors, which is the performance standard for telecommunications, the singlet system operating range was approximately 6.45m, whereas the doublet system attained a range of about 8.4m [74]. Thus, it is clear that the doublet greatly improves the range of the system.

3.4. Power

3.4.1. Overview

As mentioned in the Literature Review, most portable and self-contained electrical systems contain energy storage devices and other power electronics. Over the course of the research, the methods used to meet the power requirements of the transmitter and receiver have evolved, but each revision contained the two previously mentioned key components. As such, in this section of the Methodology, the design process and decisions made regarding power distribution elements for this project will be discussed.

3.4.2. Early Iterations

Developing power distribution hardware for the proposed UOWC system meant first understanding which voltage levels were required. Initially, the transceiver device required three different voltages in addition to a reference ground voltage: +5V, -5V, +15V. The op-amps in the receiver design required +5V and -5V supply rails, and the LED array that was designed as part of the transmitter required a +15V supply input. Additionally, the transceiver design included a digital output signal from an Arduino Uno (+5V) connected to a digital input pin on a Raspberry Pi 3B+ (+3.3V). In order to make this lower power connection possible, a simple voltage divider circuit was included local to the microcontrollers to drop the digital signal from +5V to +3.3V. As a result, the +3.3V voltage divider will not be further discussed in the PDB PCB revisions.

Initially, the different subsystems were developed separately. This meant that the transmitter, receiver, and microcontrollers relied on independent power sources. Portability wasn't initially a major concern, so a variety of methods were used to power the different components. The transmitter was powered with a benchtop power supply set to 15V, the receiver was powered by 7.2V Ni-Mh batteries whose voltage were trimmed using linear regulators, and the microcontrollers were powered using wall power supplies or laptops.

(a) (b)

Figure 29: Ni-Mh battery (a) and wall power supply (b)

As the receiver circuit transitioned from a breadboard to a perfboard, the decision was made to switch from the Ni-Mh batteries to alkaline 9V batteries. The 9V batteries were still connected to regulators to provide the required +5V and –5V (as shown in Figure 30). The Ni-Mh batteries had a larger energy capacity and were more efficient in the prototype – for a given current, regulating 7.2V to 5V wasted less energy than regulating 9V to 5V. However, the 9V batteries offered space and weight savings, making the receiver more portable. Since 9V batteries were available at a low cost, the

tradeoff was deemed justifiable. Due to their efficacy, 9V batteries continued to be used throughout testing and experimentation for the transmitter and receiver.

Figure 30: 9V batteries with linear regulators on perfboard

As both the transmitter and receiver were moved from perfboards to PCBs in order to decrease noise on the signal, several changes were made to how the devices were powered. Firstly, additional LEDs were added in series with each branch of the transmitter, increasing the required input voltage. Ultimately, the maximum voltage of the system was designed to not exceed the 32V limit at the Neutral Buoyancy Research Facility (NBRF) at the University of Maryland (UMD), one of the potential testing sites for the UOWC system. As a result, 27V was chosen as the nominal voltage for the transmitter because it was the highest voltage that could be achieved using 9V batteries while observing the testing restrictions at the NBRF. This nominal voltage was then stepped down using a linear regulator to 24V for the LED array to provide a constant voltage even as the batteries' voltages began to decrease.

Secondly, each of the linear regulators were moved from separate perfboards onto their respective transmitter or receiver PCBs. This decreased the overall footprint of the electrical components and increased the portability of the system. Each separate

subsystem continued to have dedicated power components and batteries, as opposed to the whole system having a centralized power distribution hub. This was because each subsystem was being separately tested. Ultimately, flexibility and convenience in testing were of a higher priority than space-efficiency, energy-efficiency, and cost.

3.4.3. Energy Storage System Design

To properly design the PDB and energy storage system, the required outputs from the PDB needed to be defined. The final revision of the transmitter needed 24V input to power the LEDs, while the final revision of the receiver needed +5V and -5V to power the op-amps. The supply voltage for the microcontrollers was +5V. The maximum current draw from each device is given in Table 6:

Device	**Required Voltage (V)**	**Maximum Current Draw (mA)**
Raspberry Pi 3 B+ [75]	+5	500
Arduino Uno R3 [76]	+5	100
Transmitter	+24	350
Receiver	+5, -5	100
Total	**-**	**1050**

Table 6: Maximum current draw for devices

As shown in Table 6, the maximum current draw of the prototype was 1.05A. Peripheral devices connected to the Pi or Arduino could also increase the draw from microcontrollers beyond what is listed in Table 6, meaning the maximum current

requirement for the entire system could exceed 2.5A. Given the power and voltage requirements of the entire system, a search was performed to find other batteries to replace what was being used to power each individual subsystem. Two potential replacements were selected, and they are compared to the 9V alkaline battery in Table 7.

			
Battery Type	**Energizer Max 9V** [77]	**Samsung 25R 18650** [78]	**Samsung 30Q 18650** [79]
Chemistry	Alkaline	Lithium Ion	Lithium Ion
Nominal Voltage (V)	9.0	3.6	3.6
Capacity @ 500mA Draw (mAh)	375	2500	3000
Continuous Discharge Rating (A)	<1	20	15
Weight (g)	45.6	43.8	48
Price (USD)	3.25	3.99	4.99

Table 7: Battery cell comparison

Given that the required output voltages of the PDB were +5V, +24V, and -5V, the minimum number of each type of battery required was determined. The minimum number of cells required is the multiple of the nominal voltage for each cell that is just greater than the required output voltage magnitude. As a result, four 9V batteries were

needed to power the system: three connected in series to produce 27V and one with reverse polarity to produce -9V. On the other hand, nine Li-ion batteries were needed: seven connected in series to produce 25.2V and two connected in series with reverse polarity to produce -7.2V. Keeping in mind that the capacity, and therefore the discharge time, of the entire string of series batteries is the same as for a single battery, the potential whole battery packs were compared in Table 8.

Battery Type	**Energizer Max 9V**	**Samsung 25R 18650**	**Samsung 30Q 18650**
Number Required	4	9	9
Rechargeable?	No	Yes	Yes
Discharge Time @ 500mA Draw (minutes)	45	300	360
Total Weight (g)	182.4	394.2	432
Total Price (USD)	13.00	35.91	44.91

Table 8: Battery pack comparison

Although the system using the 9V batteries was significantly less expensive and weighs less than a system using the Li-ion batteries, the Li-ion system had a much longer life and is rechargeable. Replacing four 9V batteries every 45 minutes of operation would quickly prove costly and would limit the usability of the prototype. Additionally, the 9V batteries would quickly overheat and become damaged if the system drew more than 1A at a given time. As a result, a Li-ion battery pack built out

of Samsung 25R 18650 cells was chosen. This battery type balances long life between charges with a fairly low cost and weight.

3.4.4. Power Distribution Board Revision 1

Once all the components were placed inside the waterproofed enclosures to perform system integrations, the need for a PDB became apparent. A PDB is a PCB that contains all power electronics hardware for the rest of the systems in order to easily distribute power as required. As discussed in the review of PCB design guidelines, some benefits of using a PDB include space savings and less noise injected in signals susceptible to EMI, since the power traces on the PDB are separated from the signal traces on the other PCBs.

The initial design for the PDB was straightforward. The PDB would receive input power from the batteries at +25.2V and -7.2V, then output power at +24V, +5V, and -5V using linear regulators and DC-DC converters. The output +24V would be regulated from the +25.2V supply using an LM7824 linear regulator, and the output -5V would be regulated from the -7.2V supply using an LM7905 linear regulator. Unfortunately, the output +5V couldn't be directly regulated from the +25.2V supply using a single linear regulator. The 20.2V potential difference across a regulator would mean that any significant amount of current through the regulator would dissipate a tremendous amount of power, as shown in Figure 31a. Even with only 200mA of current, the regulator would dissipate 4.04W as heat, which would destroy the regulator regardless of the size of the heat sink that was attached.

To solve this issue, a buck converter was selected to convert the 25.2V to ~7V before regulating the buck converter output to +5V using an LM7805. The OKI-T/36W-W40N-C buck converter from Murata was selected due to its high output current limit, low output voltage noise, low cost, and ability to adjust the output voltage [80]. As mentioned in the review of DC voltage conversion, buck converters operate at a much higher efficiency than linear regulators [53]. Using a buck converter allows the linear regulator to safely pass the desired amount of current: passing 200mA through the regulator while stepping down the voltage from 7V to 5V means the regulator would only dissipate 0.4W as heat. As shown in Figure 31b, using both a buck converter and a regulator is less efficient at outputting +5V than using a buck converter alone. However, both are used because a buck converter's output often has significant levels of voltage ripple. The linear regulator smoothed this ripple and outputted a constant 5V. Therefore, both were used in the PDB design in order to achieve a fairly high efficiency while producing a stable power signal.

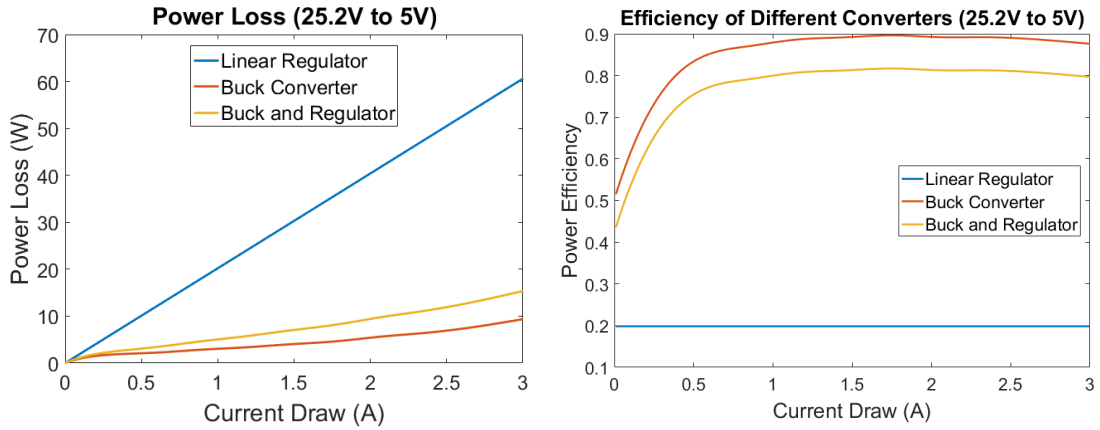

(a) (b)

Figure 31: Power loss (a) and power efficiency (b) of different converter schemes

Another significant design decision regarding the PDB was including a switch allowing input into the +5V regulator to come from a standalone supply instead of the output of the buck converter. This redundancy was included to analyze the performance of the DC-DC converter and to allow for the PDB to still be utilized in the prototype if it was determined that the new buck converter did not perform as expected. On the output side of the PDB, power is sent to the microcontrollers via USB ports soldered onto the PDB. The final notable features of the PDB are the inclusion of fuses on the main power traces to protect against overcurrent conditions, and a double-pole single-throw switch to immediately shut down all electrical systems in the enclosure. In summary, a block diagram of Revision 1 of the PDB can be found in Figure 32.

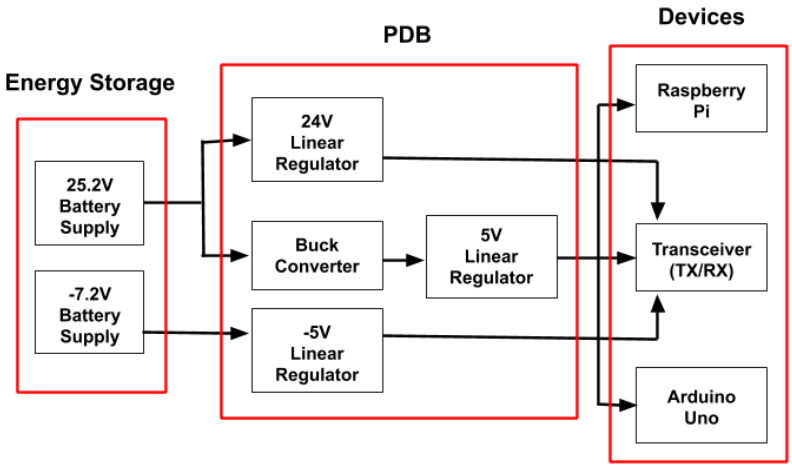

Figure 32: PDB Revision 1 block diagram

3.4.5. Power Distribution Board Revision 2

Subsequent revisions of the receiver planned to incorporate single-supply op-amps in their design, meaning the receiver no longer needed a -5V supply. This meant that the battery system could be a singular battery pack as opposed to two, and the –

5V regulator was removed from the PDB. As shown in Figure 33, Revision 2 of the PDB is simpler than the first iteration.

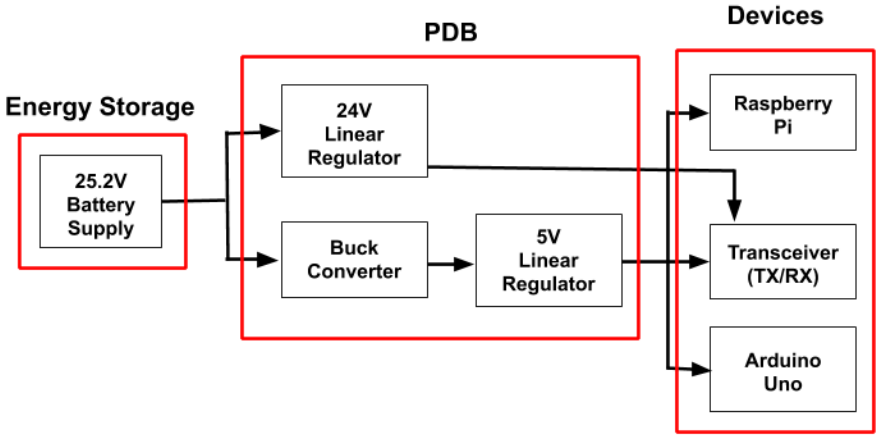

Figure 33: PDB Revision 2 block diagram

3.4.6. Implementation

As mentioned previously, 9V batteries continued to be used throughout testing and experimentation of the UOWC prototype. The PCBs for PDB Revision 1 and 2 shown in Figure 32 and Figure 33 were not produced, although the schematics and PDB PCB layouts can be found in Appendix E. Given the large improvements in energy efficiency, area efficiency, and ease of use as a result of the PDB, the production and implementation of the PDB PCB is suggested in the discussion of future directions.

3.5. Software

3.5.1. Overview

Two separate components comprise the overall system software: the transmitter program and the receiver program. The transmitter program decides what kind of data are sent over the optical link, whether it be sensor data, audio streams, or another format, while the receiver software interprets and processes the data. The received data are either streamed to a device such as a speaker or are saved to a file. These software modules exist on microcontrollers which interact with the hardware through input output (I/O) pins. This section first explains the role of microcontrollers to the system. Then, it details the process through which the system software was developed.

3.5.2. Microcontrollers

As described in the review of the OSI model, since the networking software takes a multi-layered approach, it is reasonable for the networking hardware to also take a multi-layered approach. Using multiple different hardware platforms for both the receiver and transmitter allowed significantly more modularity in the design while developing the completed system. Originally, the design used an Arduino Uno microcontroller for modulation and demodulation, which passed data via Universal Asynchronous Transmitter-Receiver (UART) to a Raspberry Pi 3B+ single board computer. This was to allow for the implementation of Manchester encoding, a scheme that provided robustness in the detection of data by the receiver. The Raspberry Pi 3B+ then controlled the rest of the software, including the remainder of the networking

layers, media control, and user interfacing. These microcontrollers can be seen in Figure 34.

(a) (b)

Figure 34: Arduino Uno R3 (a) and Raspberry Pi 3B+ (b)

Returning to the Arduino Uno R3, a microcontroller at the lowest point of the networking architecture is ideal to directly interface with the amplifier hardware and (de)modulate the physical signal. Since (de)modulation is a relatively straightforward operation that must be repeated at very high speeds, a simple but fast architecture was preferred. Microcontrollers also have the added benefit of onboard peripherals like comparators that aid in interaction with analog hardware, as well as UART interfaces. The Arduino Uno R3 was chosen due to its low cost, accessible open-source programmer, and general popularity. It succinctly implemented the desired Manchester encoding scheme and could be reprogrammed in minutes to allow for quick debugging during tests. The microcontroller communicates via UART, a very common communication protocol. This allowed either side of this interface to be easily changed without requiring a complete system redesign.

Through system integrations, it was determined that the Arduino Uno R3's role in the system was unnecessary – the UART signal from the Raspberry Pi 3B+ was sufficient to test over an optical channel without Manchester encoding. So, removing the Arduino Uno R3 eliminated the complexity, size, and power draw of an additional hardware element. Although Manchester encoding was more robust since it did not require clocking information, the costs of introducing new hardware to the system for encoding data outweighed the benefits. Yet, the system is still constructed in a way that almost any microcontroller running any encoding scheme could be introduced at the transmitter and receiver without having to modify other components

The Raspberry Pi 3B+ handled the rest of the software. The Raspberry Pi platform provided a processor with plenty of performance for the protocol prerequisites. The UART interface was easily accessible through the operating system on the Pi, and if that data stream could be properly translated, it could be used with practically any networking software.

3.5.3. I/O Methods

The microcontrollers discussed previously send an OOK signal to the transmitter in the format of a bitstream alternating between high and low voltages. For that to be possible, I/O methods must be chosen for the signal to be sent over. The Raspberry Pi has a range of I/O pins – one pair specifically corresponds to a UART serial port. Since the serial port on the Raspberry Pi operates at a default 38.4kbps, and encoded audio can use as low as 6kbps in certain encoding schemes, the serial port was

chosen for the I/O purposes of the transmitter [81]. As a result, the receiver also employed the serial port pins and UART to decode the message.

3.5.4. Non-Audio Data

Sending non-audio data in the prototype system can be generalized to sending arbitrary data or bytes over UART. This could be done in many different ways, but for testing purposes the *socat* Linux command was used, which establishes a byte stream between various data sinks and sources [82]. On the transmitter side, the *socat* command's source in the system was a variety of different options such as files, input devices, or the terminal, and the sink was the serial port. On the other hand, the *socat* command running on the receiver side used the serial port as the source and a file or the terminal as a sink. For testing, a bash script sent data from a file to the serial port on the transmitter side, a bash script redirected the incoming data to a file on the receiver side. As the process of sending non-audio data is relatively straightforward, the rest of the software section will focus on the sending of audio.

3.5.5. Audio Data

3.5.5.1. Library Selection

Unlike non-audio data, audio data transmission has many more considerations with a more complex software flow. There were three design choices evaluated for the audio data system development: Gstreamer, PortAudio, and original software developed for this prototype. Firstly, Gstreamer allows users to create a wide range of streaming applications [83]. Secondly, the PortAudio library, an audio I/O library for

C/C++ coding languages, provides a simple API for recording and/or playing sound [84]. The final choice considered was the creation of a simple audio framework, which would have involved designing a packet structure and creating transmitter and receiver software to support it.

There were three main criteria in the decision-making process to determine the optimal framework for the prototype: integrability, debuggability, and modularity. The first factor, integrability, describes the simplicity of implementing the framework in the proposed system. The second factor, debuggability, details how easy it would be to find and fix an error in the program. The last factor, modularity, is the feasibility of changing the software to reflect changes in the components of the overall system. To determine the best framework, a decision matrix was employed with these three criteria. All categories were weighted equally, and scores were given based on rank, with 3 corresponding to the highest rank and 1 corresponding to the lowest. This can be seen in Table 9.

Framework	**Gstreamer**	**PortAudio**	**From scratch**
Integrability	3	2	1
Debuggability	1	2	3
Modularity	3	2	1
Total score:	**7**	**6**	**5**

Table 9: Comparison of different possible frameworks.

In general, Gstreamer would have been simpler to use, but more difficult to debug because any issues would require searching through the Gstreamer source code and documentation to resolve. Developing an original framework would allow for easy

debugging because through iterative programming, steps could be taken to ensure each part is correct before moving onto the next. However, it would also take the most effort, and would require rewriting the code if there were any significant changes to the system such as a new audio input device. PortAudio was the middle ground between the two but did not have the advantages of either. As a result of the comparison, Gstreamer was chosen to be the basis for the software.

3.5.5.2. Streaming Format

With the I/O methods determined and the library chosen, the next step was to build the software through Gstreamer to implement the functionality of audio streaming. Gstreamer is based on pipelines, which are a series of connected elements that each perform some operation on the data and are connected to a source on one end and a sink on the other, as seem in Figure 35. The arrangement of elements in the pipeline make up the streaming format. In the case of the prototype system, two pipelines were needed, one for the transmitter and one for the receiver.

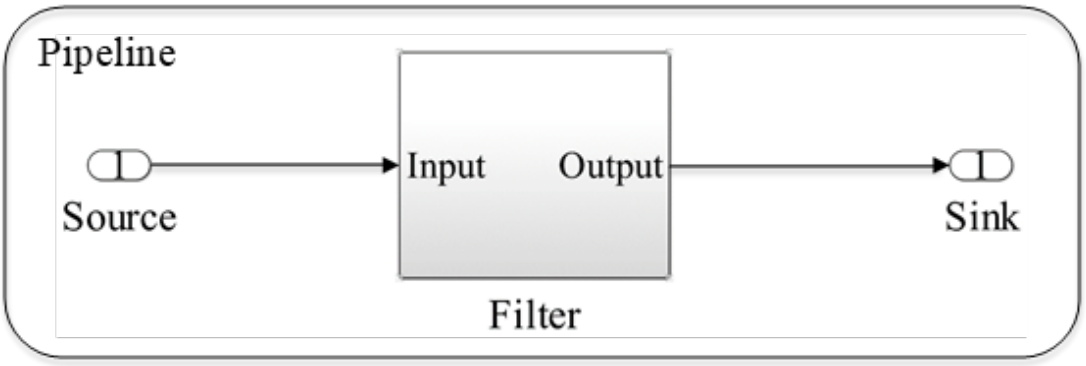

Figure 35: Example pipeline with three elements

The most important elements for the pipelines were an encoder for the transmitter side and a decoder for the receiver side. These elements allowed audio to be transmitted in an encoded state, lowering the bitrates required to send and receive it. In this case, the Opus encoding scheme was chosen, which is an open-source, royalty-free, highly versatile audio codec created by Xiph.org Foundation [81]. This means that the Opus encoder was used in the transmitter pipeline and the Opus decoder was used in the receiver pipeline. The bitrates for Opus range from 6kbps to 510kbps, and since the default serial port could handle 38.4kbps, the bitrates were compatible. The sampling rates also complied with generic audio devices, supporting up to 48kHz bandwidth. Additionally, Opus implements packet loss concealment and loss robustness, which were helpful to combat channel noise.

Opus is an audio encoding scheme, but it must be combined with a container in order to be streamed. A container is a formatting scheme that allows for multiple types of data to be combined. Thus, the default free open container format also produced by Xiph.org Foundation, Ogg, was chosen. Ogg is optimized for internet streaming and processing pipelines and can support interleaving audio and video data [85]. However, the current system does not implement video, therefore Ogg was only used to encapsulate audio data in the UOWC prototype. Relating Ogg back to pipelines, Ogg has a multiplexer element which was used in the transmitter pipeline and a demultiplexer element used in the receiver pipeline.

3.5.5.3. Finalized System

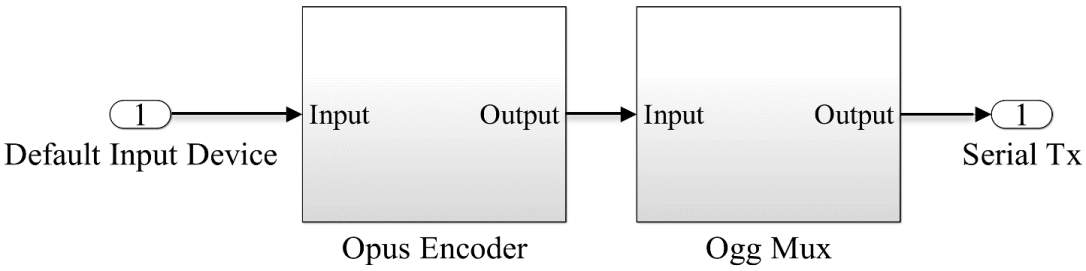

Figure 37: Transmitter side software flowchart.

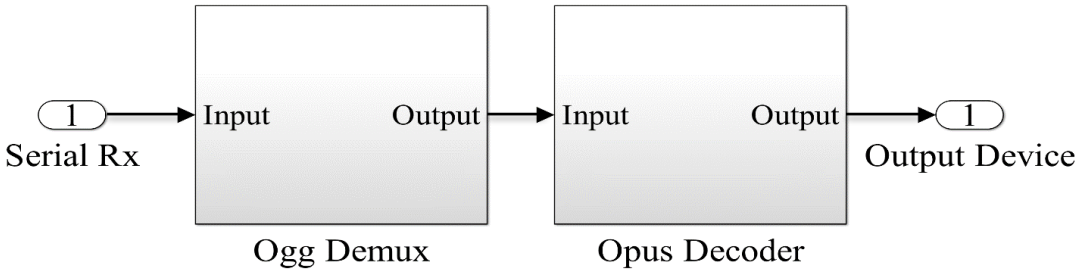

Figure 36: The receiver side software flowchart.

The final audio software system consists of the transmitter and receiver side Gstreamer pipelines. As seen in Figure 36, on the transmitter side the audio comes in from the default audio device, is encoded into Opus audio, and is then encapsulated into Ogg and sent to the serial port Tx. As seen in Figure 37, on the receiver side the data comes in from the serial port Rx, is separated from the Ogg container in the Ogg demux element, and is then decoded into raw audio by the Opus decoder and sent to the output device. The exact code is listed in Appendix F.

3.6. Testing

3.6.1. Overview

To integrate the components of the proposed system in a manner suitable for underwater operation, a chassis needed to be designed. The chassis was required to house each respective part of the system in a waterproof enclosure. The design criteria for the chassis were driven by the 18.3m depth limit for beginner scuba dives using the Professional Association of Diving Instructors (PADI) Open Water Dive Certification [86], as well as the physical dimensions of the components of the system. Three chassis revisions were designed, two of which were constructed and one of which saw underwater testing. In order to conduct the testing, testing routines were programmed to allow for expedient data collection. The three chassis revisions are described first, followed by the startup scripts, and then ending with the testing setups used for data collection.

3.6.2. Chassis Design

3.6.2.1. Chassis Revision 0

The first conceptual design of the system's chassis was to have a waterproof enclosure that could house the system's parts and transmit light. This waterproof enclosure would have the ability of attaching to a bracket on a scuba diving tank. The bracket would have an elastic band that would wrap around the scuba tank, ideally allowing for any scuba system to be used. An image of the proposed system is shown in Figure 38.

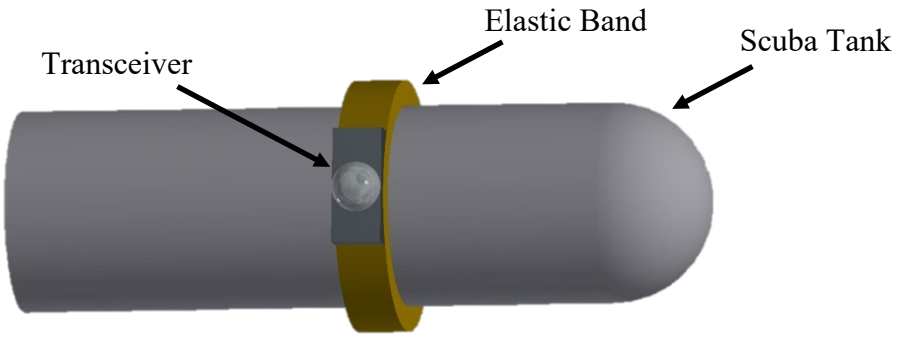

Figure 38: The proposed chassis Revision 0

This chassis would be modular allowing for the system to be mounted to many different scuba tanks as well as disconnect with ease. This idea was ultimately not pursued once research demonstrated the difficulty of designing a bracket that satisfied the design criteria. In addition, the projected time needed to design this modular system posed similar problems as there were not ample resources to accomplish this goal. With the overarching design criteria in mind, another chassis revision was pursued.

3.6.2.2. Chassis Revision 1

The goal of the next chassis revision was to utilize an off-the-shelf waterproof enclosure and modify it so that it could transmit and receive optical signals while remaining waterproof throughout the testing duration. The waterproof enclosure used in this iteration of the chassis design was the T3500 Protective Case by S3. The only modification made to the case was drilling holes into the top of the T3500 Case to allow for the transmitter and lens to be outside of the case. Although some of the S3 cases purchased were made of clear polycarbonate, holes were still drilled to eliminate any signal attenuation caused by transmission through the case. Originally, each S3 case housed a transmitter and receiver. However, the final iteration of Revision 1 of the chassis had dedicated cases for the transmitter and receiver. This was done to minimize the number of holes drilled into the dive case, thus improving the integrity of the enclosure.

Each opening was sealed with Flex Shot ®, a liquid rubber sealant, and tested on numerous occasions to ensure that the case was waterproof. These waterproof tests included submerging the sealed case in water for 30 minutes with a piece of paper inside. If the paper came out dry and no water was found inside the sealed case, it passed the test and was deemed to be waterproof. An image of Revision 1 of the chassis design can be seen below in Figure 39.

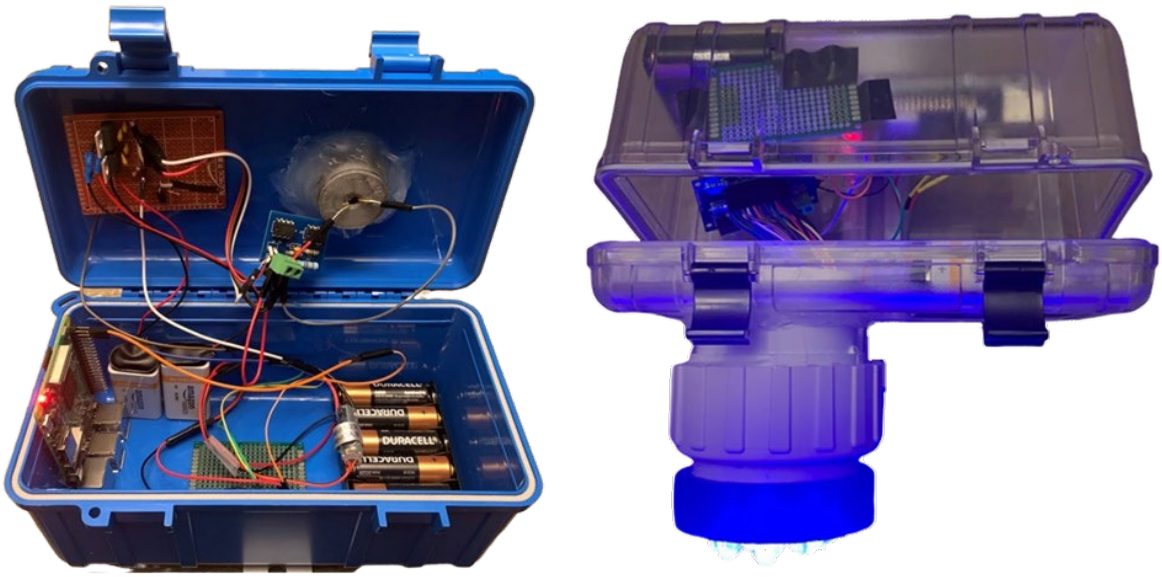

(a) (b)

Figure 39: Chassis Revision 1 with the receiver (a) and the active transmitter (b)

With this iteration of the chassis design, lens holders and transmitter housings were designed in Autodesk Inventor and SolidWorks before being 3D printed. The transmitter housing was then attached to a two-piece waterproof Polyvinyl Chloride (PVC) pipe fitting. This design feature allowed for the transmitter housing to be easily removed from the chassis and swapped out for different transmitter geometries; two of the geometries that were printed are shown in Figure 40.

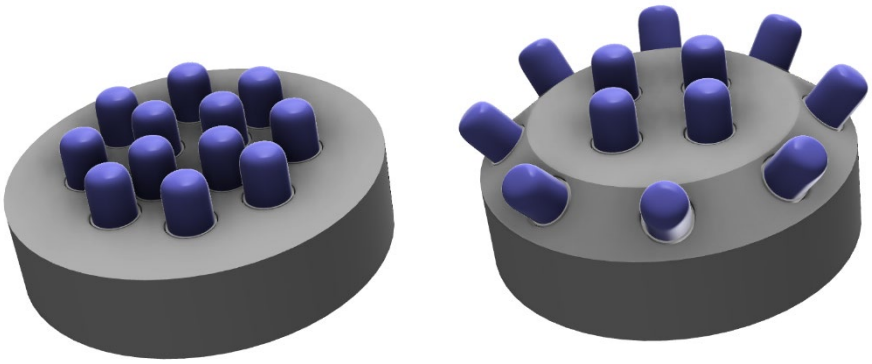

Figure 40: CAD renderings of the transmitter housings used in Revision 1 of the chassis

One issue with using the 3D printed parts for underwater testing was that the prints were not waterproof due to the nature of fuse deposition modeling (FDM) 3D printers. In FDM, 3D objects are created by printing layer by layer, which creates the possibility for small holes to be created between the layers, thus allowing water to seep through the material. This was resolved by using XTC 3D, a 3D print coating that added a sealing epoxy layer to the surfaces of the print that would be exposed to water.

The first full scale water test was conducted using this iteration of the chassis. Ultimately, this chassis revision failed due to an inability to fully waterproof the design – despite the different attempts used to seal the connections between different components in the chassis, leaks persisted. Due to this difficulty in waterproofing, a complete chassis redesign was pursued to enable true underwater testing.

3.6.2.3. Chassis Revision 2

The final chassis revision was a complete redesign in response to the issues encountered with Chassis Revision 1. Revision 2 featured industry standard Ikelite

camera cases that were custom-built to accommodate the hardware used in the prototype, and this revision featured no additional holes to ensure structural integrity. The Ikelite camera cases featured a glass cover, thus allowing for visible light signal fidelity while maintaining a watertight seal. Another advantage to using the Ikelite cases was they insulated the entire transmitter and receiver devices from the water, eliminating the need to waterproof any 3D prints.

The case used for the final chassis revision along with the transmitting and receiving hardware is shown in Figure 41. The polycarbonate case is rated to be watertight to 60m, providing a depth safety factor greater than 3.2. The case was also custom-made to remove the lens porthole and camera interaction apparatus, thus allowing for one side of the case to be a flat, glass panel [87]. These cases were recommended by the Director of the Space System Laboratory in the NBRF and were donated by Ikelite for the purposes of research. These cases are expected to have higher reliability to work underwater as they are designed to house expensive Nikon cameras for underwater photography/videography.

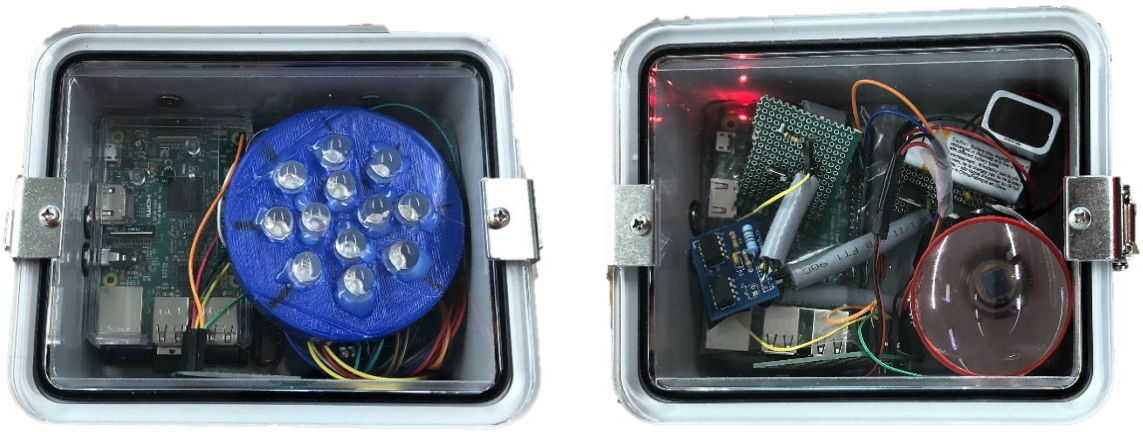

(a) (b)

Figure 41: Chassis Revision 2 with the transmitter (a) and the receiver (b)

In addition to the new housing, a new lens holder was designed to integrate a bigger lens into the system. The new lens had a focal length of 52.42mm compared to the 25.4mm used in the previous iteration of the chassis. This design iteration was planned to be used in the second round of underwater testing conducted at the NBRF, which was unable to be conducted for reasons explained in the discussion of future directions.

3.6.3. Startup Scripts

In order to efficiently test underwater without the need of manually running a program between each test run, startup scripts were designed to run test programs upon boot. To do this, the startup routine of the Raspberry Pis on both the transmitter and receiver were modified to call bash scripts through the file rc.local, which controls a portion of startup services. On the transmitter side, the bash script

continuously transmitted a predetermined message to the transmitter circuit. On the receiver side, the bash script continuously wrote the messages that it received through the serial port and stored them into a text file, dated and marked appropriately. These scripts allowed for the capability to do multiple tests by simply restarting the Raspberry Pis. These scripts can be seen in Appendix G.

3.6.4. Testing Setup

3.6.4.1. Testing Setup 1: Through Air

Before performing any underwater experiments on the UOWC prototype, the system performance was first tested through air to troubleshoot any issues that arose and to refine the testing procedures for subsequent underwater tests. Testing through air meant that the chassis could be opened and that the signal lines within the transmitter and receiver could be probed during data transmission, as seen in Figure 42. This meant that errors in the physical setup of the test rig, such as the alignment of the transmitter and receiver, or errors in the test procedure, such as issues with the startup scripts written for data collection, were more quickly found and solved. Experiment 1 reviews the data collected from the formalized test of the UOWC prototype through air.

Figure 42: Photo of the setup for tests through air

3.6.4.2. Testing Setup 2: Quasi-Underwater

Following the through air test, the prototype was then tested in quasi-underwater conditions using glass tanks filled with tap water, as seen in Figure 43. The transmitter and receiver were placed outside the glass tanks, but the chassis were sealed during testing to simulate the test procedure that would be used when the prototype was fully submerged. Although the testing setup did not fully encapsulate the conditions of underwater data transmission due to the narrow channel created by the tanks and the reflections and refractions at the tank walls, it did provide preliminary results that were

used to gauge the efficacy of the prototype for underwater data transmission. The results of this experiment are described in Experiment 2.

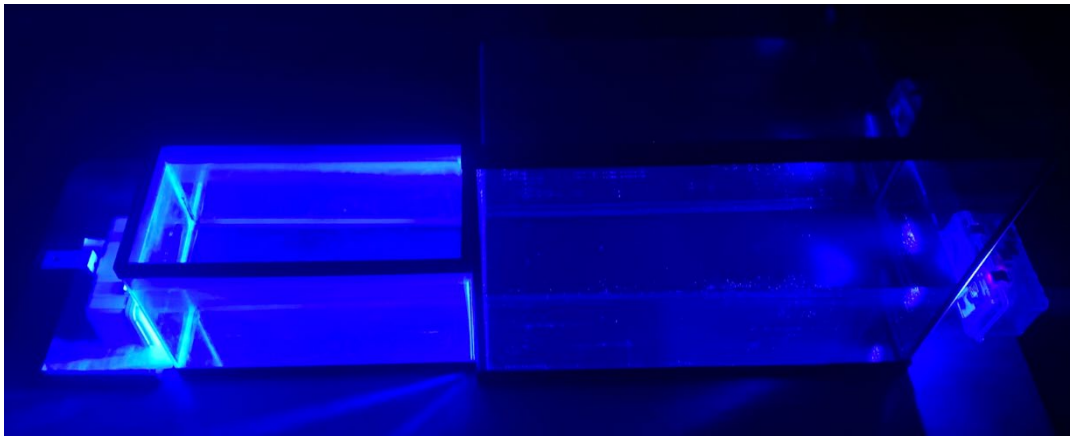

Figure 43: Photo of the rig used for quasi-underwater testing

3.6.4.3. Testing Setup 3: Underwater

After the tests over air and in the quasi-underwater environment, the focus then turned to testing in a true underwater environment. This environment posed several new challenges: the integrity of the chassis was now paramount, and the amount of interaction with the rig during testing became more limited. In the first two testing setups, the process for ensuring that the transmitter was reliably sending data to the receiver was straightforward: the chassis was opened, and the receiver signal was probed to see if data were being successfully transmitted. In the underwater experiments, this was no longer possible because the chassis was completely submerged. This issue was resolved by attaching the transmitter and receiver to an 80/20 T-slot beam using L-brackets and Loctite Marine Epoxy. As a result of this testing rig, the alignment could be verified out of the water, and then would not change as the entire rig was submerged. Additionally, the versatility of the 80/20 and the L-

brackets meant that the transmission distance was easily modifiable, being used to for testing at distances of 0.72m, 1.4m, and 1.5m. This testing rig was first experimented with using a small recreational pool, then was used for testing at the NBRF. An image of the third testing setup is shown in Figure 44 and the resulting experiment results are described in Experiment 3.

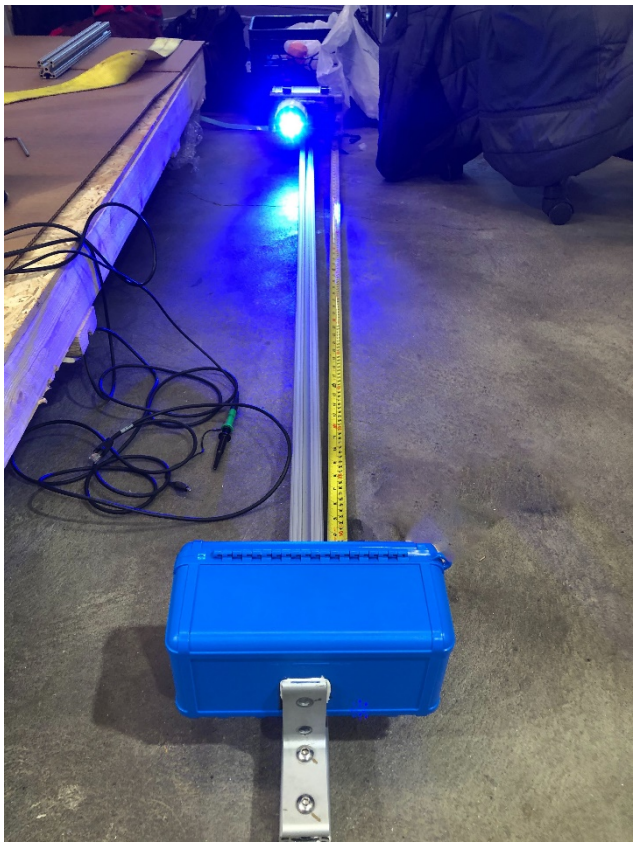

Figure 44: Photo of the rig used for underwater testing

Chapter 4. Results

4.1. Overview

This chapter describes the results of three major experiments that were conducted using the UOWC prototype and the testing setups described in the previous section. The first experiment tested BER versus distance through air for direct LoS transmission. The second experiment tested for transmission success through tanks of tap water at variable distances. A third experiment, which was not completed, planned to test BER versus distance underwater. A fourth test with further revisions was planned but never executed – this will be detailed in the discussion of future directions for testing.

4.2. Experiment 1

Experiment 1 tested BER versus distance through air at normal incidence, or at a 0° angle. Table 10 states each hardware revision used in the system integration.

Hardware Component	**Revision Number**
Transmitter	1
Optical Collection System	0
TIA	1
PDB	N/A
Chassis	N/A

Table 10: Hardware component revisions

As referenced in the Methodology, transmitter Revision 1 was the final transmitter revision, consisting of the full 12 LED array, switching circuit, current

mirror, and on-board power. Furthermore, Revision 0 of the optical collection system utilized the plano-convex lens, and Revision 1 of the TIA included the finalized circuit PCB without the power components on board. For this test, the TIA dual-regulated power supply was soldered to a separate perfboard and connected externally to the TIA PCB. As discussed in the Methodology, the PDB revisions were not incorporated into the final designs, so the power generation and regulation elements were local to each component. Finally, this experiment was conducted outside of the dive cases – the components were not confined together as they would be in the final chassis Revision 1 design. This difference has significant implications, which will be reviewed in the Discussion.

To test BER, a 977kB file consisting of one million random characters was transmitted at a rate of 38.4kbps – while this was a serial transmission, the selected data speed was well within the range for audio transmission. The received data were then stored to a file and compared bitwise to the original data and the error rate was recorded. The distance was increased after each subsequent successful transmission, and the test was repeated. Figure 45 below displays the calculated BER versus distance on a linear scale.

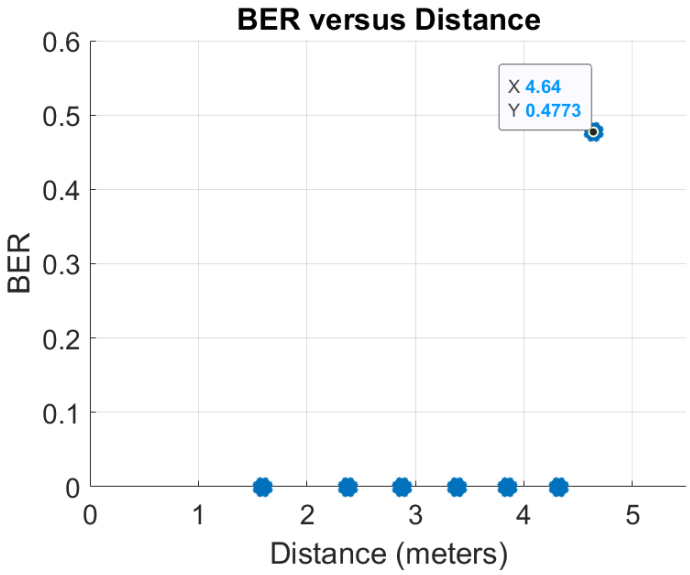

Figure 45: BER versus distance for experiment 1

The results of this experiment show that the system was either able to achieve perfect transmission, corresponding to a BER of 0, or no transmission at all, corresponding to a BER of approximately 0.5. The maximum measured transmission distance was approximately 4.4m, so accordingly distances further than 4.4m would yield completely unsuccessful transmission. The reasoning and impact of this will be discussed in detail in the Discussion, but this result served as a basis for the measurements taken in Experiment 2, which will be reviewed next.

4.3. Experiment 2

Experiment 2 tested the feasibility of data transmission through water using the quasi-underwater environment described in the second testing setup. These trials through water are expected to be conservative compared to trials conducted completely

underwater due to the refraction and reflection from the air-glass-water interfaces. Once again, a set of characters was sent from the transmitter to the receiver. Despite the differing transmission medium, Experiment 2 utilized the same hardware revisions as Experiment 1, except the integrated system was deployed inside the chassis Revision 1 design. Therefore, both the transmitter and receiver were battery powered and confined to a small volume.

For this experiment, 10 trials were run: two trials through 0.51m of water in one tank, four trials through 0.76m of water in one tank, and four trials through 1.42m of water through two tanks. The experimental setup for 0.51m transmission can be seen in Figure 46.

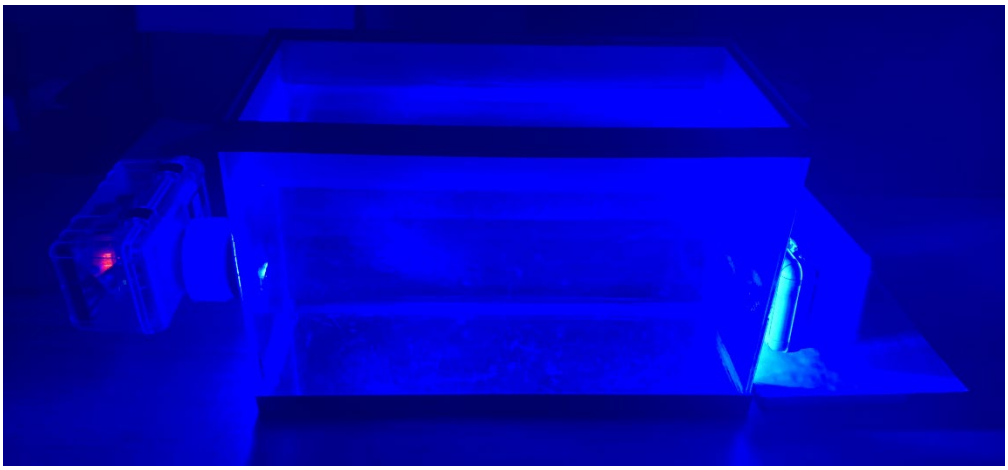

Figure 46: Experimental setup for transmission through 0.51m of tap water

As discovered in Experiment 1, transmission was either wholly successful or unsuccessful. Therefore, the results were recorded as either a success or a failure, as seen in Table 11.

Trial	Distance through Water (m)	Number of Tanks	Result
1	0.51	1	Failure
2	0.51	1	Success
3	0.76	1	Failure
4	0.76	1	Failure
5	0.76	1	Success
6	0.76	1	Success
7	1.42	2	Failure
8	1.42	2	Failure
9	1.42	2	Failure
10	1.42	2	Success

Table 11: Transmission success versus distance of Experiment 2

In summary, the tests through 0.51m and 0.76m were 50% successful and the tests through 1.42m was 25% successful. The sole purpose of this experiment was to demonstrate that transmission through water was possible – this was shown to be true. The performance analysis would be tested in Experiment 3, which will be explained next.

4.4. Experiment 3

Experiment 3 was devised to test BER versus distance in a full underwater setting at the NBRF. Revision 1 of the waterproof chassis was used for this experiment in conjunction with the testing rig constructed out of 80/20. In addition, the hardware used was consistent with the previous two experiments. Unfortunately, both the transmitter and receiver waterproofing failed, so no data were collected from the experiment.

Chapter 5. Discussion

5.1. Discussion of Results

5.1.1. Overview

This section will explain in detail the results obtained from Experiment 1 and Experiment 2 and discuss their broader implications. To recapitulate, Experiment 1 tested BER versus distance through air and Experiment 2 tested the viability of communication through tanks of water.

5.1.2. Experiment 1

Experiment 1 demonstrated that error-free transmission was possible from a maximum distance of 4.4m; beyond that, the system would fail. This maximum measured distance differs from the maximum range measured in the Methodology, which for the singlet lens was 3.3m. This discrepancy was due to the fact that Experiment 1 was conducted out of the dive cases, whereas the maximum distance measurements from previously referenced were obtained in-case. When the components were sealed in the case, it was found that the signal fidelity decreased due to EMI. The unshielded wires used for all component connections, including power, ground, and signal lines, produced and conducted EMI when confined within the case and thus injected more noise into the system.

Besides EMI, an interesting observation from Experiment 1 was that transmission was either completely perfect or a total failure, dependent on a maximum cutoff distance. This is due to the nature of the TIA circuit. The TIA circuit was designed to saturate the input signal from the photodiode to the maximum voltage of

the op-amp because of its high gain. When the incident signal power dipped below the necessary saturation power, the signal was lost. This is contrasted in Figure 47 and Figure 48 below.

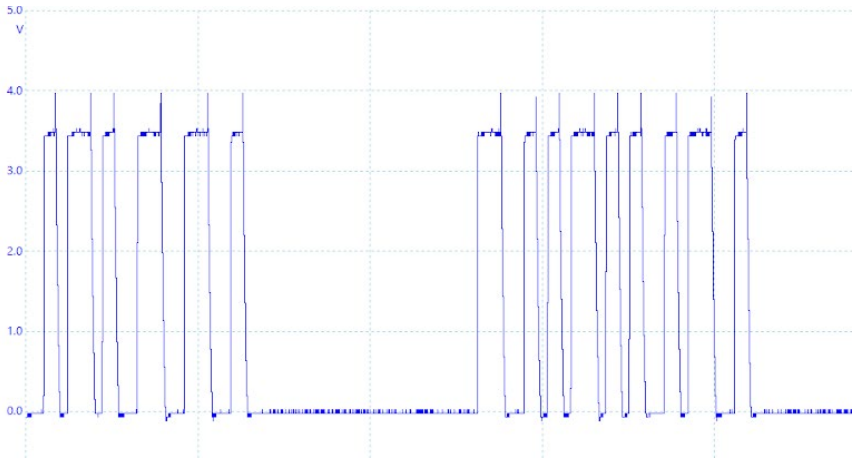

Figure 47: Output signal saturated to the maximum op-amp voltage

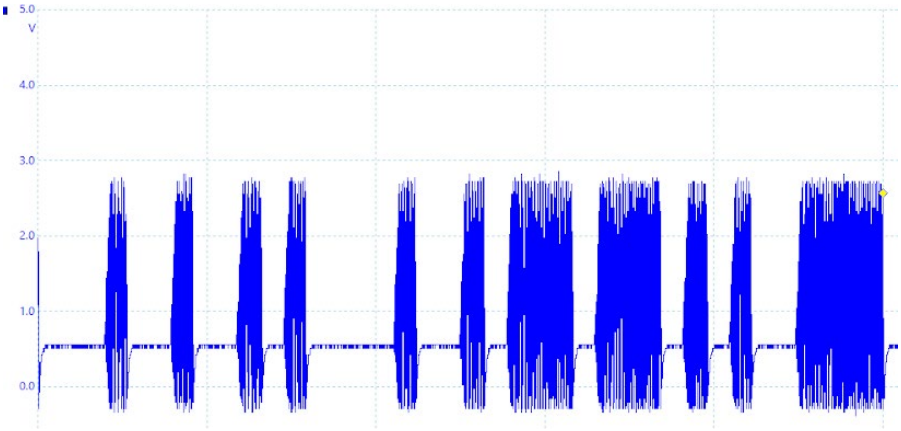

Figure 48: Output signal when the input signal was below saturation power

In Figure 47, each bit is either fully saturated to the signal high or fully dropped to the signal low. To the contrary, Figure 48 shows oscillations in the signal throughout

the bit timing. This saturation caused irrecoverable errors in the bit detection, thus resulting in unsuccessful transmission.

5.1.3. Experiment 2

Experiment 2 demonstrated that transmission through water was possible. This was tested successfully at distances of 0.51m, 0.76m, and 1.42m. These three distances were created as a result of the two glass tanks of fixed size used for this test. No maximum transmission range was measured, but these distances are expected to be conservative compared to the true maximum distance due to the attenuating interface between the tanks, as described in the Experiment 2 results. Despite this, Experiment 2 still proved that this proposed UOWC system is feasible, albeit at a short range. If the final TIA, PDB, and optical collection system revisions were integrated and tested as planned in Experiment 4, the transmission range would likely be much closer to the ranges simulated in the Methodology. Additionally, greater improvements to the system to boost operation are outlined in the following section, which would further prove the viability of this proposed system.

5.2. Future Directions

5.2.1. Hardware

Due to time constraints, there were ultimately several hardware features between the transmitter, receiver, and power distribution unit that were designed but not fully integrated in the final iteration of the UOWC prototype. One of the design goals for the hardware was to consolidate the different components in the prototype into fewer PCBs to reduce redundant parts and improve the ease-of-use of the prototype. As discussed in the design iterations of the PDB, schematics and PCBs for the PDB were designed (see Appendix E) but never manufactured. Additionally, Appendix E shows schematics for a single transmitter/receiver board. If given more time, the future iterations of the prototype's hardware would consist of a single board dedicated to distributing the power supplied by the batteries and another board dedicated to the transmission and detection of optical signals. Future plans would also include making the design of these boards stackable, which would make the hardware more modular and reduce the overall footprint.

There is also additional research that could be done to increase the performance of the transmitter. The range of the UOWC system is dependent on the optical intensity of the transmitter circuit, so there are several research avenues that could be investigated to increase its range. For example, new LEDs were found that were smaller and had a higher luminous intensity than what was used in the transmitter revisions, as mentioned in the discussion of design decisions for the transmitter. Incorporating these into the transmitter design has the potential to increase the range of the transmitter while maintaining or reducing the size of the LED housing, thus improving the usability

of the prototype. Additionally, the design strategies used to suppress thermal runaway, although effective, could be further investigated. For example, additional experiments could be performed to compare the effectiveness of current mirror circuits to heat sinks in controlling the current and temperature of LED arrays.

Finally, there were measures that could have been taken to reduce the noise in the TIA circuit. As mentioned in the Discussion of Results, EMI was a large inhibiting factor for closed-case tests. Thus, insulating PVC-jacketed copper wire was selected for the signal and power wires of the TIA circuit in an effort to reduce EMI. Preliminary testing indicated that the shielded wires eliminated the receiver EMI, but no further experiments were executed to confirm this improvement.

5.2.2. Software

One natural direction for improvement of the software is the design of user interfaces (UIs). Implemented on both the transmitter and receiver, the UI would consolidate all the functions of the system into usable, easy to understand controls. The transmitter UI would include options to transmit audio or data from a file source or input device, while the receiver UI would have options to display incoming string data, play incoming audio data through a speaker, and compare incoming string data to files for differences. A preliminary UI was designed to display transmitted data as seen in Figure 49; however, the UI was not implemented in the prototype because the chassis revision were not yet capable of real-time data monitoring.

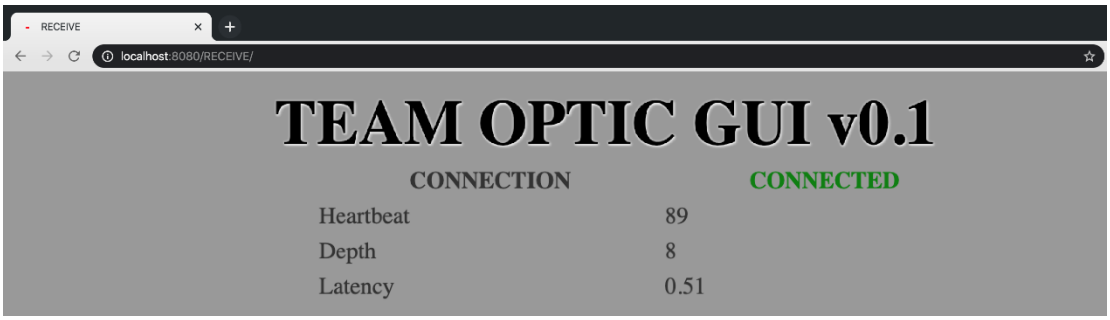

Figure 49: Preliminary UI

Another future step for the software is to create more robust pipelines for audio that are optimized relative to elements in Gstreamer and their properties. Gstreamer elements can have many tunable parameters which change how they interact with data. An optimized system could have lower latency, higher audio quality, and better error prevention/protection.

5.2.3. Testing

Previously, Experiment 4 was anticipated to be conducted in the NBRF using the chassis Revision 2 with the customized Ikelite casings. Due to unforeseen circumstances resulting from the COVID-19 pandemic, the NBRF and UMD at large were under severe research restrictions that prohibited Experiment 4 from being conducted. Therefore, the next step for testing would be to mount the transmitter and receiver units to the testing rig made using the 80/20 and conduct variable-distance BER trials in the NBRF. A direct extension of these trials would be to vary the depth of the units, including trials with either the transceiver or receiver being at different depths. A photo of the NBRF can be seen in Figure 50.

Figure 50: The NBRF at UMD

During testing, it was also noted that monitoring the data stream from the receiver module in real-time for underwater testing was not possible with the chassis Revision 1 and Revision 2 designs. As detailed in the third testing setup, the submerged chassis had to be reopened and closed for every trial. This lengthened underwater testing and the repeated opening and closing of the cases increased the strain placed on the waterproofing measures on the cases. This also meant that if a test failed during its operation, the failure would not be noticed until after the entire trial had been conducted. Therefore, future work to build from the chassis Revision 2 design should include measures that would permit real-time monitoring of underwater trials. This would likely take the form of additional ports to allow for ethernet cables to stream data to a monitor above water.

Additionally, trials may be conducted in water with varying turbidity, environmental lighting, and transmitter-receiver transmission angles. Given the aquatic conditions the NBRF must maintain for other research activities, an alternative setting would need to be found to conduct conditions with varying these parameters.

5.2.4. Implications for Other Research

Extending the research as described above would ideally allow for the improvement of UOWC systems while reducing the average cost to research and produce these systems. This is due to the relatively inexpensive components that were used in this research. While the research discussed in this thesis has emphasized incoherent light produced by LEDs, many of the future research directions previously mentioned could be generalized to benefit laser diode UOWC systems, namely the stackable, modular boards and the software improvements.

These improvements would also contribute to closing the gaps in UOWC research by demonstrating the effects of refraction on data transmission alongside varying turbidity, lighting, and transmission angles. Such research would serve to make future UOWC systems increasingly robust in a diverse array of environments and uses.

Chapter 6. Conclusion

This thesis proposed a design for a portable, consumer-grade UOWC system capable of short-range data transmission. An affordable model with the presented capabilities is necessary to make underwater communications more accessible, therefore promoting technological advancements in multiple areas of the underwater domain. Existing UOWC systems have been shown to achieve propagation distances further than RF and data rates faster than acoustic – these create unique applications to which modern high-speed communications can be applied, such as scuba diver audio and vitals streaming. However, these UOWC systems are far from ubiquitous, as they are deficient in terms of price, size or production. This research showed that a reliable UOWC prototype can be created using only commercial-grade products, in a small enough package for divers to reasonably use as a hand-held device.

This investigation into a UOWC design was unique because of its sourcing of cost-effective, modular components that allowed the transmitter, receiver, PDB, and software to be updated without necessarily changing other aspects of the system. Firstly, the transmitter was constructed with inexpensive LEDs and MOSFETS while still generating switching speeds suitable for audio transmission at bit rates of at least 96kbps. As for the receiver, a PIN photodiode was purposely selected for its low cost in comparison to other possible options: PMTs and APDs. Then, using an achromatic doublet lens, the receiver extended its maximum theoretical range to 8.4m, all inside a compact Ikelite dive case. Also enclosed were the widely used Raspberry Pi single-board computers that controlled the system using open-source software

packages like GStreamer and Opus. Finally, common household 9V batteries were used to power the entire system.

To confirm the functionality of this module, the system was tested under different channel conditions. The system was first proven to work sufficiently through air. Then, before its final revision, it reliably transmitted data up to 1.42m through water. These results suggest that an inexpensive consumer-grade UOWC is feasible. Moving forward, the efficacy could be vastly improved by implementing the final revisions and the future directions mentioned above.

In conclusion, the hope is that continued research efforts in the field of UOWC will yield a commercialized and affordable system in the consumer market. This research would empower marine researchers, improve live-time ocean monitoring, streamline underwater search-and-rescue, and more. Above all, this thesis seeks to advance the field of underwater technology to be more accessible to both consumers and researchers.

References

[1] A. Celik, T. Y. Al-Naffouri, M.-S. Alouini and N. Saeed, "Underwater optical wireless communications, networking, and localization: A survey," *Ad Hoc Networks,* vol. 94, June 2019.

[2] C. Coglan, "The ocean economy of the United States: Measurement, distribution, & trends," *Ocean & Coastal Management,* 2018.

[3] US Department of Commerce, National Oceanic and Atmospheric Association, ""How much of the ocean have we explored?," NOAA's National Ocean Service, 2009.

[4] M. F. Ali, D. N. K. Jayakody, Y. A. Chursin, S. Affes and S. Dmitry, "Recent Advances and Future Directions on Underwater Wireless Communications," *Archives of Computational Methods in Engineering,* 2019.

[5] N. Mohamed, I. Jawhar, J. Al-Jaroodi and Zhang Liren, "Sensor Network Architectures for Monitoring Underwater Pipelines," *Multidisciplinary Publishing Institute,* vol. 11, no. 11, pp. 10738-10764, 2011.

[6] I. F. Akyildiz, D. Pompili and T. Melodia, "Challenges for Efficient Communication in," *Ad Hoc Networks,* vol. 3, no. 3, pp. 1-23, 2005.

[7] L. Liu, . S. Zhou and J.-H. Cui, "Prospects and Problems of Wireless Communication for Underwater Sensor Networks," *Wireless Communications and Mobile Computing,* vol. 8, no. 8, pp. 1-18, 2008.

[8] J. Heidemann, M. Stojanovic and M. Zorzi, "Underwater sensor networks: applications, advances and challenges," *Philosophical Transactions of the Royal Society A,* vol. 370, no. 1958, pp. 1-18, 2012.

[9] Z. Zeng, "A Survey of Underwater Wireless Optical Communication," University of British Columbia, Vancouver, 2015.

[10] H. M. Oubei, C. Li, K.-H. Park, T. K. Ng, M.-S. Alouini and B. S. Ooi, "2.3 Gbit/s underwater wireless optical communications using directly modulated 520 nm laser diode," *Optics Express,* vol. 23, no. 16, pp. 20743-20748, 2015.

[11] H. Kaushal and G. Kaddoum, "Underwater Optical Wireless Communication," *IEEE Access,* vol. 4, pp. 1518-1547, 2016.

[12] J. Benjamin and R. MacKintosh, "Regulating scientific diving and underwater archaeology: Legal and historical considerations," *International Journal of Nautical Archaeology,* vol. 45, no. 1, pp. 153-169, 2016.

[13] M. Deleau, P. White, G. Pierson, T. Leighton and P. Kemp, "The response of anguilliform fish to underwater sound under an experimental setting," *River Research and Applications,* vol. 36, no. 3, pp. 441-451, 2020.

[14] V. Tavrizov, "Experience in removing blasted underwater rock," *Hydrotechnical Contruction,* vol. 26, no. 2, pp. 114-118, 1992.

[15] C. Edmonds, B. McKenzie, R. Thomas and J. Pennefather, "Diving medicine for scuba divers, 3rd edition," *Diving and Hyberbaric Medicine – South Pacific Underwater Medicine Society,* vol. 40, no. 2, pp. 98-99, 2010.

[16] G. Chang, M. Honda and F. Nencioli, "Innovations in optics for coastal and open-ocean mooring applications," *Sea Technology,* vol. 49, no. 8, pp. 17-18, 20-22, 2008.

[17] J. Lloret, M. Garcia, S. Sendra and G. Lloret, "An underwater wireless group-based sensor network for marine fish farms sustainability monitoring," *Telecommunication Systems: Modelling, Analysis, Design and Management,* vol. 60, no. 1, pp. 67-84, 2015.

[18] E. McCarthy, "International regulation of underwater sound," *Oceans,* vol. 1, pp. 221-228, 2000.

[19] S. S. Butler, "Exclusions and exemptions from OSHA's commercial diving standard. U.S. Department of Labor," *OSHA Divistion of Maritime Compliance Assistance,* pp. 1-6, 1996.

[20] G. Kumar, C. Engle and C. Tucker, "Factors driving aquaculture technology adoption," *Journal of the World Aquaculture society,* vol. 49, no. 3, pp. 447-476, 2018.

[21] D. Liu, "Autonomous Vessel Technology, Safety, and Ocean Impacts," *The Future of Ocean Governance and Capacity Development,* pp. 490-494, 2019.

[22] L. Weilgart, "Keeping the Noise Down: Approaches to the Mitigation and Regulation of Human-Caused Ocean Noise," *The Future of Ocean Governance and Capacity ,* pp. 298-302, 2019.

[23] H. M. Brundage, "Designing a wireless underwater optical communication system," Massachusetts Institute of Technology, 2010.

[24] C. P. Gates, "Towards a Modular, Low-Power, Low-Cost, and High-Speed Underwater Optical Wireless Communication Transmitter," *UC San Diego Electronic Theses and Dissertations,* 2019.

[25] S. Arnon, "Underwater Optical Wireless Communication Network," *Optical Engineering,* vol. 49, no. 1, 2010.

[26] W. C. Cox, K. F. Gray, J. A. Simpson, B. Cochenour, B. L. Hughes and J. F. Muth, "A MEMS blue/green retroreflecting modulator for underwater optical communications," *OCEANS 2010 MTS/IEEE SEATTLE,* pp. 1-4, 2010.

[27] R. J. Green and F. Jasman, "Monte carlo simulation for underwater optical wireless communications," *2013 2nd International Workshop on Optical Wireless Communications (IWOW),* pp. 113-117, 2013.

[28] Z. Zeng, S. Fu, H. Zhang, Y. Dong and J. Cheng, "A Survey of Underwater Optical Wireless Communications," *IEEE Communications Surveys & Tutorials,* vol. 19, no. 1, pp. 204-238, 2017.

[29] T. Youssef Elganimi, "Performance Comparison between OOK, PPM and PAM Modulation Schemes for Free Space Optical (FSO) Communication Systems: Analytical Study," *International Journal of Computer Applications,* vol. 79, no. 11, pp. 22-27, 2013.

[30] "S2C R 48/78 Underwater Acoustic Modem," EvoLogics GmbH, 2014.

[31] "Datasheet BlueComm 100 - Optical Communications System," Yateley: Sonardyne International Limited, 2016.

[32] "Datasheet BlueComm 200 - Optical Communications System," Yateley: Sonardyne International Limited, 2016.

[33] "Sonardyne International Limited," Sonardyne BlueComm Underwater Wireless Optical Communication System, 2016.

[34] A. Al-Kinani, C. Wang, L. Zhou and W. Zhang, "Optical Wireless Communication Channel Measurements and Models," *IEEE Communications Surveys & Tutorials,* vol. 20, no. 3, pp. 1939-1962, 2018.

[35] C. Gabriel, M. Khalighi, S. Bourennane, P. Leon and V. Rigaud, "Monte-Carlo-Based Channel Characterization for Underwater Optical Wireless Communication Systems," *IEEE/OSA Journal of Optical Communications and Networking,* vol. 5, no. 1, pp. 1-12, 2013.

[36] V. I. Haltrin, "Chlorophyll-Based Model of Seawater Optical Properties," *Appl. Opt.,* vol. 38, no. 33, pp. 6826-6832, 1999.

[37] P. Horowitz and W. Hill, The Art of Electronics, 1st ed., Cambridge: Cambridge University Press, 1980.

[38] R. Baker, CMOS: Circuit Design, Layout, and Simulation, 3rd ed., Hoboken: Wiley-Blackwell, 2015.

[39] V. Lakshminarayanan and N. Sriraam, "Analyzing Thermal Runaway in Semiconductor Devices Using the Constrained Method of Optimization," in *Internation Conference on Circuits, Controls and Communications*, Bengaluru, 2013.

[40] N. G. M. Yang, B. Y. R. Shieh, T. F. Y. Zeng and S. W. R. Lee , "Analysis of Pulse-Driven LED Junction Temperature and its Reliability," in *China Internation Forum on Solid State Lighting: International Forum on Wide Bandgap Semiconductors China (SSL China: IFWS)*, Shenzhen, 2018.

[41] H. K. Ma, B. R. Chen, H. W. Lan and C. Y. Chao, "Study of an LED Device with a Honeycomb Heat Sink," in *IEEE Semiconductor Thermal Measurement and Management Symposium (SEMI-THERM)*, Santa Clara, 2010.

[42] C. Davis, Lasers and Electro-Optics, Cambridge: Cambridge University Press, 2014, pp. 602-627.

[43] Japan Agency for Marine-Earth Science and Technology, "Study of Adaptive Underwater Optical Wireless Communication with Photomultiplier Tube," 2017.

[44] Sonardyne, *Bluecomm 200 - Optical Communications System,* 2019.

[45] W. G. Lawrence, G. Varadi, G. Entine, E. Podniesinski and P. K. Wallace, "A Comparison of Avalanche Photodiode and Photomultiplier Tube Detectors for Flow Cytometry," *The International Society for Optical Engineering,* 2008.

[46] C. Lu, J. Wang, S. Li and Z. Xu, "60m/2.5Gpbs Underwater Optical Wireless Communication with NRZ-OOK Modulation and Digital Nonlinear Equalization," *Optical Society of America,* 2019.

[47] OSI Optoelectronics, "Photodiode Characteristics and Applications," 24 June 2015. [Online]. Available: http://osioptoelectronics.com/technology-corner/application-notes.aspx.

[48] G. Dolci, C. Tua, M. Grosso and L. Rigamonti, "Life Cycle Assessment of Consumption Choices: A Comparison Between Disposable and Rechargeable Household Batteries," *The International Journal of Life Cycle Assessment,* vol. 21, no. 12, pp. 1691-1705, 2016.

[49] Y. Liang, C. Zhao, H. Yuan, Y. Chen, W. Zhang, J. Huang, D. Yu, Y. Liu, M. Titirici, Y. Chueh, H. Yu and Q. Zhang, "A Review of Rechargeable Batteries for Portable Electronic Devices," *Infomat,* vol. 1, no. 1, pp. 6-32, 2019.

[50] H. Zumbahlen, Linear Circuit Design Handbook, Amsterdam: Elsevier/Newnes Press, 2008.

[51] I. Mayergoyz and P. McAvoy, Fundamentals of Electric Power Engineering, 1st ed., Toh Tuck: World Scientific, 2015.

[52] D. Mercer, "Chapter 20: Analog to Digital Conversion," Analog Devices, 2013. [Online]. Available: https://wiki.analog.com/university/courses/electronics/text/chapter-20. [Accessed 7 March 2020].

[53] Texas Instruments, "Switching regulator fundamentals (Rev. C)," *Texas Instruments,* 2012.

[54] W. Kester and B. Erisman, "Switching Regulators," in *Practical Design Techniques for Power and Thermal Management*, Norwood, Analog Devices, 1998.

[55] B. P. Systems, "components101 Breadboard," 8 June 2018. [Online]. Available: https://components101.com/sites/default/files/component_datasheet/Breadboard%20Datasheet.pdf. [Accessed 11 March 2020].

[56] T. Instruments, *PCB Design Guidelines For Reduced EMI,* Texas Instruments, 1999.

[57] ITU-T, "Forward error correction for high bit-rate DWDM submarine systems," *Recommendation.*

[58] Z. Chen and H. Haas, "Space division multiple access in visible light communications," in *IEE International Conference on Communications (ICC)*, London, 2015.

[59] M. A. Khalighi and M. Uysal, "Survey on free space optical communication: a communication theory perspective," *IEEE Comun. Surv. Tut.,* vol. 16, no. 4, pp. 2231-2258, 2014.

[60] F. Akhoundi, A. Minoofar and J. A. Salehi, "Underwater positioning system based on cellular underwater wireless optical CDMA networks," in *26th Wireless and Optical Communication Conference (WOCC)*, Newark, NJ, 2017.

[61] C. C. Kao, Y. S. Lin, G. D. Wu and C. J. Huang, "A comprehensive study on the internet of underwater things: applications, challenges, and channel models Sensors," *Sensors 17,* vol. 1477, pp. 1-20, 2017.

[62] "IEEE Standard for Advanced Audio Coding," *IEEE Std 1857.2-2013,* pp. 1-343, 2013.

[63] M. Laughton and D. Warne, Electrical Engineer's Reference Book, 16th ed., Oxford: Newnes, 2003.

[64] China Young Sun LED Technology, "YSL-R1042B5C-D13," Shenzhen.

[65] Kingbright, "WP7113QBC/G," 2018.

[66] Cree, "Cree® 5-mm Blue and Green Round LED C503B-BAS/BAN/GAS/GAN," Durham, 2019.

[67] ON Semiconductor, "P2N2222A," 2013.

[68] Supertex Inc., "TN0702: N-Channel Enhancement-Mode Vertical DMOS FET," Sunnyvale, 2013.

[69] Supertex Inc., "VN0300: N-Channel Enhancement-Mode Vertical DMOS FET," Sunnyvale, 2009.

[70] ThorLabs, "Si Photodiode FDS1010," *FDS1010 photodiode datasheet,* Feb 2017.

[71] ThorLabs, "Si Photodiode FDS100," *FDS100 photodiode datasheet,* September 2017.

[72] First Sensor, "First Sensor PIN PD Data Sheet, Part Description PS13-6b TO," *PS13-6b TO photodiode datasheet,* Jan 2018.

[73] Texas Instruments, "Transimpedance amplifier circuit," in *Analog Engineers Circuit Cookbook: Amplifiers*, Dallas, TX, 2018.

[74] C. DeCusatis, Handbook of Fiber Optic Data Communication, vol. 4, 2014.

[75] "FAQs - Raspberry Pi Documentation," [Online]. Available: https://www.raspberrypi.org/documentation/faqs/#power. [Accessed 9 March 2020].

[76] Arduino, "Arduino Uno Rev3 - FAQ," [Online]. Available: https://store.arduino.cc/usa/arduino-uno-rev3. [Accessed 9 March 2020].

[77] Energizer, *Energizer Max Alkaline 9V datasheet.*

[78] Samsung SDI, "Introduction of INR 18650-25R," *Samsung INR18650-25R datasheet,* October 2013.

[79] Samsung SDI, "Specification of Product: Lithium-io rechargeable cell of power tools, Model Name: INR18650-30Q," *Samsung INR18650-30Q datasheet,* March 2014.

[80] Murata Power Solutions, "Selectable Output 36-Watt DOSA-SMT DC-DC Converters," *Murata Okami OKI-T/36W_W40 DC/DC power converters datasheet,* 2020.

[81] "Opus Codec," Xiph.org, [Online]. Available: http://www.opus-codec.org/.

[82] G. Rieger, "socat - Multipurpose relay (SOcket CAT)," [Online]. Available: https://linux.die.net/man/1/socat.

[83] GStreamer, "Gstreamer Documentation," [Online]. Available: https://gstreamer.freedesktop.org/documentation/?gi-language=c. [Accessed 12 March 2020].

[84] "PortAudio," [Online]. Available: http://www.portaudio.com/.

[85] "The Ogg container format," Xiph.org, [Online]. Available: https://xiph.org/ogg/.

[86] "Become a Certified Scuba Diver FAQs," Professional Association of Diving Instructors, [Online]. Available: https://www.padi.com/help/scuba-certification-faq. [Accessed 2020].

[87] Ikelite, "Underwater Housing for Nikon COOLPIX A1000," Ikelite, 2017. [Online]. Available: https://www.ikelite.com/products/underwater-housing-for-nikon-coolpix-a1000-digital-cameras. [Accessed 11 March 2020].

[88] B. Streetman and S. Kumar, Solid State Electronic Devices, 6th ed., Upper Saddle River: Prentice-Hall, 2006.

[89] A. Sedra and K. Smith, Microelectronic Circuits, 7th ed., New York: Oxford University Press, 2015.

[90] W. S. Bochu, L. L. Biao and D. Chuanren, "Soundwave stimulation triggers the content change of the endogenous hormone of the chrysanthemum mature callus," *Colloids and Surfaces B: Biointerfaces,* vol. 37, no. 3, pp. 107-112, 2004.

Appendix

A. Regulatory Constraints

Regulatory constraints imposed by institutions are contained within this appendix. These excerpts deal work to control the environmental, economic, and labor-based impact of and marine ventures. The use of UOWC in a practical setting would require adherence to these regulations. As such, conventions and establishments were referenced for necessary information. Of the existing considerations, the relevant regulations are:

United Nations Convention on the Law of the Sea (UNCLOS)

Part XII,

Section 1, Article 194, 195;

Section 4, Article 205, 206;

Section 5, Article 208, 209;

Section 9, Article 236;

Section 11

Part XIII

Section 1, Article 240;

Section 4, Article 258, 260;

Part XIV

Section 1, Article 267.

Safety of Life at Sea Convention (SOLAS):

Chapter II, Article 7;

Chapter V, Article 47;

Chapter VI, Article 51, 56.

Standards of Training, Certification, and Watchkeeping Convention (STCW):

Resolution 8;

Resolution 11.

International Safety Management (ISM) Code:

Part A

Section 6, Article 2;

Section 10, Article 3.

B. Difference Between BJTs and MOSFETS in Digital Switching Applications

The BJT and MOSFET are two semiconductor architectures that are commonly used in digital switching applications. The theory of operation is the same for both: both devices have a current-conducting channel that can be switched on or off with a third terminal in the device (in the BJT this terminal is called the base, and in the MOSFET this terminal is called the gate). The BJT is a current-controlled device, meaning the conducting channel is controlled using a current signal sent to the base which adjusts the biasing of the internal p-n junctions, thus controlling the current that flows through the device [88]. On the other hand, the MOSFET is a voltage-controlled device, meaning the conducting channel is controlled using a voltage applied to the gate which induces a channel for current to pass through [88]. The n^+pn BJT, one common BJT configuration, is shown in Figure 51, and the n-channel MOSFET, one common MOSFET configuration, is shown in Figure 52.

.

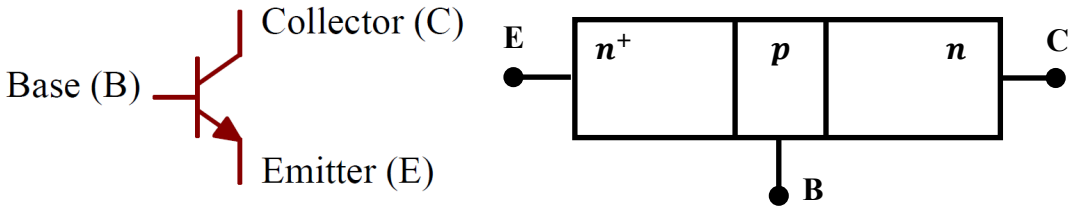

(a) (b)

Figure 51: n^+pn BJT (a) circuit schematic and (b) device configuration

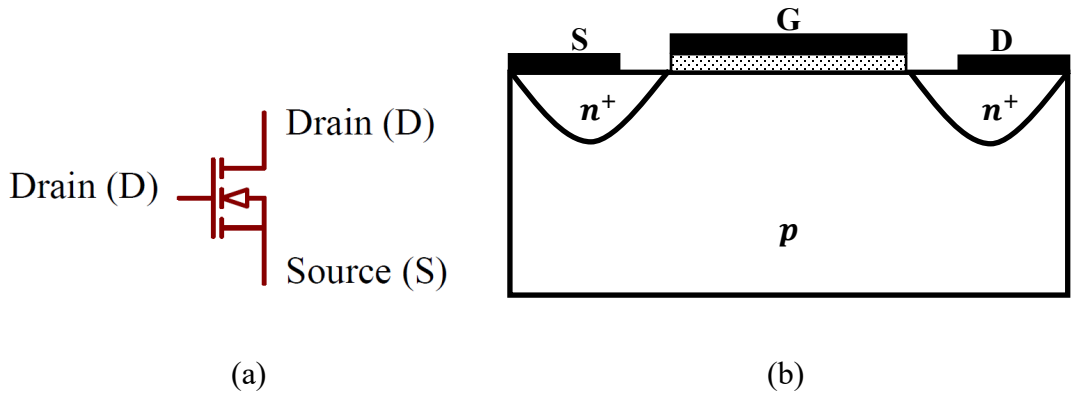

Figure 52: N-channel MOSFET (a) circuit schematic and (b) device configuration

One of the advantages of using a BJT is that it has a very low on-state resistance, meaning that the device typically draws less power and has a lower voltage drop across the channel [51]. This means that the BJT acts more like an ideal switch compared to the MOSFET because it generates a lower voltage drop in the on-state, thus acting more like a short circuit. However, one drawback with using a BJT for switching purposes is that its switching frequency is limited due to the physics of the device. The rate that the BJT's channel can turn on or off is dependent on the rate that charges can flow in and out of the base region. Before the channel is turned on, charges must flow into the base and diffuse across the base in order to properly bias the p-n junctions in the device. The opposite must happen when the channel is turned off, and both these events reduce the effective switching speed of the BJT [51]. Another drawback of the BJT is that it is a current-controlled device. This can create limitations if, for example, the signal used to modulate the channel is coming from a source that is power-limited or cannot drive a current high enough to achieve the desired channel current [89].

On the other hand, the voltage-controlled gate of the MOSFET can switch at much higher speeds because there is no diffusion of carriers in or out of the terminal [89]. As a result, these devices have become ubiquitous in high frequency digital switching circuits [51] [38]. However, MOSFETs typically have higher on-state resistances compared to BJTs resulting in lower efficiencies. Additionally, MOSFETs have less clearly defined on and off states compared to the BJT [89]. In a BJT, the channel is only present if there is a continuous current that is injected into the base to bias the junctions within the device. On the other hand, the gate of the MOSFET is electrically isolated from the channel, which means charges that are inadvertently deposited onto the gate will stay there and can result in an unintentional changed of state of the channel [89]. This charge accumulation comes from a variety of sources: electrostatic discharge and the intrinsic capacitances between the channel and the gate are two examples [38]. As a result, MOSFETs can be inadvertently turned on or off, resulting in less deterministic states compared to the BJT.

C. Switching Converter Schematics

The resistor symbols in the schematics below are symbolic of any load that is being powered by the switching converters. The loads do not need to be purely resistive. Additionally, the switch in each of the converters is implemented using a transistor.

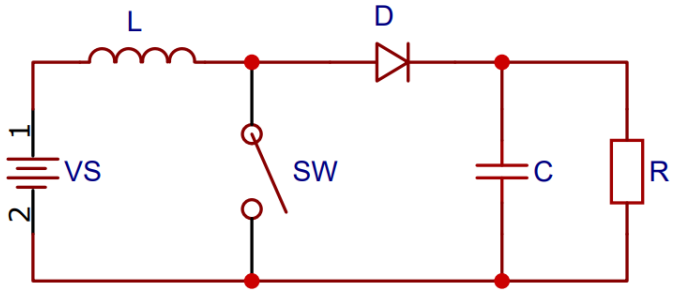

Figure 53: Boost converter

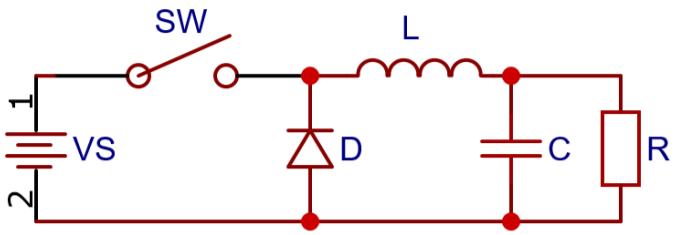

Figure 54: Buck converter

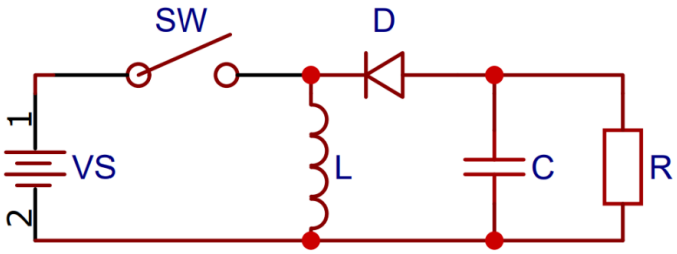

Figure 55: Buck-boost converter

D. Lens Spot Sizes

The spot diagram of a lens refers to the locations of the light rays at the focused spot. For these simulations, 100 paraxial rays were propagated through each lens. Figure 55 and Figure 56 show the simulated spot diagrams of the doublet and singlet.

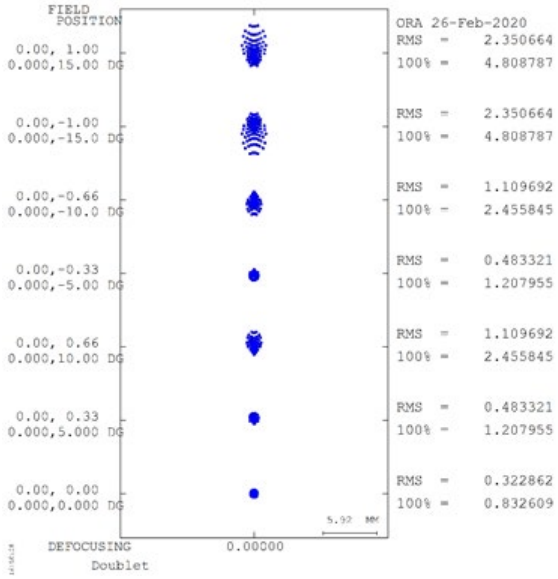

Figure 56: Spot sizes for doublet lens

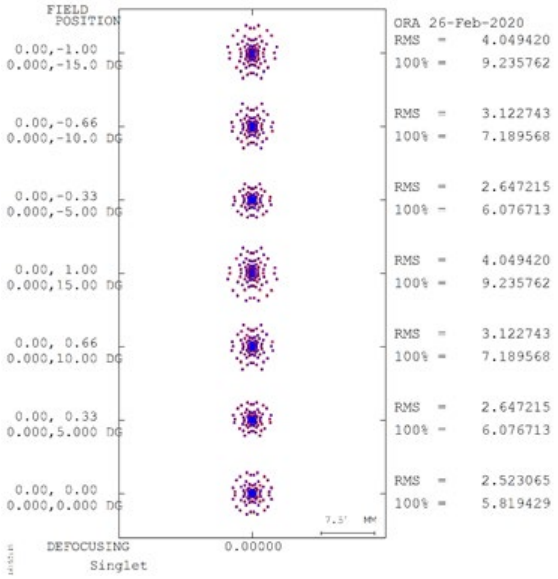

Figure 57: Spot sizes for singlet lens

E. Circuit Revision Bill of Materials (BOM), Schematics, and PCB Layouts

E.1. LED Transmitter Board Revision 1

Item No	Qty	Designator	Part Number	Description	Manufacturer	Notes
1	1	C1	-	0.1 uF THRU HOLE CAP 50V	-	-
2	1	D1	SB240TA	DIODE SCHOTTKY 40V 2A DO15	SMC DIODE	-
3	1	J1	PPTC122LFBN-RC	24 POS HEADER CONN THRU HOLE	SULLINS	-
4	1	J2	691137710005	TERM BLK 5POS SIDE ENTRY 5MM PCB	WURTH ELECTRONIK	-
5	12	L1-L12	YSL-R1042B5C-D13	BLUE LED 10MM	CHINA YOUNG SUN	-
6	3	Q1-Q3	TN0702	N-CH 20V 530mA (Tj) 1W (Tc) THRU HOLE TO-92-3	MICROCHIP TECHNOLOGY	Can use either TN0702 or VN0300
7	3	Q1-Q3	VN0300	MOSFET N-CH 30V 640MA TO92-3	MICROCHIP TECHNOLOGY	Can use either TN0702 or VN0300
8	1	R1	-	1kOHM THRU HOLE RES 1/4W	-	-
9	2	R2,R3	-	10OHM THRU HOLE RES 1W	-	-
10	1	U1	LM7824CT	IC REG LINEAR 24V 1A TO220-3	ON SEMICONDUCTOR	-

Table 12: LED transmitter board Revision 1 BOM

NOTES:
1. Q1-Q3 CAN BE EITHER TN0702 OR VN0300

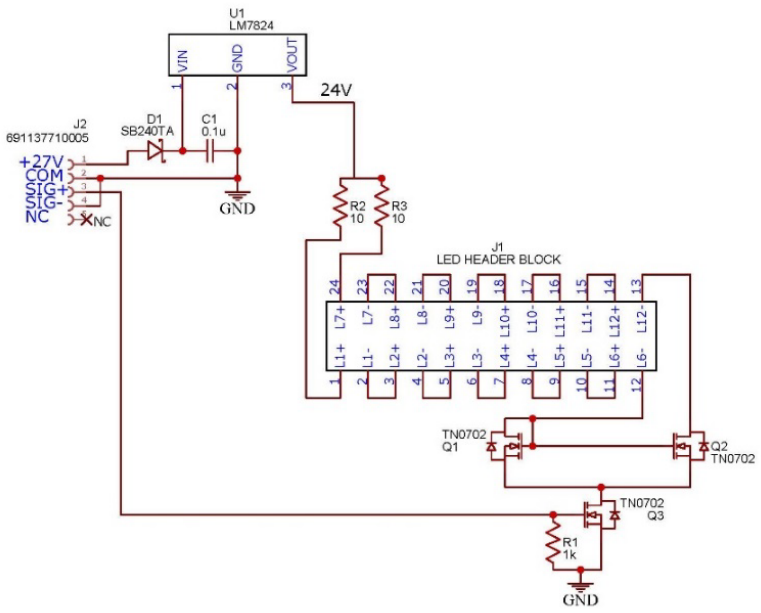

Figure 58: LED transmitter board Revision 1 schematic

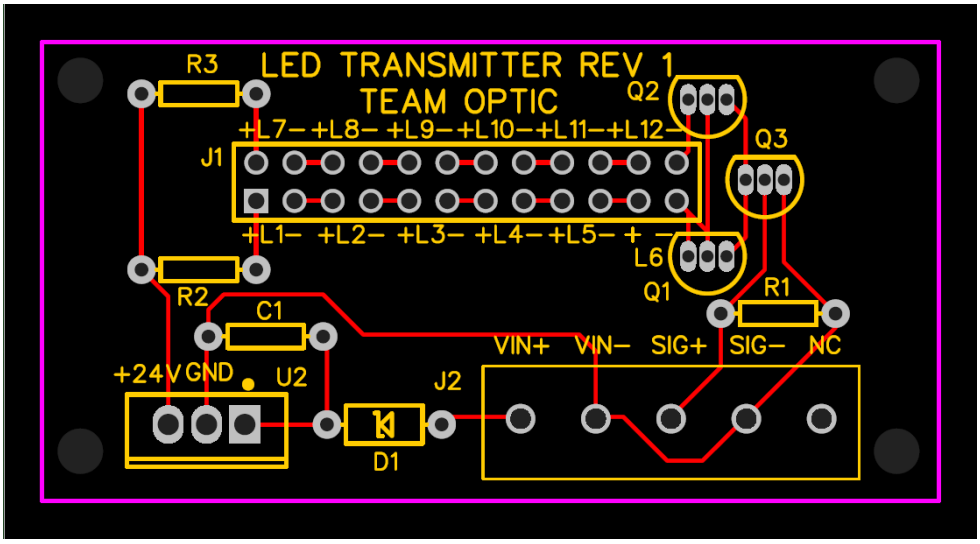

Figure 59: LED transmitter board Revision 1 PCB

E.2. Receiver Board Revision 1

Item No	Qty	Designator	Part Number	Description	Manufacturer	Notes
1	1	C1	-	1pF THRU HOLE CAP	-	-
2	4	C2-C5	-	0.1UF THRU HOLE CAP	-	-
3	1	J1	691137710005	TERM BLK 5POS SIDE ENTRY 5MM PCB	WURTH ELECTRONIK	-
4	1	J2	PS13-6-TO5	13mm PIN PHOTODIODE	FIRST SENSOR	-
5	1	R1	-	47kOHM THRU HOLE RES 1/4W	-	-
6	1	R2	-	470kOHM THRU HOLE RES 1/4W	-	-
7	3	R3	-	1kOHM THRU HOLE RES 1/4W	-	-
8	2	U1, U2	OP37EZ	63MHz GBW OP AMP	ANALOG DEVICES	-
9	1	U3	LM7805CT/NOPB	IC REG LINEAR 5V 1A TO220-3	TEXAS INSTRUMENTS	-
10	1	U4	LM7905CT/NOPB	IC REG LINEAR -5V 1.5A TO220-3	TEXAS INSTRUMENTS	-

Table 13: Receiver board Revision 1 BOM

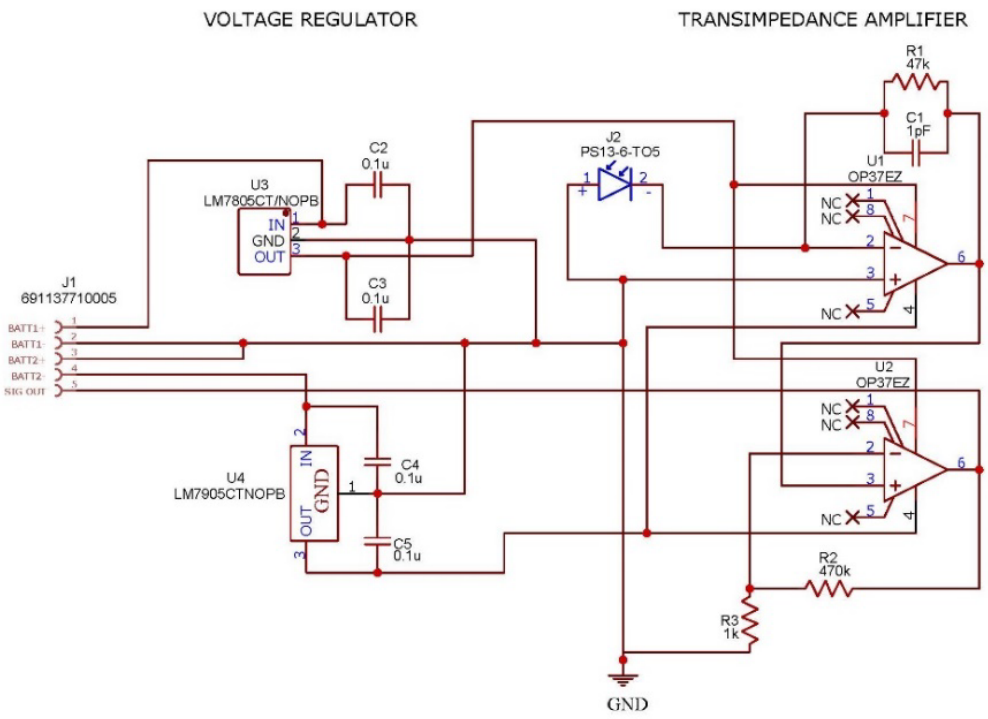

Figure 60: Receiver board Revision 1 schematic

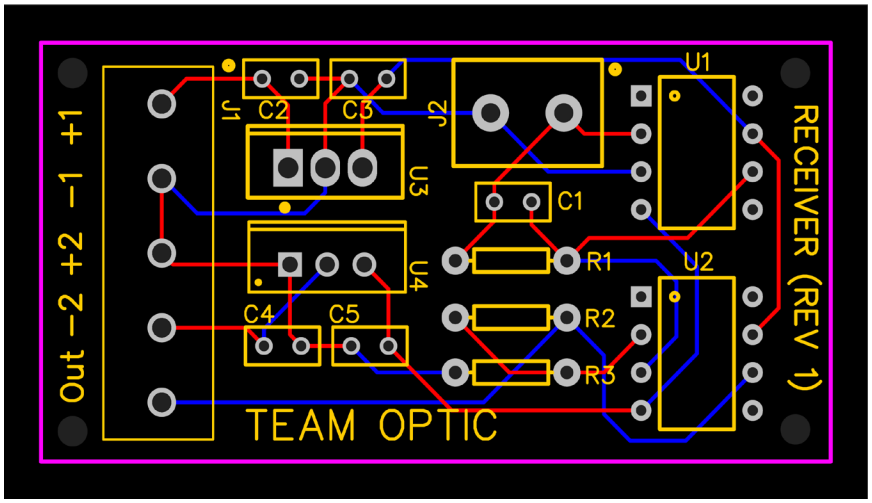

Figure 61: Receiver board Revision 1 PCB

E.3. Transmitter/Receiver Board Revision 1

Item No	Qty	Designator	Part Number	Description	Manufacturer	Notes
1	4	-	1053002300	CONN 20-22AWG CRIMP GOLD	MOLEX	NOT SHOWN
2	1	C1	-	1pF THRU HOLE CAP	-	-
3	1	D1	SB240TA	DIODE SCHOTTKY 40V 2A DO15	SMC DIODE	-
4	1	H1	1053131304	CONN HEADER R/A 4 POS 2.5MM	MOLEX	-
5	1	H2	1848749	TERM BLOCK 12POS TOP ENTRY 3.5MM	PHOENIX CONTACT	-
6	1	H3	691137710005	TERM BLK 5POS SIDE ENTRY 5MM PCB	WURTH ELECTRONIK	-
7	1	J1	1053071204	CONN RCPT HSG 4POS 2.50MM	MOLEX	NOT SHOWN
8	12	L1-L12	YSL-R1042B5C-D13	BLUE LED 10MM	CHINA YOUNG SUN	-
9	3	M1-M3	TN0702	N-CH 20V 530mA (Tj) 1W (Tc) THRU HOLE TO-92-3	MICROCHIP TECHNOLOGY	Can use either TN0702 or VN0300
10	3	M1-M3	VN0300	MOSFET N-CH 30V 640MA TO92-3	MICROCHIP TECHNOLOGY	Can use either TN0702 or VN0300
11	1	P1	PS13-6-TO5	13mm PIN PHOTODIODE	FIRST SENSOR	-
12	3	R1, R4,R7	-	1kOHM THRU HOLE RES 1/4W	-	-
13	2	R2,R3	-	10OHM THRU HOLE RES 1W	-	-
14	1	R5	-	470kOHM THRU HOLE RES 1/4W	-	-
15	1	R6	-	47kOHM THRU HOLE RES 1/4W	-	-
16	1	R8	-	2.2kOHM THRU HOLE RES 1/4W	-	-
17	1	R9	-	10kOHM THRU HOLE RES 1/4W	-	-
18	1	TP1	5011	PC TEST POINT MINIATURE BLACK	KEYSTONE	-
19	3	TP2-TP4	5010	PC TEST POINT MINIATURE RED	KEYSTONE	-
20	2	U1, U2	LM7171BIN/NOPB	200MHz GBW OP AMP	ANALOG DEVICES	-

Table 14: Transmitter/receiver board Revision 1 BOM

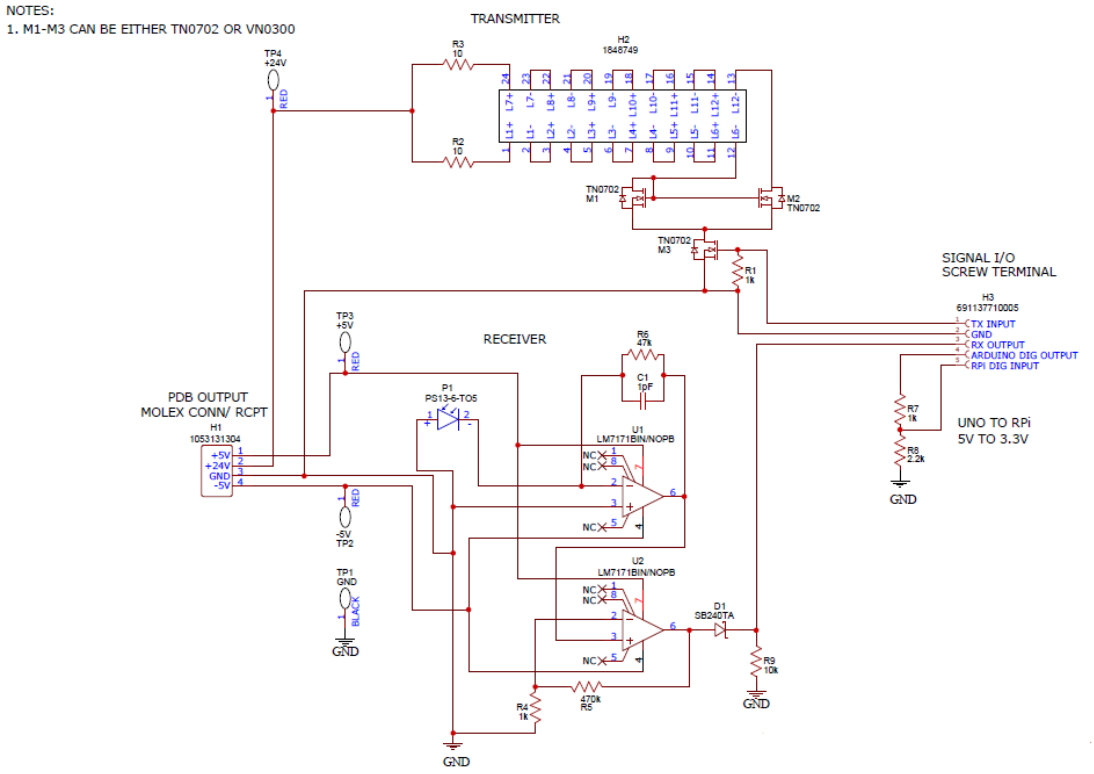

Figure 62: Transmitter/receiver board Revision 1 schematic

E.4. Transmitter/Receiver Board Revision 2

Item No	Qty	Designator	Part Number	Description	Manufacturer	Notes
1	4	-	1053002300	CONN 20-22AWG CRIMP GOLD	MOLEX	NOT SHOWN
2	1	C1	-	1pF THRU HOLE CAP	-	-
3	1	H1	1053131304	CONN HEADER R/A 4 POS 2.5MM	MOLEX	-
4	1	H2	1848749	TERM BLOCK 12POS TOP ENTRY 3.5MM	PHOENIX CONTACT	-
5	1	H3	691137710005	TERM BLK 5POS SIDE ENTRY 5MM PCB	WURTH ELECTRONIK	-
6	1	J1	1053071204	CONN RCPT HSG 4POS 2.50MM	MOLEX	NOT SHOWN
7	12	L1-L12	YSL-R1042B5C-D13	BLUE LED 10MM	CHINA YOUNG SUN	-
8	3	M1-M3	TN0702	N-CH 20V 530mA (Tj) 1W (Tc) THRU HOLE TO-92-3	MICROCHIP TECHNOLOGY	Can use either the TN0702 or the VN0300
9	3	M1-M3	VN0300	MOSFET N-CH 30V 640MA TO92-3	MICROCHIP TECHNOLOGY	Can use either TN0702 or VN0300
10	1	P1	PS13-6-TO5	13mm PIN PHOTODIODE	FIRST SENSOR	-
11	3	R1, R4,R7	-	1kOHM THRU HOLE RES 1/4W	-	-
12	2	R2,R3	-	10OHM THRU HOLE RES 1W	-	-
13	1	R5	-	470kOHM THRU HOLE RES 1/4W	-	-
14	1	R6	-	47kOHM THRU HOLE RES 1/4W	-	-
15	1	R8	-	2.2kOHM THRU HOLE RES 1/4W	-	-
16	1	TP1	5011	PC TEST POINT MINIATURE BLACK	KEYSTONE	-
17	4	TP2-TP5	5010	PC TEST POINT MINIATURE RED	KEYSTONE	-
18	2	U1, U2	LTC6268	500MHZ SINGLE SUPPLY OP AMP	ANALOG DEVICES	-

Table 15: Transmitter/receiver board Revision 2 BOM

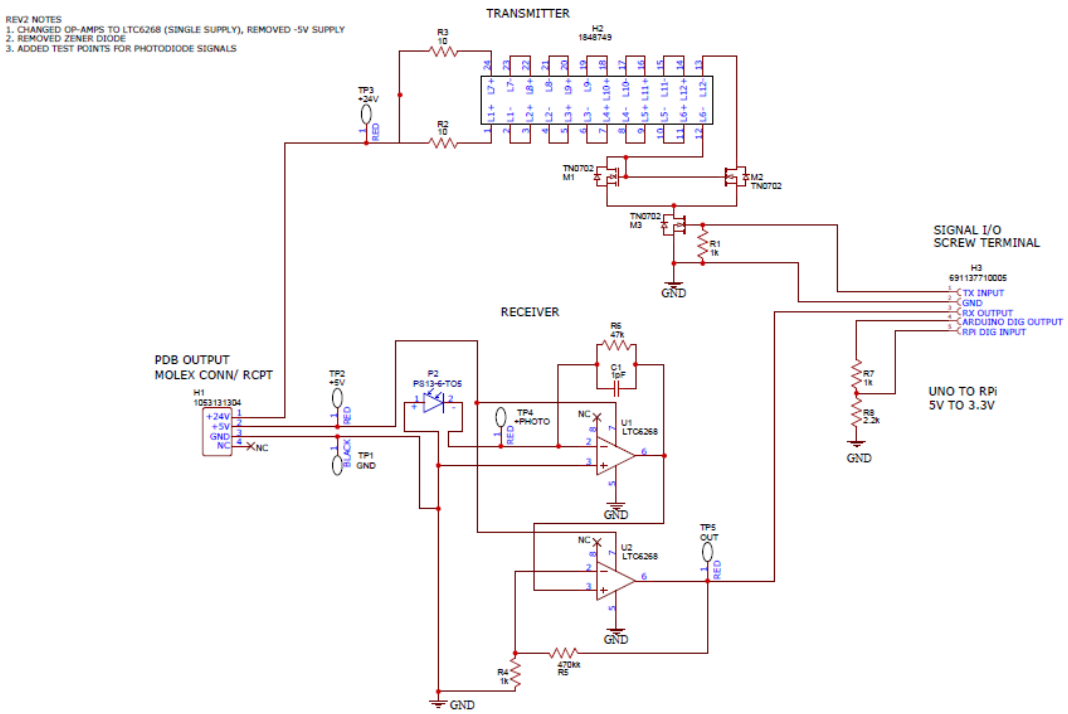

Figure 63: Transmitter/receiver board Revision 2 schematic

E.5. Power Distribution Board Revision 1

Item No	Qty	Designator	Part Number	Description	Manufacturer	Notes
1	2	-	577002B00000G	REGULATOR HEATSINK	AAVID	NOT SHOWN
2	10	-	1053002300	CONN 20-22AWG CRIMP GOLD	MOLEX	NOT SHOWN
3	4	C1-C4	-	1uF THRU HOLE CAP	-	-
4	1	F1	0698Q2500-01	FUSE 2.5A 350V RADIAL	BEL FUSE	-
5	3	H1-H3	1053131304	CONN HEADER R/A 4POS 2.5MM	MOLEX	-
6	1	H4	61300311121	CONN HEADER VERT 3POS 2.54MM	WURTH	-
7	2	J1-J3	1053071204	CONN RCPT HSG 4POS 2.50MM	MOLEX	NOT SHOWN
8	1	J4	QPC02SXGN-RC	CONN JUMPER SHORTING .100" GOLD	SULLINS	NOT SHOWN
9	1	SW1	RBW2ABLKREDIF0	SWITCH ROCKER DPST 16A (AC) 125V	E-SWITCH	-
10	1	TP1	5011	PC TEST POINT MINIATURE BLACK	KEYSTONE	-
11	3	TP2-TP4	5010	PC TEST POINT MINIATURE RED	KEYSTONE	-
12	1	U1	LM7905CT/NOPB	IC REG LINEAR -5V 1.5A TO220-3	TEXAS INSTRUMENTS	-
13	1	U2	LM7824CT	IC REG LINEAR 24V 1A TO220-3	ON SEMICONDUCTOR	OBSOLETE
14	2	U3	OKI-T/36W-W40N-C	DC/DC CONVERTER (VARIABLE OUTPUT)	MURATA	-
15	5	U4	MIC29310-5.0WT	IC REG LINEAR 5V 3A TO220-3	MICREL	-
16	2	USB1, USB2	614004190021	USB TYPE A FEMALE PCB RECEPTACLE	WURTH	-

Table 16: PDB Revision 1 BOM

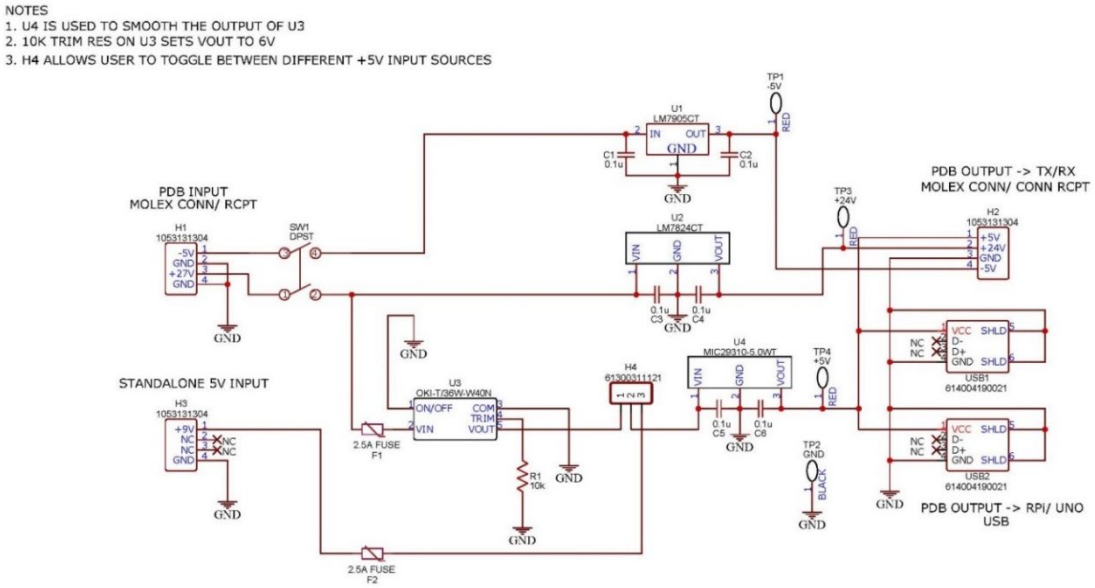

Figure 64: PDB Revision 1 schematic

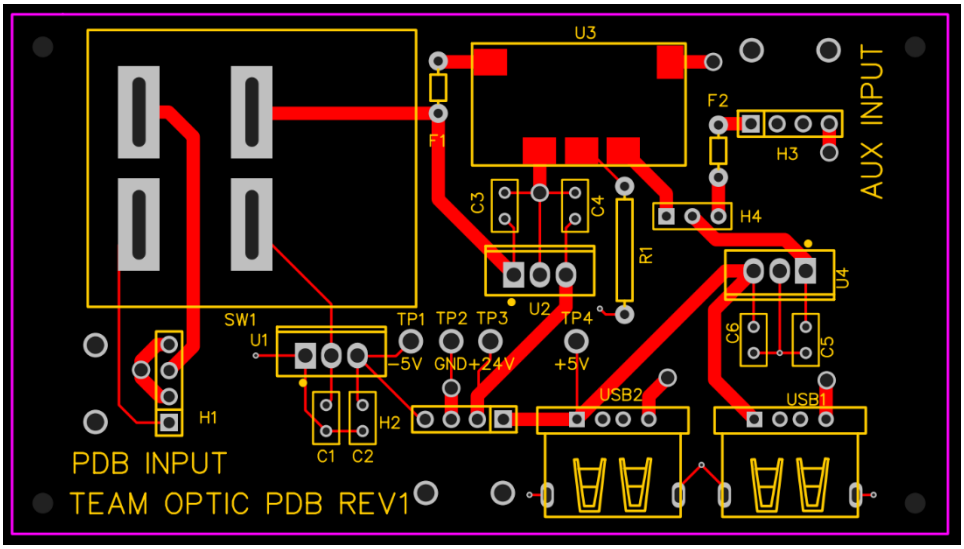

Figure 65: PDB Revision 1 PCB

E.6. Power Distribution Board Revision 2

Item No	Qty	Designator	Part Number	Description	Manufacturer	Notes
1	2	-	577002B00000G	REGULATOR HEATSINK	AAVID	NOT SHOWN IN SCHEM
2	10	-	1053002300	CONN 20-22AWG CRIMP GOLD	MOLEX	NOT SHOWN IN SCHEM
3	4	C1-C4	-	1uF THRU HOLE CAP	-	-
4	1	F1	0698Q2500-01	FUSE 2.5A 350V RADIAL	BEL FUSE	-
5	2	H1-H3	1053131304	CONN HEADER R/A 4POS 2.5MM	MOLEX	-
6	1	H4	61300311121	CONN HEADER VERT 3POS 2.54MM	WURTH	-
7	2	J1-J3	1053071204	CONN RCPT HSG 4POS 2.50MM	MOLEX	NOT SHOWN
8	1	J4	QPC02SXGN-RC	CONN JUMPER SHORTING .100" GOLD	SULLINS	NOT SHOWN
9	1	SW1	RBW2ABLKREDIF0	SWITCH ROCKER DPST 16A (AC) 125V	E-SWITCH	-
10	1	TP1	5011	PC TEST POINT MINIATURE BLACK	KEYSTONE	-
11	3	TP2-TP4	5010	PC TEST POINT MINIATURE RED	KEYSTONE	-
13	1	U2	LM7824CT	IC REG LINEAR 24V 1A TO220-3	ON SEMICONDUCTOR	OBSOLETE
14	2	U3	OKI-T/36W-W40N-C	DC/DC CONVERTER (VARIABLE OUTPUT)	MURATA	-
15	5	U4	MIC29310-5.0WT	IC REG LINEAR 5V 3A TO220-3	MICREL	-
16	2	USB1, USB2	614004190021	USB TYPE A FEMALE PCB RECEPTACLE	WURTH	-

Table 17: PDB Revision 2 BOM

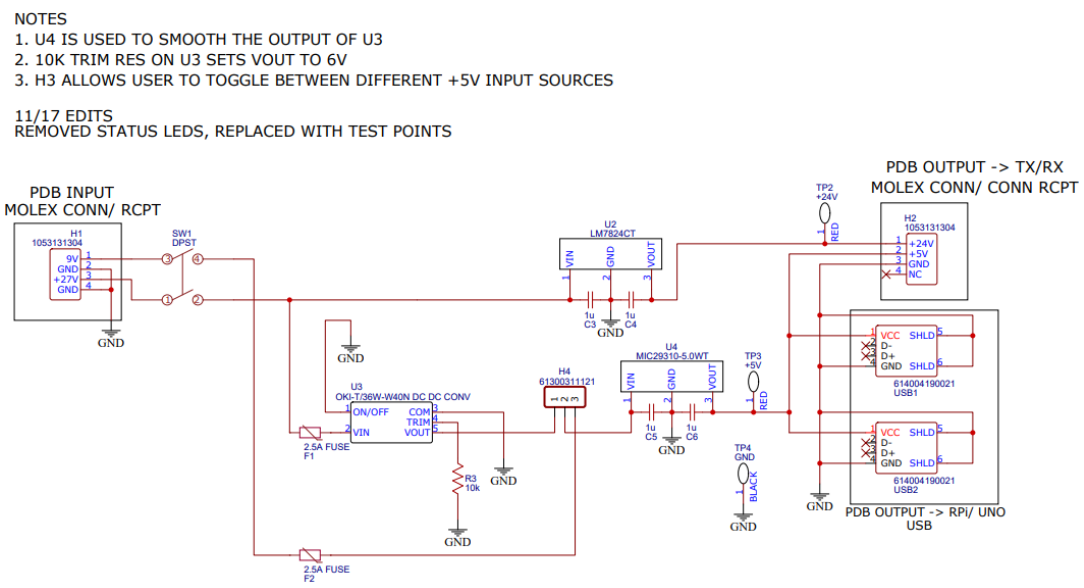

Figure 66: PDB Revision 2 schematic

F. Audio Streaming Programs

F.1. Audio Transmitter Code:

```
#include <gst/gst.h>

static void on_pad_added (GstElement *element, GstPad *pad, gpointer data) {
  GstPad *sinkpad;
  GstElement *decoder = (GstElement *) data;
  g_print ("dynamic pad created, linking demuxer/decovder \n");
  sinkpad = gst_element_get_static_pad (decoder,"sink");
  gst_pad_link (pad, sinkpad);
  gst_object_unref(sinkpad);
}

int
main (int argc, char *argv[])
{
  GstElement *pipeline, *source, *sink, *oggdemux, *opusdec, *audioconvert, *audioresample;
  GstBus *bus;
  GstMessage *msg;
  GstStateChangeReturn ret;

  /* Initialize GStreamer */
  gst_init (&argc, &argv);

  /* Create the elements */

  source = gst_element_factory_make ("filesrc", "source");
  sink = gst_element_factory_make ("autoaudiosink", "sink");
  oggdemux = gst_element_factory_make("oggdemux", "oggdemux");
  opusdec = gst_element_factory_make("opusdec","opusdec");
  audioconvert = gst_element_factory_make("audioconvert","audioconvert");
  audioresample = gst_element_factory_make("audioresample","audioresample");

  /* Create the empty pipeline */
  pipeline = gst_pipeline_new ("test-pipeline");

  if (!pipeline || !source || !sink || !oggdemux || !opusdec || !audioconvert || !audioresample) {
    g_printerr ("Not all elements could be created.\n");
    return -1;
  }

  /* Build the pipeline */
  gst_bin_add_many (GST_BIN (pipeline), source, oggdemux, opusdec, audioconvert,
audioresample,sink, NULL);
```

```
if (gst_element_link(source,oggdemux) != TRUE) {
  g_printerr ("source and demux cannot be linked");
  gst_object_unref (pipeline);
  return -1;
}
if (gst_element_link_many(opusdec,audioconvert,audioresample,sink, NULL) != TRUE) {
  g_printerr ("sink cannot be linked");
  gst_object_unref (pipeline);
  return -1;
}
if (g_signal_connect (oggdemux, "pad-added", G_CALLBACK(on_pad_added), opusdec) <= 0) {
  g_printerr ("signal cannot be connected");
  gst_object_unref(pipeline);
  return -1;
}

/* Modify the source's properties */
g_object_set (source, "location", "/dev/ttyS0", NULL);

/* Start playing */
ret = gst_element_set_state (pipeline, GST_STATE_PLAYING);
if (ret == GST_STATE_CHANGE_FAILURE) {
  g_printerr ("Unable to set the pipeline to the playing state.\n");
  gst_object_unref (pipeline);
  return -1;
}
/* Wait until error or EOS */
bus = gst_element_get_bus (pipeline);
msg =
    gst_bus_timed_pop_filtered (bus, GST_CLOCK_TIME_NONE,
    GST_MESSAGE_ERROR | GST_MESSAGE_EOS);

/* Parse message */
if (msg != NULL) {
  GError *err;
  gchar *debug_info;

  switch (GST_MESSAGE_TYPE (msg)) {
    case GST_MESSAGE_ERROR:
      gst_message_parse_error (msg, &err, &debug_info);
      g_printerr ("Error received from element %s: %s\n",
          GST_OBJECT_NAME (msg->src), err->message);
      g_printerr ("Debugging information: %s\n",
          debug_info ? debug_info : "none");
      g_clear_error (&err);
      g_free (debug_info);
      break;
```

```
      case GST_MESSAGE_EOS:
        g_print ("End-Of-Stream reached.\n");
        break;
      default:
        /* We should not reach here because we only asked for ERRORs and EOS */
        g_printerr ("Unexpected message received.\n");
        break;
    }
    gst_message_unref (msg);
  }

  /* Free resources */
  gst_object_unref (bus);
  gst_element_set_state (pipeline, GST_STATE_NULL);
  gst_object_unref (pipeline);
  return 0;
}
```

F.2. Audio Receiver Code:

```
#include <gst/gst.h>

static void on_pad_added (GstElement *element, GstPad *pad, gpointer data) {
  GstPad *sinkpad;
  GstElement *decoder = (GstElement *) data;
  g_print ("dynamic pad created, linking demuxer/decovder \n");
  sinkpad = gst_element_get_static_pad (decoder,"sink");
  gst_pad_link (pad, sinkpad);
  gst_object_unref(sinkpad);
}

int
main (int argc, char *argv[])
{
  GstElement *pipeline, *source, *sink, *oggdemux, *opusdec, *audioconvert, *audioresample;
  GstBus *bus;
  GstMessage *msg;
  GstStateChangeReturn ret;

  /* Initialize GStreamer */
  gst_init (&argc, &argv);

  /* Create the elements */

  source = gst_element_factory_make ("filesrc", "source");
  sink = gst_element_factory_make ("autoaudiosink", "sink");
  oggdemux = gst_element_factory_make("oggdemux", "oggdemux");
  opusdec = gst_element_factory_make("opusdec","opusdec");
  audioconvert = gst_element_factory_make("audioconvert","audioconvert");
  audioresample = gst_element_factory_make("audioresample","audioresample");

  /* Create the empty pipeline */
  pipeline = gst_pipeline_new ("test-pipeline");

  if (!pipeline || !source || !sink || !oggdemux || !opusdec || !audioconvert || !audioresample) {
    g_printerr ("Not all elements could be created.\n");
    return -1;
  }

  /* Build the pipeline */
  gst_bin_add_many (GST_BIN (pipeline), source, oggdemux, opusdec, audioconvert,
audioresample,sink, NULL);

  if (gst_element_link(source,oggdemux) != TRUE) {
    g_printerr ("source and demux cannot be linked");
```

```
  gst_object_unref (pipeline);
  return -1;
}
if (gst_element_link_many(opusdec,audioconvert,audioresample,sink, NULL) != TRUE) {
  g_printerr ("sink cannot be linked");
  gst_object_unref (pipeline);
  return -1;
}
if (g_signal_connect (oggdemux, "pad-added", G_CALLBACK(on_pad_added), opusdec) <= 0) {
  g_printerr ("signal cannot be connected");
  gst_object_unref(pipeline);
  return -1;
}

/* Modify the source's properties */
g_object_set (source, "location", "/dev/ttyS0", NULL);

/* Start playing */
ret = gst_element_set_state (pipeline, GST_STATE_PLAYING);
if (ret == GST_STATE_CHANGE_FAILURE) {
  g_printerr ("Unable to set the pipeline to the playing state.\n");
  gst_object_unref (pipeline);
  return -1;
}
/* Wait until error or EOS */
bus = gst_element_get_bus (pipeline);
msg =
    gst_bus_timed_pop_filtered (bus, GST_CLOCK_TIME_NONE,
    GST_MESSAGE_ERROR | GST_MESSAGE_EOS);

/* Parse message */
if (msg != NULL) {
  GError *err;
  gchar *debug_info;

  switch (GST_MESSAGE_TYPE (msg)) {
    case GST_MESSAGE_ERROR:
      gst_message_parse_error (msg, &err, &debug_info);
      g_printerr ("Error received from element %s: %s\n",
          GST_OBJECT_NAME (msg->src), err->message);
      g_printerr ("Debugging information: %s\n",
          debug_info ? debug_info : "none");
      g_clear_error (&err);
      g_free (debug_info);
      break;
    case GST_MESSAGE_EOS:
      g_print ("End-Of-Stream reached.\n");
```

```
      break;
    default:
      /* We should not reach here because we only asked for ERRORs and EOS */
      g_printerr ("Unexpected message received.\n");
      break;
   }
   gst_message_unref (msg);
 }

 /* Free resources */
 gst_object_unref (bus);
 gst_element_set_state (pipeline, GST_STATE_NULL);
 gst_object_unref (pipeline);
 return 0;
}
```

G. Startup Scripts

G.1. Audio Transmitter Startup Script:

```
while true
do
        sleep 1s
        killall socat
        socat -b1048576 -u OPEN:/home/pi/OPTIC/testData.txt /dev/ttyS0
done
```

G.2. Audio Receiver Startup Script

```
#!/bin/bash


socat -b1048576 -u /dev/ttyS0 STDOUT > "/home/pi/OPTIC/Test_Results/`date
'+%Y_%m_%d__%H_%M_%S'`.txt"
```